ELEMENTA Science of the Anthropocene

Kohlbach, D, et al. 2025. Nansen and Amundsen basins: Gradients of physico-chemical properties and biota composition with implications for future resource management of the central Arctic Ocean. *Elem Sci Anth*, 13: 1. DOI: https://doi.org/10.1525/elementa.2024.00016

RESEARCH ARTICLE

Nansen and Amundsen basins: Gradients of physico-chemical properties and biota composition with implications for future resource management of the central Arctic Ocean

Doreen Kohlbach[1,2,*], Agneta Fransson[3], Martí Amargant-Arumi[1], Karen M. Assmann[4], Philipp Assmy[3], Gunnar Bratbak[5], Melissa Chierici[4], Anca Cristea[1,3], Dmitry V. Divine[3], Emily Down[6], Wenche Eikrem[7,8], Øyvind Foss[3], Jessie Gardner[1], Rolf R. Gradinger[1], Mats A. Granskog[3], Silvia Hess[9], Randi B. Ingvaldsen[4], Zoé Koenig[1], Sławomir Kwaśniewski[10], Sanna Majaneva[11,12], Miriam Marquardt[1], Oliver Müller[5], Iliana Vasiliki Ntniou[5], Mateusz Ormańczyk[10], Bonnie Raffel[3], Paul Renaud[11], Angelika H. H. Renner[4], Thaise Ricardo de Freitas[9], Arunima Sen[13], Zofia Smoła[10], Camilla Svensen[1], Anna Vader[13], Selina Våge[5], Józef Wiktor[10], Anette Wold[3], Monika Zabłocka[10], Amanda Ziegler[1,11], and Bodil A. Bluhm[1]

The projected transition of the central Arctic Ocean (CAO) into a warmer, seasonally ice-free ocean requires more knowledge of this environment to predict changes in the structure and dynamics of its ecosystems. We aimed to compare the state and underlying processes of Nansen Basin and Amundsen Basin ecosystems observed in August–September 2021 and assess impacts of Atlantic Water inflow and fresher Transpolar Drift waters, respectively, on these ecosystems. The basins differed in features of sea ice, hydrography, and chemical and biological compositions. The near-slope open water in western Nansen Basin showed a clear fingerprint of warm, saline Atlantic Water, with larger vertical turbulent fluxes facilitating nutrient transport across the pycnocline and supporting larger standing stocks of bacteria, protists, and zooplankton. Pelagic primary production and microbial and faunal stocks decreased northward and into Amundsen Basin, likely due to lower nutrient concentrations, stronger stratification, and reduced light through the more continuous and thicker ice and snow cover in Amundsen Basin, possibly also impacted by seasonally declining light levels. Transpolar Drift signals included lower salinity, stronger stratification, and higher silicate concentrations in Amundsen Basin surface waters. Similarities to earlier observations included the increase in small-sized algae from Nansen Basin into Amundsen Basin and overall low faunal abundances in the CAO, suggesting that overarching patterns remained unchanged over past decades. Examples of species range extensions and notable taxon absences relative to earlier studies, however, could be due to borealization and changes in sea-ice conditions, respectively. Higher density ecosystem sampling and consistent time series are recommended to confirm such conclusions. The distinct basin differences call for a regional approach to future management of the CAO. We especially caution against using the area of strong Atlantic Water inflow in southern Nansen Basin as representative of the entire basin, let alone Amundsen Basin or the CAO.

Keywords: Central Arctic Ocean, Ecosystem status, Climate change, Sustainable management

[1] Department of Arctic and Marine Biology, UiT The Arctic University of Norway, Tromsø, Norway

[2] Alfred Wegener Institute Helmholtz Centre for Polar and Marine Research, Bremerhaven, Germany

[3] Norwegian Polar Institute, Fram Centre, Tromsø, Norway

[4] Institute of Marine Research, Tromsø, Norway

[5] Department of Biological Sciences, University of Bergen, Bergen, Norway

[6] Department of Remote Sensing and Data Management, Norwegian Meteorological Institute, Tromsø, Norway

[7] Norwegian Institute for Water Research, Oslo, Norway

[8] Natural History Museum, University of Oslo, Oslo, Norway

[9] Department of Geosciences, University of Oslo, Oslo, Norway

[10] Institute of Oceanology Polish Academy of Sciences, Sopot, Poland

[11] Akvaplan-niva, Tromsø, Norway

[12] Norwegian University of Science and Technology, Trondheim, Norway

[13] Department of Arctic Biology, University Centre in Svalbard, Svalbard, Norway

* Corresponding author:
Emails: d.kohlbach@googlemail.com; doreen.kohlbach@awi.de

1. Introduction

The central Arctic Ocean (CAO; here defined as the Eurasian and Amerasian basins) is one of the last regions with old and thick multiyear ice (MYI), which, due to global warming, is being replaced continuously with younger and thinner first-year ice (FYI; Kwok, 2018; IPCC, 2019). Furthermore, the entire Arctic Ocean (including CAO and shelves) is predicted to become largely sea-ice free during the summer months as early as the middle of the 21st century (Laliberté et al., 2016; Guarino et al., 2020; Kim et al., 2023). In addition to changes in the sea-ice habitat, significant changes in the water column, including temperature increase (Tsubouchi et al., 2021), changes in ocean chemistry (Terhaar et al., 2020), circulation patterns (Valk et al., 2019), stratification (Hordoir et al., 2022), and nutrient availability (Tuerena et al., 2022), are the consequences of warming as well as altered atmospheric circulation and inflow of water masses, with partly contrasting ecosystem responses to these environmental changes in the Eurasian versus Amerasian Basin (Polyakov et al., 2017; 2020; Muilwijk et al., 2023).

The Eurasian Basin consists of two main deep basins: the Nansen Basin and the Amundsen Basin, which are separated by the Gakkel Ridge. Atlantic Water (AW) is subducted under the fresher Arctic surface layer as it enters the Eurasian Basin through eastern Fram Strait (warmer, more saline) and from the Barents Sea (colder, less saline; Rudels, 2015; Rudels et al., 2015; Rudels and Carmack, 2022). In the past decades, a salinification of the upper ocean in the Eurasian Basin has been detected, accompanied by weakened upper ocean stratification and changes in nutrient fluxes (Polyakov et al., 2020), which is strongly influenced by a large-scale weather pattern called the Arctic Dipole (Polyakov et al., 2023). The increased inflow of warmer AW into the Nansen Basin brings large amounts of heat into the CAO and causes "Atlantification" of this deep-sea basin, which results in rising temperature and salinity as well as reduction in sea-ice cover (Polyakov et al., 2017; Aksenov et al., 2018). Atlantification has occurred to a lesser extent in the Amundsen Basin (Polyakov et al., 2017; 2020).

Previous studies suggested different environmental regimes in the two basins. The stronger influence of AW (**Figure 1a**; Rudels et al., 2013) results in higher nutrient concentrations in the Nansen Basin compared to the Amundsen Basin (Flores et al., 2019; Castellani et al., 2020). The presence of the Transpolar Drift (TPD; **Figure 1a**) also leaves a distinct riverine/terrestrial geochemical imprint on the surface waters in the Amundsen Basin (e.g., Charette et al., 2020; Liguori et al., 2021). Primary production rates are low in the Nansen and Amundsen basins compared to shelf seas (Nöthig et al., 2020b), but higher than in the more oligotrophic Beaufort Gyre overlying the Amerasian Basin (Wiedmann et al., 2020). Vertical particle flux rates were estimated to be somewhat higher and particle composition differing in the Amundsen Basin compared to the Nansen Basin, which was explained by the influence of the TPD/Lena River bringing particles from the shelf into the Amundsen Basin (Nöthig et al., 2020a). Moreover, differences in meso- and macrozooplankton community structure between the two basins were observed (Auel and Hagen, 2002; David et al., 2015; Ingvaldsen et al., 2023). Based on these variations in environmental settings and ecosystem structure, ongoing and future climate change might be argued to impact the two basins differently. Comparative investigations of ecosystem properties on either side of the Gakkel Ridge are therefore warranted.

Due to heavy ice conditions year-round and associated restricted human access, the CAO is still relatively underexplored in comparison to seasonally ice-covered systems and shelf regions of the Arctic. Consequently, there is limited information on the functioning of the CAO ecosystem under current environmental conditions (e.g., Bluhm et al., 2015; Ingvaldsen et al., 2021; Solomon et al., 2021; Pnyushkov and Polyakov, 2022). A holistic ecological inventory—in addition to interdisciplinary research—is therefore crucial to better understand system links and anticipate future changes. The expansion of open-water areas in the decades to come will introduce new opportunities for enhanced shipping and fishing activities in the CAO. The potential for commercial fisheries after the end of the current fishing ban in 2037 (Central Arctic Ocean Fisheries Agreement; Haug et al., 2017; Vylegzhanin et al., 2020) warrants a thorough assessment of biotic (including harvestable) and abiotic resources in this region (Snoeijs-Leijonmalm et al., 2020; Ingvaldsen et al., 2023) as well as of the potential consequences of human activities in the CAO to ensure an intact and functioning ecosystem.

Sea-ice decline and changes of seawater properties have a direct impact on the structure and functioning of the sympagic (ice-associated), pelagic, and benthic compartments of the CAO ecosystem (Lannuzel et al., 2020; Steiner et al., 2021). For example, evidence for changed community composition and diversity of sea-ice protists in the CAO over the past decades is attributed to reduced sea-ice extent and loss of MYI (Hop et al., 2020). Impacts on pelagic protist communities are complex and likely to show regional differences depending on changes in the main environmental drivers. Thus, increased stratification and lowered nitrate concentrations in the upper water column of the Amerasian Basin have resulted in a change in dominance from nano- to picophytoplankton concomitant with resource control of phytoplankton size structure (Li et al., 2009; Li et al., 2013; Zhang et al., 2015), while range expansion of temperate phytoplankton species into the Arctic Ocean, such as the coccolithophore *Geophyrocapsa huxleyi* (former synonym *Emiliania huxleyi*) (Neukermans et al., 2018; Oziel et al., 2020) and cyanobacteria of the genus *Synechococcus* (Paulsen et al., 2016), as a result of Atlantification are likely to be more pronounced in the Eurasian Basin. Ship-board incubation experiments testing the effects of changes in temperature, salinity, and acidification state on phytoplankton community

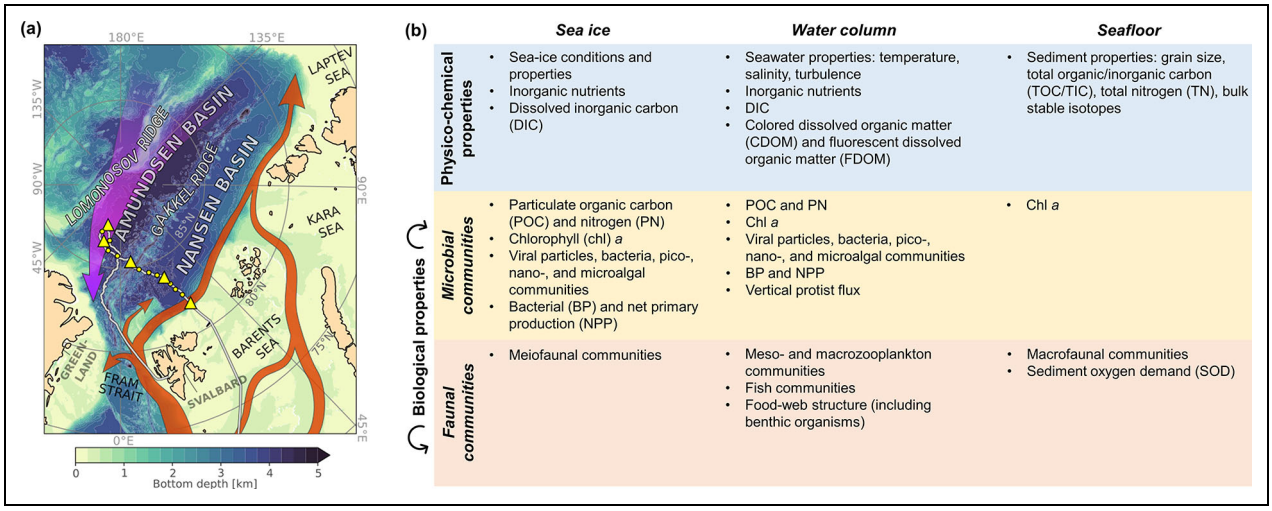

Figure 1. Study region and research foci. Overview of (a) the study region highlighting the Atlantic Water inflow (orange arrows) influencing the Nansen Basin and the Transpolar Drift (purple arrow) influencing the Amundsen Basin (map created using Python/Matplotlib) and (b) physico-chemical and biological properties of the central Arctic Ocean ecosystem investigated in this study.

structure from the Atlantic and Pacific inflow regions to the Arctic Ocean showed complex response patterns, with temperature increases generally favoring diatoms while changes in salinity and acidification state tended to increase growth of small-sized phytoplankton (<10 µm; Sugie et al., 2020; Ahme et al., 2023). Additionally, the higher water temperature facilitates the northward expansion of boreal zooplankton and fish (Fossheim et al., 2015; Ingvaldsen et al., 2021; Snoeijs-Leijonmalm et al., 2021), which will likely compete with true Arctic species, altering the structure of current CAO food webs. Sea-ice algae can be a fresh and nutritious food source for benthic food webs in the high Arctic (Boetius et al., 2013; Rybakova et al., 2019; Wiedmann et al., 2020). Less sea ice in the future, potentially associated with a more spatio-temporally restricted availability of ice algae, might therefore also change benthic community structure and functioning (Kędra et al., 2015; Yunda-Guarin et al., 2020; Zhulay et al., 2023).

For this study, comprehensive and interdisciplinary research was conducted in the western Nansen Basin across the Gakkel Ridge into the western Amundsen Basin. Thereby, we provide an extensive ecosystem inventory of the two basins during late summer 2021, contrasting chemical, physical, and biological components of sympagic, pelagic, and benthic environments (**Figure 1b**). Our work was conducted along a transect of 15 stations with five process-oriented sampling locations from a whole-system perspective. Specifically, we aimed to compare: (i) environmental properties of sea ice, water column, and seafloor sediments; (ii) composition and productivity of ice-associated and pelagic microbial communities; and (iii) composition and stocks of faunal communities inhabiting sea ice, water column, and sediments. This holistic approach allowed us to identify and evaluate links between environmental drivers, biological communities, and their responses as well as their variability between the two basins in a descriptive manner. Understanding the environmental drivers and ecological mechanisms that have led to the CAO structure and functioning we observe today can help project future Arctic ecosystem status in response to climate change. This understanding of ecosystem status and its spatial variability contributes to the development of sound governance and management strategies for these largely international waters (Mason et al., 2024).

2. Material and methods

2.1. Sampling campaign

Physical, chemical, and biological samples of sea ice, water column, and benthic environments were collected during August–September 2021 (cruise JC2-2, cruise number 2021710; August 24 to September 24) onboard the Norwegian icebreaker RV *Kronprins Haakon* within the framework of the Norwegian Nansen Legacy project (https://arvenetternansen.com). The northward transect covered areas from 81.8°N to 87.5°N in the CAO featuring five main process stations (stations P7 to P11) at which nearly all ecosystem properties studied were observed, measured, and sampled and additional stations (NLEG stations) at which mostly environmental variables were collected (**Figure 2a** and **Table 1**). Stations P7 and P8 were located in the Nansen Basin, station P9 at the Gakkel Ridge, and stations P10 and P11 in the Amundsen Basin. All stations except for the southernmost location P7 were ice-covered at the time of sampling (Figure S1). Details on individual sampling procedures can be found in the project sampling protocols (The Nansen Legacy, 2020: https://doi.org/10.7557/nlrs.5719) and the cruise report (Fransson et al., 2022: https://doi.org/10.7557/nlrs.6413). Given the comprehensive sampling approach and deep-sea habitat, the total number of stations that could be covered

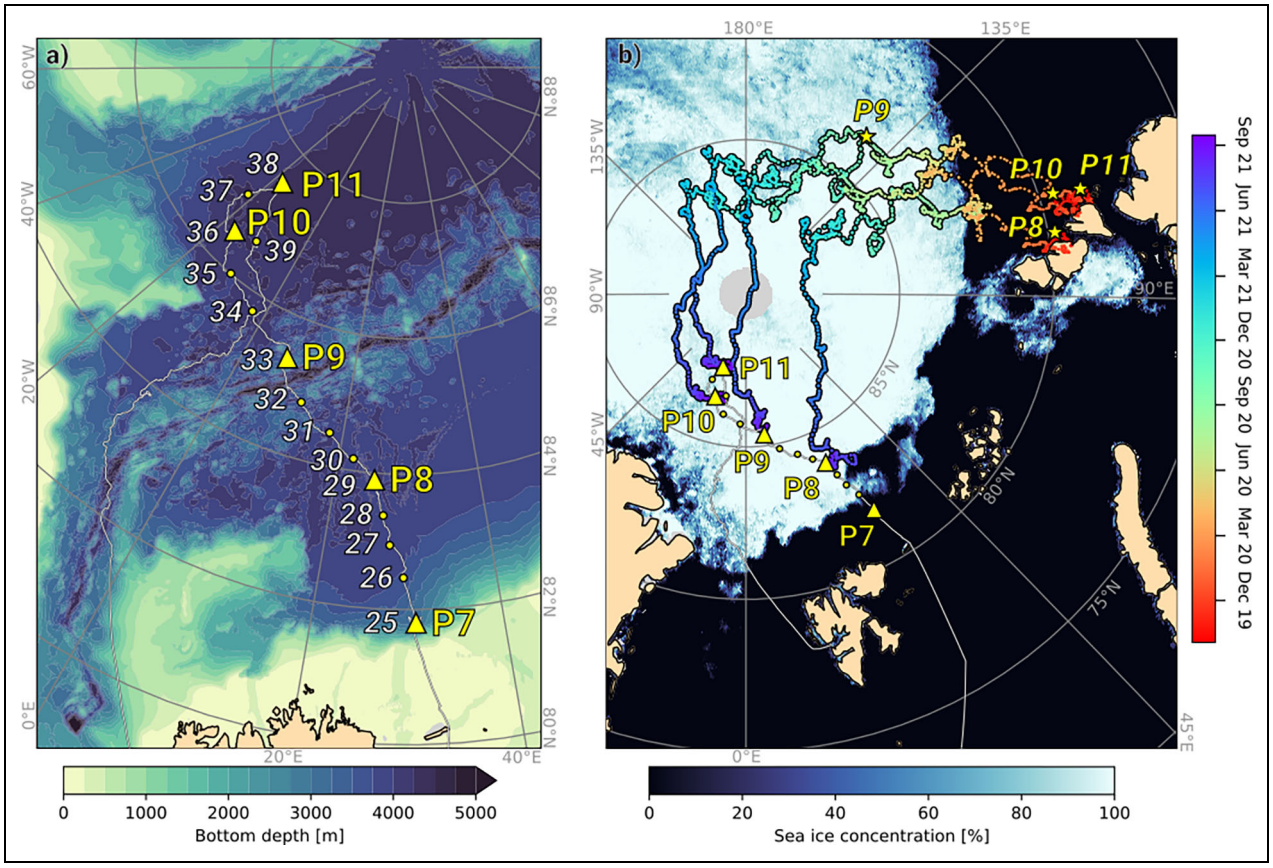

Figure 2. Sampling area, stations, sea-ice concentration, and drift back-trajectories. (a) Bathymetry of the sampling area with cruise track (white line), including main process (P) stations (yellow triangles) and additional stations (yellow circles; see **Table 1** for station information), and (b) cruise track with stations plotted along with sea-ice concentration from 06/09/2021 (blue/white background colors). Sea-ice drift back-trajectories from stations P8–P11 are shown as dots colored by date, and trajectory origins as yellow stars. Maps were created using Python/Matplotlib.

Table 1. Stations sampled during the Nansen Legacy JC2-2 cruise in August–September 2021

Location	Station	Start Date (2021)	End Date (2021)	Start Latitude (°N)	Start Longitude (°E)	End Latitude (°N)	End Longitude (°E)	Bottom Depth (m)	Temperature (°C)[a]	Salinity (g kg^{-1})[a]
Nansen Basin	P7/NLEG25	28/08	30/08	81.803	30.885	81.803	30.884	3,056	−0.10	33.45
	NLEG26	30/08	31/08	82.470	29.536	82.477	29.440	3,661	−1.39	33.45
	NLEG27	31/08	31/08	82.947	27.857	82.947	27.769	3,924	−1.43	33.79
	NLEG28	31/08	31/08	83.382	26.878	83.379	26.776	3,983	−1.50	33.44
	P8/NLEG29	01/09	04/09	83.899	25.411	83.857	24.999	4,002	−1.47	33.53
	NLEG30	04/09	04/09	84.178	22.090	84.176	22.140	4,013	−1.57	33.57
	NLEG31	04/09	05/09	84.496	17.916	84.504	17.983	4,014	−1.60	33.02
Gakkel Ridge	NLEG32	05/09	05/09	84.824	12.337	84.828	12.351	3,713	−1.66	32.06
	P9/NLEG33	06/09	08/09	85.371	7.455	85.392	7.460	3,573	−1.59	31.33
	NLEG34	09/09	09/09	85.747	−2.544	85.749	−2.637	4,166	−1.61	29.99
Amundsen Basin	NLEG35	10/09	10/09	86.005	−10.692	85.999	−10.750	4,172	−1.61	30.06
	P10/NLEG36	11/09	14/09	86.505	−16.708	86.497	−16.692	4,235	−1.63	30.35
	NLEG37	14/09	14/09	87.004	−21.525	87.004	−21.395	4,285	−1.61	29.86
	P11/NLEG38	15/09	18/09	87.501	−17.372	87.497	−17.252	4,290	−1.61	30.00
	NLEG39	19/09	19/09	86.610	−11.015	86.611	−10.981	4,246	−1.65	30.62

[a]Average conservative temperature and absolute salinity for uppermost 15–20 m of water column.

for all parameters was low ($n = 5$), allowing only for limited statistical analysis of selected parameters; rather, the strength lies in the holistic presentation from sea ice through the water column to the seafloor, and from physics and chemistry to biology, including stock estimates, taxon composition, and rate measurements.

2.2. Environmental properties of the sea-ice, water column, and benthic environments

2.2.1. Sea-ice conditions and properties

2.2.1.1. Regional-scale sea-ice conditions and origin of sea ice at the ice stations (P8–P11)

Regional-scale sea-ice conditions for the study area (Steer and Divine, 2023) were derived from daily Advanced Microwave Scanning Radiometer for EOS (AMSR-E) and Advanced Microwave Scanning Radiometer 2 (AMSR2) satellite-based passive microwave gridded sea-ice concentrations (Spreen et al., 2008; available at https://seaice.uni-bremen.de/sea-ice-concentration/amsre-amsr2/information/). We also carried out bridge-based observations of local sea-ice conditions along the cruise route following the ASSIST Ice Watch protocol (see cruise report for details and https://icewatch.met.no/cruises/129 for the data).

To understand the origin of sea ice at the sea-ice stations (**Figure 2b**), Lagrangian back-trajectories were calculated from daily gridded sea-ice drift (OSI SAF, 2010; 2022a; Lavergne and Down, 2023) and concentration data (OSI SAF, 2022b; 2022c). More details on the data and methods used as well as the associated uncertainties and limitations of the product are found in Down et al. (2023). The derived back-trajectories in combination with physical properties of sea ice from ice cores (see Section 2.2.1.2) and visual assessment of sea-ice surface topography in situ were used to infer the most likely age of the sampled ice floes (Figure S2).

In order to assess the representativeness of the sea-ice stations on a regional scale, we conducted sea-ice thickness surveys using a helicopter-towed electromagnetic instrument (EM-bird, details and principles of operation and data acquisition in Haas et al., 2009) in three areas: at P8, between NLEG35 and P10, and at NLEG40.5 (opportunistic point at 8.23°E and 83.85°N, not discussed in the following as no sampling was conducted at this station). The flights covered a total distance of 845 km.

2.2.1.2. In situ work: Sea-ice coring, ice floe-scale sea-ice, and snow thickness surveys

At each ice station, a set of ice cores was recovered for analysis of the physical, chemical, and biological properties of sea ice using an ice corer (Mark II coring system, Kovacs Enterprise, LLC; Table S1). All cores were collected from the same site on level ice in an area of about 10×10 m size. In particular, ice cores were retrieved for measurements of ice temperature and bulk salinity, bulk concentrations of nutrients (nitrate, NO_3^-; nitrite, NO_2^-; silicate, $Si(OH)_4$; phosphate, PO_4^{3-}; Section 2.2.3) and total dissolved inorganic carbon (DIC; Section 2.2.4), particulate organic carbon (POC) and nitrogen (PN; Section 2.3.1) and chlorophyll *a* (chl *a*; Section 2.3.2), diversity, abundance and productivity estimates of microbial communities (Sections 2.3.3 and 2.3.4) and diversity and abundance of sea-ice meiofauna (Section 2.4.1) as well as isotopic compositions of ice-associated particulate organic matter (iPOM; Section 2.4.4). Table S2 provides an overview of parameters sampled from the same pooled ice cores and which ice sections were used for the respective analysis. All ice sections of biological cores were melted onboard in the dark at 4°C with 100 mL filtered seawater (<0.22 μm) added per centimeter of ice to reduce potential negative impacts due to osmotic stress. Core sections for nutrient and DIC analyses were melted without the addition of seawater. All values are presented per volume melted sea ice after correcting for dilution with filtered seawater.

Sea-ice temperature profiles were obtained from one ice core within a few minutes after core extraction. The measurements were made using a thermistor probe (Testo-720) in holes drilled at 5 cm spacing. Onboard the ship, bulk salinity of melted ice core sections was measured using a conductivity meter (Cond3110 SET3). Salinity is reported on the practical salinity scale (dimensionless).

To put the local sea-ice properties inferred from ice cores in a floe-scale context, variability in sea-ice thickness and snow depth at a floe-scale was obtained from ski-bound transects across sea-ice station floes using a GEM-2 (Geophex Ltd) electromagnetic sensor and a Magnaprobe (SnowHydro LLC) snow probe (Table S3; see Itkin et al., 2023, for details on the method). The transect lengths varied between ice stations from a few hundred meters to a few kilometers, dictated by sea-ice conditions and visibility, but were designed to be representative of the ice conditions at the sea-ice stations.

2.2.2. Water-column sampling

Water-column hydrography was investigated using vertical profiles of temperature and salinity obtained with a conductivity-temperature-depth sensor (CTD; SBE 911plus, Sea-bird Scientific; Fransson, 2022) mounted on a rosette equipped with 24 Niskin bottles (10 L each) used for seawater sampling (see below). Pressure, temperature, and practical salinity data from the CTD are accurate to ± 0.5 dbar, $\pm 10^{-3}$°C, and $\pm 3 \times 10^{-3}$, respectively. CTD data were processed using the standard SBE Data Processing software. Data points shallower than 15 m were removed due to biases resulting from deploying the CTD through the ship's moonpool. We present the hydrographic data in this study as conservative temperature (in °C) and absolute salinity (in g kg^{-1}) using the TEOS-10 equation of state (McDougall and Barker, 2011). For the Eurasian Basin, conservative temperature values are roughly the same as potential temperature, and absolute salinity around 0.15 higher than practical salinity.

We define AW as water with a temperature >0°C, a density anomaly with respect to the surface (σ_0) >27.7 kg m^{-3}, and a density anomaly with respect to 500 m ($\sigma_{0.5}$) <30.444 kg m^{-3} following Rudels et al. (2005). The Upper Polar Deep Water just below has the same density limits, but is colder than 0°C. Any water below/denser than these two water masses is defined as Deep Water for the purpose

of this work (Rudels et al., 2005). The Surface Mixed Layer is defined as the depth where σ_0 (z) – σ_0 (15 m) > 0.125 kg m^{-3} (following Monterey and Levitus, 1997). The Cold Halocline Layer in the Amundsen Basin is defined as the layer below the Surface Mixed Layer with a base depth defined as the depth where the density ratio R = 0.05, that is, where the vertical temperature gradient starts to be significant with respect to the salinity gradient (Bourgain and Gascard, 2011). Turbulence measurements were collected using free-fall MSS-90 microstructure profiles (see more detail in Text S1; Koenig et al., 2023a).

Water samples were collected at discrete depths (Table S4) from Niskin bottles on the CTD rosette for salinity calibration, analysis of inorganic nutrients (Section 2.2.3), DIC (Section 2.2.4), colored (or chromophoric) dissolved organic matter (CDOM) and fluorescent DOM (FDOM; Section 2.2.5), POC and PN (Section 2.3.1), chl *a* (Section 2.3.2), microbial community properties (Sections 2.3.3 and 2.3.4), and isotopic compositions of pelagic POM (pPOM; Section 2.4.4). Water samples from shallower depths (<10 m) were collected either through an ice hole or over the side of the ship using a Niskin bottle or a bucket attached to a rope.

2.2.3. Inorganic nutrients in sea ice and seawater

Ice cores for nutrients collected at all ice stations were sliced into 10–15 cm sections from the sea-ice top to the ice-water interface (Table S2). Each section was put into a bag (same as for inorganic carbon; Section 2.2.4) and placed in a dark and cool place (10–15°C) for sea-ice melting.

Melted ice and seawater samples (Table S4) for the determination of [NO_3^-], [NO_2^-], [$Si(OH)_4$], and [PO_4^{3-}] were filled into 20 mL pre-rinsed plastic HDPE vials and preserved with 250 µL chloroform and stored in the dark at 4°C (Gundersen et al., 2022). Post-cruise analysis was performed using a spectrophotometric method on an automated analyzer (Skalar F, Analytical B.V., The Netherlands) following standard procedures (Grasshoff et al., 2009; Gundersen et al., 2022) at the Institute of Marine Research (IMR), Bergen, Norway. The analyzer was calibrated by routine measurements of reference seawater obtained from Ocean Scientific International Ltd., UK, and was also used in regional and global intercalibration studies, such as QUASIMEME (http://www.quasimeme.org) and IOCCP. Moreover, comparisons between unfiltered frozen samples and samples with chloroform additions stored at 4°C with post cruise analysis showed no difference than between fresh samples analyzed immediately (Dore et al., 1996; Gundersen et al., 2022). Detection limits were 0.5 µmol kg^{-1} for [NO_3^-], 0.06 µmol kg^{-1} for [PO_4^{3-}], and 0.7 µmol kg^{-1} for [$Si(OH)_4$], respectively. NO_2^- concentrations were below detection limit at <0.06 µmol kg^{-1}; here [NO_3^-] refers to the sum of [NO_3^-] and [NO_2^-]. The analytical precision was <0.2% for [NO_3^-] and [$Si(OH)_4$] and <1% for [PO_4^{3-}], and the accuracy was <1% for [NO_3^-] and [$Si(OH)_4$] and <2% for [PO_4^{3-}] (Gundersen et al., 2022). Nutrient fluxes were derived from the nutrient-water sampling and the MSS-derived eddy diffusivity (see more detail in Text S1). The complete dataset for nutrients in sea ice and seawater can be found in Fransson et al. (2025b) and Chierici et al. (2025), respectively.

2.2.4. Dissolved inorganic carbon (DIC) in sea ice and seawater

Ice cores were sectioned and melted in 10–15 cm sections (Table S2); each section was put into a gas-tight bag, air was removed, and bags were placed in a dark and cool place (10–15°C) for sea-ice melting. Each melted sample was transferred to a 250 mL borosilicate bottle and analyzed following the same procedure as for the seawater samples. Seawater samples were collected at all P and NLEG stations (Table S4) in 250 mL borosilicate bottles following standard sampling protocols (Dickson et al., 2007). Bulk sea-ice samples and seawater samples were stored dark at 4°C and analyzed onboard within 5–24 h. DIC was determined by coulometric titration (Johnson et al., 1985) using a Versatile Instrument for the determination of total inorganic carbon (VINDTA 3D, Marianda, Germany). The precision and accuracy were ±2 µmol kg^{-1} for DIC, based on replicates of Certified Reference Material supplied by A. Dickson (San Diego, USA). A correction factor to the measured values was applied based on the ratio between the certified value and the measured reference values. The complete dataset for DIC in sea ice and seawater can be found in Fransson et al. (2025a) and Chierici and Fransson (2025), respectively.

2.2.5. Colored dissolved organic matter (CDOM) and fluorescent dissolved organic matter (FDOM) in seawater

Seawater samples for CDOM and FDOM were collected only at stations P10, P11, and NLEG37 (upper approximate 100 m and a few deeper samples) directly from the Niskin bottles by gravity filtration through a 0.22 µm cartridge filter (Opticap XL4 Durapore) and stored refrigerated at 4°C in the dark in pre-combusted amber glass vials until measurement. CDOM absorbance was measured using a double-beam PerkinElmer LAMBDA 650 spectrophotometer in the spectral range of 240–700 nm, using a 10 cm quartz cuvette, and reported here as an absorption coefficient (m^{-1}) at 350 nm. FDOM was measured as fluorescence excitation-emission matrices (EEMs) of the samples collected with a HORIBA Aqualog spectrofluorometer with a 1 cm quartz cuvette (for details see Zabłocka et al., 2020). Fluorescence intensity was measured and reported in Raman units (RU). Here, the EEMs were analyzed to extract the intensity of typical fluorescence peaks, representing different types of DOM as defined by Coble (see table 2 in Coble, 1996), including peak A (humic-like), peak C (humic-like), and peak M (marine humic-like). The intensity calculations for these peaks were performed by averaging the values within an approximate 21 nm range, centered on the excitation and emission wavelengths of these peaks. Analyses took place at the Institute of Oceanology, Polish Academy of Sciences (IO PAN), Sopot, Poland.

2.2.6. Seafloor sediment properties: Grain size, total organic/inorganic carbon (TOC/TIC), total nitrogen (TN), and bulk stable isotopes of sediment particulate organic matter (sPOM)

At each P station, short sediment cores (55 mm diameter; three replicates) were subsampled from replicate deployments of a large box corer (50 × 50 cm, 0.25 m^2 surface area) for sediment property analyses. All short sediment cores were sectioned onboard into 1 cm slices (0–6 cm) and immediately stored at −20°C for further analysis onshore.

Prior to grain-size and bulk organic geochemical analyses of sediment, all samples were lyophilized. Grain size distributions, performed on non-acidified samples, were determined using a Beckman Coulter LS 13320 Particle Size Analyzer at the Department of Geoscience at UiT. Organic matter was removed with 10% H_2O_2 and deflocculated with a 5% Calgon solution (sodium hexametaphosphate and sodium carbonate) prior to analysis. The abundance of particles within the range of 0.04–2,000 μm were classified with this method: clay, <4 μm; silt, 4–63 μm; sand, 63–2,000 μm. Three replicate measurements were performed per sample, of which the average values were used.

Approximately 1 g of homogenized, freeze-dried sediment from each core interval was ground for total organic and inorganic carbon (TOC/TIC), total nitrogen (TN), their stable carbon ($\delta^{13}C$) and nitrogen ($\delta^{15}N$) isotopic compositions as well as TOC:TN ratios. Pulverized sediment samples were analyzed via elemental analyzer isotope ratio mass spectrometry at Iso-Analytical Laboratories in Crewe, UK. Prior to TOC and $\delta^{13}C$ analyses, inorganic carbon was removed from the sediments by acid treatment (1 M HCl). Elemental composition was reported in dry weight percent (dw %). The resulting isotope data were reported in delta notation: $\delta X\,(‰) = [(R_{sample} - R_{standard}) / R_{standard}] \times 1{,}000$, where R is the ratio of heavy:light isotopes of the element X in our sample relative to the reference standards Vienna PeeDee Belemnite (VPDB, carbon; Craig, 1957) and atmospheric air (nitrogen; Mariotti, 1983). Approximately 20% of the samples were analyzed in duplicate, of which the mean values were used. The complete dataset can be found in Hess et al. (2024).

Sedimentation rates were estimated from carbon-dating fish otoliths found in the upper 2 cm at station P9 at the National Laboratory for Age Determination at the Norwegian University of Science and Technology, Trondheim, Norway. Constant sedimentation rates were assumed since the otoliths were deposited.

2.3. Microbial communities

2.3.1. Particulate organic carbon (POC) and nitrogen (PN) in sea ice and seawater

Ice cores were sampled at the four ice-covered stations and sectioned as listed in Table S2. For seawater (Table S4), duplicate (about 20% of samples) or triplicate subsamples (about 80% of samples; 1,000–2,850 mL filtered each) were filtered onto pre-combusted Whatman GF/F filters; the limited volume of melted sea-ice sample allowed for only one but occasionally duplicate (about 15% of samples) or triplicate subsamples (about 10% of samples; 290–2,350 mL each). Filters were stored at −20°C and analyzed within one year on a CE 440 Exeter analytical CHN analyzer at the Department of Arctic and Marine Biology at UiT The Arctic University of Norway, Tromsø, according to the procedures described by Reigstad et al. (2008). POC and PN concentrations are published in Marquardt et al. (2022).

2.3.2. Chlorophyll (chl) *a* measurements

Ice cores sampled at the ice-covered stations were sliced inside a tent to avoid exposure to direct sunlight. For the lowermost 30 cm of the cores, the matching sections of five ice cores were pooled to have sufficient volume for analysis (Table S2). Typically, between 0.25 L and 0.5 L of melted sea-ice water was filtered through 25 mm Whatman GF/F filters under low vacuum pressure (approximately 30 kPa). For water column chl *a,* subsamples were collected at discrete depths from the Niskin bottles at all P stations and at some NLEG stations (Table S4). At the ice-covered stations P8–P11, seawater was also collected through a hole in the ice (Table S4). Water was stored dark and cold in plastic bottles until further processing within 1 h. A single sample was taken at each depth and between 0.15 L and 0.5 L of seawater was filtered through GF/F filters. Chl *a* in sediments was subsampled from box corers with 4.7 cm (inner diameter) cores and cut into 1 cm sections (to 6 cm sediment depth, targeting $n = 3$ per site and section), wrapped in aluminium foil and frozen at −20°C. Chl *a* samples were extracted overnight in 5 mL of methanol at 4°C. Acid-corrected chl *a* concentrations were measured in the dark according to Holm-Hansen and Riemann (1978) with a Turner Trilogy fluorometer. Complete sea-ice and seawater chl *a* datasets can be found in Vader and Marquardt (2022), while sediment chl *a* data can be found in Akvaplan-niva (2023).

The CTD was equipped with an additional factory-calibrated sensor for chl *a* fluorescence (WET Labs ECO fluorometer). The in situ fluorescence chl *a* fluorometer measurements ($[chl]_{con}$) were corrected using laboratory measurements of chl *a* concentrations ($[chl]_{meas}$) from filtered water samples (see above; Vader and Marquardt, 2022), which were used to calculate a relationship with in situ fluorescence: $[chl]_{con} = 0.797 \cdot [chl]_{meas}^2 + 0.22833[chl]_{meas} + 0.010286$ ($R^2 = 0.94$, $n = 42$; Figure S3). This relationship was valid for measured chl *a* concentrations of less than 1 mg m^{-3}, a requirement met at all stations but P7 where chl *a* concentrations exceeded 1 mg m^{-3}. We did not correct the in situ chl *a* fluorometer measurements at station P7. For global ocean datasets, fluorometers have been found to overestimate chl *a* concentrations by around 100%, with large residual spread in the data (Roesler et al., 2017). Other factors, such as growth phase, nutrient limitation, grazing, photoacclimation, and non-photochemical quenching may also affect the in situ fluorescence, which may therefore be interpreted as a high-resolution interpolation of the discrete chl *a* concentrations, with some additional sources of error introduced through the calibration relationship.

2.3.3. Abundances of viral particles, bacteria, pico- and nanoalgae, and heterotrophic nanoflagellates (HNF) in sea ice and water column

Sea-ice samples were collected and sectioned as listed in Table S2. Seawater was collected at discrete depths at all stations (**Tables 1** and S4). Samples for flow cytometric abundance analysis were prepared in triplicate by fixing 1.8 mL of sample water (seawater or melted sea-ice sample) with 36 µL 25% glutaraldehyde (0.5% final concentration) at 4°C in the dark for a minimum of 2 h. Samples were then flash-frozen in liquid nitrogen and stored at –80°C until further processing was done at the Department of Biological Sciences at the University of Bergen, Norway.

Abundances of viral particles and bacteria were determined using a FACS Calibur (Becton Dickinson, San Jose, California, USA) flow cytometer. Frozen samples were thawed, diluted 10 times with 0.2-µm-filtered TE buffer (Tris 10 mM and EDTA 1 mM, pH 8), stained with SYBR Green I (Invitrogen, Eugene, Oregon, USA) and incubated at 80°C in a water bath for 10 min (Marie et al., 1999). The stained samples were counted at a low flow rate of around 60 µL min^{-1}, and different groups were discriminated on biparametric plots of green fluorescence versus side scatter. Viral particles were separated into three common subgroups: low fluorescence, medium fluorescence, and high fluorescence viral particles. In addition to total bacterial abundance, we quantified three different groups of bacteria (Lebaron et al., 2002; Hammes and Egli, 2010): low and high nucleic acid content bacteria and "very large" high nucleic acid bacteria having an unusually high fluorescence signal.

The abundances of pico- (approximately 0.2–2 µm) and nano-sized algae (approximately 2–20 µm) and heterotrophic nanoflagellates (HNF) were determined using an Attune® NxT Acoustic Focusing Cytometer (Invitrogen by Thermo Fisher Scientific) with a syringe-based fluidic system and a 20 mW 488 nm (blue) laser. Autotrophic pico- and nanoplankton were counted after thawing the sample, and the various groups of protists were discriminated based on their red fluorescence versus orange fluorescence, red fluorescence versus side scatter, and orange fluorescence versus side scatter (Paulsen et al., 2016). For HNF analysis, samples were stained with SYBR Green I (Invitrogen, Eugene, Oregon, USA) for 2 h in the dark, and subsequently 1–2 mL was measured at a flow rate of 500 µL min^{-1} following the protocol of Zubkov et al. (2007). Abundances of viral particles, bacteria, and small protists (pico- and nanoalgae, HNF) in the water column, as well as abundances of the latter two in sea ice, are reported in Bratbak et al. (2023).

2.3.3.1. Bacterial production (BP) estimates

BP was estimated based on incorporation of ^{3}H-leucine according to Smith and Azam (1992) in depth horizons in ice cores listed in Table S2 and water depths listed in Table S4. Three replicates of 1.5 mL seawater samples were incubated with 25 nM ^{3}H-leucine (final concentration) for 2 h at in situ temperature (0–1°C) in 2 mL Eppendorf vials. The incubations were stopped by adding 80 µL of 100% trichloroacetic acid (TCA). A fourth replicate served as control and was stopped immediately with TCA as above. The samples were centrifuged before the supernatant was removed and the pellet washed with 1.5 mL 5% TCA. This procedure was repeated twice before 1 mL of scintillation cocktail (Ultima Gold XR, PerkinElmer, Massachusetts, USA) was added and the radioactivity counted in a PerkinElmer Liquid Scintillation Analyzer Tri-Carb 2800TR. Leucine incorporation was estimated and converted to µg C incorporated L^{-1} d^{-1} using the specific activity of the isotope and the conversion factor 1,545 g C mol^{-1} leucine incorporated according to Simon and Azam (1989), assuming no isotope dilution (Kirchman et al., 2009). BP datasets for sea ice and water column can be found in Müller et al. (2023b).

BP in ice samples was estimated using ice melted in 0.22 µm filtered seawater as described above. The samples were incubated at approximately 1°C, and the dilution was accounted for in the final production estimates. These estimates should thus be considered relative, and care should be exercised when comparing to bacterial production estimates in seawater.

2.3.4. Protist communities in sea ice and water column (nano- and microplankton)

For the microscopic analysis of sea-ice protists, ice cores and sections listed in Table S2 were used. A volume of 90 mL of melted sea ice was transferred into a 100 mL brown glass bottle and fixed with 0.4 mL of 25% glutaraldehyde and 10 mL of 20% hexamethylenetetramine-buffered formalin solutions to yield final concentrations of 0.1% and 2%, respectively. For the analysis of pelagic protists, 190 mL of seawater from four to five discrete depths (Table S4) in the upper 90 m of the water column, including the subsurface chl *a* maximum, was filled into 200 mL brown glass bottles. Samples were fixed with 0.8 mL of 25% glutaraldehyde and 10 mL of 20% hexamethylenetetramine-buffered formalin solutions to yield final concentrations of 0.1% and 1%, respectively. All samples were stored cool (about 15°C) and dark until further processing at IO PAN.

Identification and quantification of protists were carried out with a Nikon Eclipse TE300 inverted light microscope equipped with phase and differential interference contrasts and objectives 10–60× (resulting in 100–600× magnification) following the Utermöhl method (Utermöhl, 1958; modified by Edler et al., 2010). Organisms were identified to the lowest possible taxonomic level according to the World Register of Marine Species and grouped as diatoms, dinoflagellates, (other) flagellates or ciliates. The category "flagellates" includes unidentified flagellated forms in different size classes and flagellates of known systematic affiliation such as chrysophytes and green algae (like *Pyramimonas* sp. or *Chlamydomonas* sp.). Further details on the method can be found in Kohlbach et al. (2023) and Marquardt et al. (2023b). Taxonomic data of sea-ice protists can be found in Assmy et al. (2022b), and pelagic protist data can be found in Assmy et al. (2022a).

Live imagery onboard the ship was carried out on the same ice sections, net hauls (10 µm mesh) and samples

concentrated (5 L to 20 mL) by tangential flow (Vivaflow 200, 0.2 µm, Sartorius Stedim Lab LTD) using a Leica DM 1000 LED microscope fitted with a Leica EC3, 3 pcs. camera. Samples for scanning electron microscopy (SEM) were preserved in 1.5x PHEM buffer at pH 7.8 with final concentrations of (freshly prepared) 0.4% glutaraldehyde and 2% formalin (Montanaro et al., 2016). The samples were rinsed in PHEM buffer, dehydrated in an ethanol series (30–100%), critical-point dried (BAL-TEC CPD 030, UK), mounted on stubs and sputter-coated (Cressington 308r coating system, UK) with platinum. The stubs were examined in a Hitachi S-4800 SEM at the Electron Microscopy Laboratory, Institute for Biosciences, University of Oslo, Norway.

2.3.4.1. Net primary production (NPP) rates

The primary production rates of sea-ice algae and phytoplankton were determined using in situ ^{14}C uptake incubations. Discrete water samples (Table S4) were collected from the upper 90 m of the water column. From each depth, 250 mL were transferred to one light and one dark acid-washed polystyrene bottle each, and $NaH^{14}CO_3$ was added to each bottle at a final activity of about 0.1 mCi mL^{-1}. After spiking, two 250 µL subsamples were taken from each incubation bottle and fixed with 250 µL pure ethanolamine for later determination of the total concentration of added carbon. For sea-ice algae, the bottom 3 cm of two sea-ice cores (Table S2) were crushed, pooled, and mixed with filtered surface seawater to simulate conditions at the ice-water interface and allow for tracer access to the sea-ice algae. The mixture was filled into 250 mL bottles and treated similarly to the water column samples (ratio of ice volume to seawater volume: 0.15).

The in situ incubation bottles were deployed for 23–28 h at the original sampling depths from directly under the sea ice (for ice samples) to a maximum depth of 90 m using an ice-attached mooring rig. After retrieval, the contents of the bottles were filtered onto 25 mm Whatman GF/F filters in the dark; for sea ice, the crushed ice pieces had melted over the course of the incubation. The filters were placed into 20 mL scintillation vials, and 750 µL concentrated HCl were added. The vials were incubated for 24 h, after which they were ventilated to remove all inorganic carbon. In the home laboratory (Department of Arctic and Marine Biology, UiT), 10 mL of scintillation cocktail (Ecolume) were added to each vial prior to the analysis of the samples in a Tri-Carb 2900TR liquid scintillation counter (PerkinElmer). Each sample was counted twice for 10 min, and an average of the two counts was taken. A normalization of NPP relative to irradiance was not possible because deployment of the CTD profiler through the ship's moonpool did not provide accurate irradiance profiles for the water column under the ice.

2.3.4.2. Vertical protist flux

To assess vertical flux of protists, short-term sediment traps (KC-Denmark) were deployed at the P stations. The sediment trap mooring contained four cylindrical collection cups attached at each of eight depths (Table S4). Prior to deployment, the cylinders were filled with pre-filtered deep water (500 m, filtered through a Sartorius filtration system) from the NLEG station preceding the P station to ensure that the water within the cylinders had a higher density than at the sampling depths. At the ice-free station P7, the trap was freely drifting, while at the ice-covered stations P8–P11 the mooring was attached to the edge of the ice floes. An additional set of under-ice sediment traps were deployed at P8–P11 through an ice hole, with two cups deployed at 1, 5, 10, and 20 m (with 1 m and 10 m shown) for approximately 23 h and 26 h. Upon retrieval, the cups at each depth from both traps were pooled into a canister and processed.

2.4. Faunal communities

Taxonomic names and systematic affinities used for all faunal communities are as currently accepted in the World Register of Marine Species.

2.4.1. Sea-ice meiofauna

Three replicate ice cores were cut into sections listed in Table S2. The melted ice core sections were carefully mixed before taking a 90 mL subsample for protist identification and quantification (Section 2.3.4). The entire remaining volume was measured and concentrated over a 20 µm sieve for meiofauna analysis. Sea-ice meiofauna were identified and counted alive onboard with Leica stereomicroscope (M80, 7.5–60× or M125, 7.8–160× magnification). Counted samples were fixed (two cores by adding 37% formalin for a final concentration of 2%, one additional core by addition of 96% ethanol for a 90–95% final concentration) and stored for further analysis in the laboratory at UiT, Tromsø, Norway. More detailed descriptions of sampling, sample processing, and identification are published in Marquardt et al. (2023b). Sea-ice meiofauna counts, abundance, and biomass are published in Marquardt et al. (2023a).

2.4.2. Pelagic meso- and macrozooplankton and fish

Mesozooplankton were sampled with stratified vertical net hauls using MultiNet Mammoth (Hydro-Bios, nine nets, opening of 1.0 m^2, net length of 550 cm) and MultiNet Midi (Hydro-Bios, five nets, opening of 0.25 m^2, net length of 250 cm; Table S5). The MultiNet Mammoth was equipped with a 180 µm mesh size, and the maximum operation depth was 3,000 m; therefore, it was used only at station P7 for community sampling. MultiNet Midi was used with both 180 µm and 64 µm meshes, performing one tow at the station with each mesh to cover all size groups, including small copepod taxa and copepod nauplii, which may be sampled inefficiently using nets with meshes that are coarse (e.g., 180 µm). At station P7, the Multinet Mammoth samples were taken with finer depth resolution than the Multinet Midi samples but the results were merged to match the layers sampled with the Multinet Midi. For the MultiNet Midi, the standard sampling depths were bottom–2,000 m, 2,000–600 m, 600–200 m, 200–50 m, and 50–0 m. The deepest sampling depth was 4,100–3,000 m at stations P10 and P11 depending on the water depth at the individual station (Table S5). Collected zooplankton samples were processed immediately upon

retrieval of the nets. Zooplankton collected using coarse and fine mesh gauze nets were concentrated on sieves with mesh sizes of 180 µm and 64 µm, respectively, gently flushed with filtered seawater before being transferred into 125 mL plastic bottles and preserved in a 4% solution of acid-free formalin in seawater.

The zooplankton organisms were identified and counted in the laboratory under a stereomicroscope equipped with an ocular micrometer according to standard procedures (Postel, 2000; Wold et al., 2023). Smaller-sized zooplankters (maximum dimension <5 mm, including most copepods and juvenile stages of pteropods, euphausiids, ostracods, amphipods, appendicularians, and chaetognaths) were identified and counted in subsamples obtained from the fixed sample volume by automatic pipette, with no fewer than 500 individuals from the sample always examined. Larger zooplankters (maximum dimension >5 mm, including large copepods, pteropods, euphausiids, ostracods, amphipods, decapods, appendicularians, chaetognaths, and fish larvae) were sorted and identified from the entire sample. Representatives of *Calanus* spp. were identified at the species level based on morphology and prosome lengths of individual copepodid stages (Kwasniewski et al., 2003). The samples from 64 µm and 180 µm nets were analyzed separately and the results were later merged by selecting the small taxa and stages from the 64 µm net and the larger taxa and stages from the 180 µm net. A list of species and stages selected from the two mesh sizes is provided in Wold et al. (2023).

Macrozooplankton was collected using a Midwater Ring Net (MIK net) with 3.14 m^2 opening, of approximate 13 m length, with a 1,600 µm mesh size except for the last 1 m having 500 µm. The MIK net was hauled vertically from 1,000 m to the surface, with a hauling speed of about 1.5 m s^{-1}. The gelatinous zooplankton captured by the MIK net (here cnidarians and ctenophores) were gently removed using filtering spoons or wide-mouthed pipettes, counted, and identified to the lowest taxonomic level possible. Finally, subsamples of the MIK catch were stored in hexamine-buffered 4% formalin for detailed taxonomic analyses at the IMR laboratory. In the laboratory, the zooplankton kept in formalin were sorted and identified to the lowest possible taxonomic level.

Additionally, two pelagic trawls were used to catch macrozooplankton and fish: a Harstad 320 trawl (Godø et al., 1993) and a macrozooplankton 92 m trawl. The Harstad trawl (opening area of approximately 250 m^2) is graded from 200 mm mesh in the front of the trawl to 60 mm before the cod-end. The cod-end has an 8-mm mesh net. The trawl was used with modified rigging which included wire instead of spectra sweeps (both 60 m long), reducing the total buoyancy of the trawl net (from 1,047 kg to 50 kg), and applying 150 kg weights in front of each lower wing and a 40 kg weight at the end of the cod-end. The macrozooplankton 92 m trawl (trawl opening area of approximately 36 m^2; Krafft et al., 2010; Klevjer et al., 2020) was used with ordinary rigging, except that a 40 kg weight was added at the back part of the cod-end. The macrozooplankton trawl is a non-graded trawl with an 8 mm mesh opening (EN ISO 1107:2003) from the front of the trawl to the cod-end. Trawling was conducted in leads with very thin new ice. Fishing depth was determined by acoustic registrations on the EK80. With weak acoustic registrations, one trawl was set at approximately 50 m, and another one in the mesopelagic depth layer of 300–450 m. Details on the trawling operations can be found in Ingvaldsen et al. (2023). Trawl catches were sorted immediately, and organisms were identified to species level when possible. Representative subsamples of 100 g were preserved in 4% hexamine-buffered formalin solution in 500 mL plastic bottles. The preserved samples were species-identified, when possible, at the IMR laboratory.

Stable isotope compositions ($\delta^{13}C$ and $\delta^{15}N$) of selected pelagic zooplankton taxa, including arthropods, ctenophores, cnidarians, chaetognaths, and molluscs collected by MIK nets and macrozooplankton trawls, were analyzed as described in Section 2.4.4. Loose fish otoliths were retrieved from box core samples by sieving the surface sediment (see Section 2.4.3.1). Fish species were identified from otoliths by L. Lindblom and L. Heggebakken at IMR, Tromsø, Norway. Age of the otoliths was determined by ^{14}C-dating at the National Laboratory for Age Determination at the Norwegian University of Science and Technology, Trondheim, Norway.

2.4.3. Benthic biota

2.4.3.1. Macrobenthos communities

Macrobenthos was sampled by taking short sediment cores (11.7 cm inner diameter, targeting $n = 4$ for community analysis) typically distributed over three box cores taken per site (P7–P11) after draining surface water. The core samples were first used for quantifying sediment oxygen demand (SOD; Section 2.4.3.2) and subsequently sieved over a 0.25 mm mesh to remove the sediment (approximately 20 cm thick layer). The remaining fauna was preserved in 10% buffered formalin seawater solution and later identified to the lowest taxonomic level possible at IO PAN. Meiofaunal taxa were identified to phylum (nematodes) or order (harpacticoid copepods). The data for P7 can be found in Jordà-Molina et al. (2024) and for P8–P11 in Bluhm et al. (2023).

2.4.3.2. Sediment oxygen demand (SOD)

SOD of the whole benthic community in sediment cores was determined as described in Sen et al. (2024). Briefly, sealed sediment cores were incubated in the dark after a 12 h acclimation period with air stones to ensure oxygen saturation. Calibrated oxygen spot sensors, affixed to the core lids, were used with a Fibox 4 optical sensor (PreSens Precision Sensing GmbH) to measure oxygen concentration every 6 h until about 30% of the oxygen was consumed (about 2 days). SOD was calculated based on the (negative) slope of the rate of oxygen consumption. Experiments were run at near-ambient bottom water temperature (on average 0.4–0.6°C given limitations and variations in the cold room with no intended difference among stations), with additional treatments mimicking an increase in future temperature and food availability. These treatments included: (i) 30 mg of added algae per core, run at ambient temperature; (ii) increased

temperature (ambient temperature plus 2°C); and (iii) the combined increase of temperature (ambient plus 2°C) and food availability (30 mg of added algae). Each incubation treatment was run in replicates of three or five depending on the number of successful box cores that could be retrieved.

2.4.4. Food-web structure based on isotopic compositions

POM was sampled from the sea ice (iPOM) and water column (pPOM) to characterize stable isotope and C:N ratios of these dominant carbon sources in the study area. The bottom 0–10 cm section (from ice-water interface) of three sea-ice cores was melted and subsamples of 500–1,600 mL filtered onto pre-combusted GF/F filters (targeting $n = 3$ per site) and frozen at –20°C. Seawater was sampled from the chl *a* maximum layer where present and from 20 m otherwise, and separate samples were taken from ice floes about 0.5 m below the sea-ice surface. Between 1,050 and 2,500 mL of water were filtered as above (targeting $n = 3$ per site). Benthic fauna was sampled from the surface sediment layer (0–5 cm) of box cores and sieved over 0.25 mm mesh. Due to the overall low density of macrofauna and small body size of individuals, fauna from replicate box cores per site were pooled. All samples were subsequently frozen at –20°C until further analysis. iPOM and pPOM samples were analyzed at the CLIPT stable isotope biogeochemistry laboratory at the University of Oslo, Norway (see Ziegler et al., 2023, for details on procedure and equipment). Faunal samples were prepared for stable isotope analysis as described in Ziegler et al. (2023). Approximately 0.5–2.0 mg of each sample was analyzed at the Alaska Stable Isotope Facility at the University of Alaska Fairbanks (see Ziegler et al., 2023, for details on procedure and equipment). The resulting data were reported in standard delta notation as described in Section 2.2.6 with precision of 0.04‰ ($\delta^{13}C$) and 0.12‰ ($\delta^{15}N$). Stable isotope data of sea ice, seawater, and invertebrates can be found in Ziegler et al. (2024a, 2024b, 2024c), respectively.

3. Results

3.1. Environmental properties of sea ice, water column, and the benthic environment

3.1.1. Sea-ice environment

3.1.1.1. Sea-ice cover, thickness, and ice types

The sea-ice cover in the study area during the cruise was consolidated with over 80% sea-ice concentration north of approximately 82°N (**Figure 2b**). Seasonal variations in sea-ice conditions at the ice stations (NLEG27, P8–P11) during 2020–2021 inferred from remote sensing data indicated perennial sea-ice cover at all ice stations but NLEG27 (Steer and Divine, 2023).

Surface freeze-up had occurred by the time of the cruise. New ice formation in leads and openings was observed, and melt-pond surfaces on all ice stations were already refrozen. Moreover, snowfall during the cruise led to a gradual snow accumulation on the sea ice and on refrozen melt ponds (Fransson et al., 2022). Snow thickness increased progressively northward along the cruise track, from a few centimeters at NLEG27 to up to 20 cm deep snow at P11. Table S3 provides specific details on ice conditions at the ice stations.

Station NLEG27, >100 km away from the ice edge, was in an area dominated by big, thick refrozen floes and very thin newly formed sea ice. Stations P8–P11 were set on big to vast floes, with a mixture of ice types (FYI, MYI, including thick, old ridged floes) at P8 and P9, while stations P10 and P11 featured significant areas of heavily deformed (ridged) ice, contributing up to 20–30% to total sea-ice area according to bridge-based ASSIST Ice Watch observations. Sea-ice back trajectory analysis (**Figure 2b**) together with regional ice-age distribution (Figure S2) suggested a common origin of the oldest ice in the area from the western Laptev Sea (**Figure 2b**), further indicating that (parts of) the ice floes sampled included ice that might have survived more than one summer season.

Comparison of in situ ice-thickness measurements with ice-thickness data from airborne surveys suggested that the ice floes at the sea-ice sampling stations were representative for the area (Table S3). The 320 km of airborne ice-thickness surveys around P8 indicated relatively thin ice (modal thickness of 0.9 m). The flight in the Amundsen Basin at 86°N between P9 and P10 also showed modal (1.6 m) and median (1.7 m) ice thicknesses similar to the values measured in situ at P9 and P10, the virtual absence of open water, and a maximum ice-thickness value of approximately 9.5 m. Both satellite imagery and on-site visual observations were consistent in showing few substantial leads in the P10 area, which was also reflected in the ice-thickness measurements.

3.1.1.2. Sea-ice temperature, salinity, DIC, and nutrient concentrations

Sea-ice temperatures varied throughout the core depths and between stations. At P8 and P9, the sea-ice temperatures decreased from the top of the ice to the ice-water interface (**Figure 3a**). At P10 and P11, the sea-ice temperature was lower at the top of the ice than at the ice-water interface. The top ice was warmest at P8 (–0.9°C) and coldest at P11 (–2.5°C). In contrast, bulk salinity (0 to 3.5) showed higher values in the bottom 10 cm of ice at the Amundsen Basin stations P10 and P11 compared to P8 and P9 (**Figure 3b**). Salinity at P8 showed a C-shaped profile that may indicate FYI at the coring site (e.g., Malmgren, 1927; Backstrom and Eicken, 2006). The bulk sea-ice DIC showed a similar pattern as salinity with large variability between the stations. At Amundsen Basin stations P10 and P11, the highest DIC (approaching 250 μmol kg^{-1}) was observed at the bottom 10 cm (**Figure 3c**). This increase toward the bottom was also observed at the same stations for $[Si(OH)_4]$, except at P8 where the lowest $[Si(OH)_4]$ was found at mid-depth (**Figure 3e**). $[NO_3^-]$, $[Si(OH)_4]$, and $[PO_4^{3-}]$ showed generally large variability between the stations (**Figure 3d**–**3f**). At P9, NO_3^- concentrations were relatively similar throughout the core, whereas at P10, the highest $[NO_3^-]$ was found at mid-depth and at P11 in the top section of the ice core

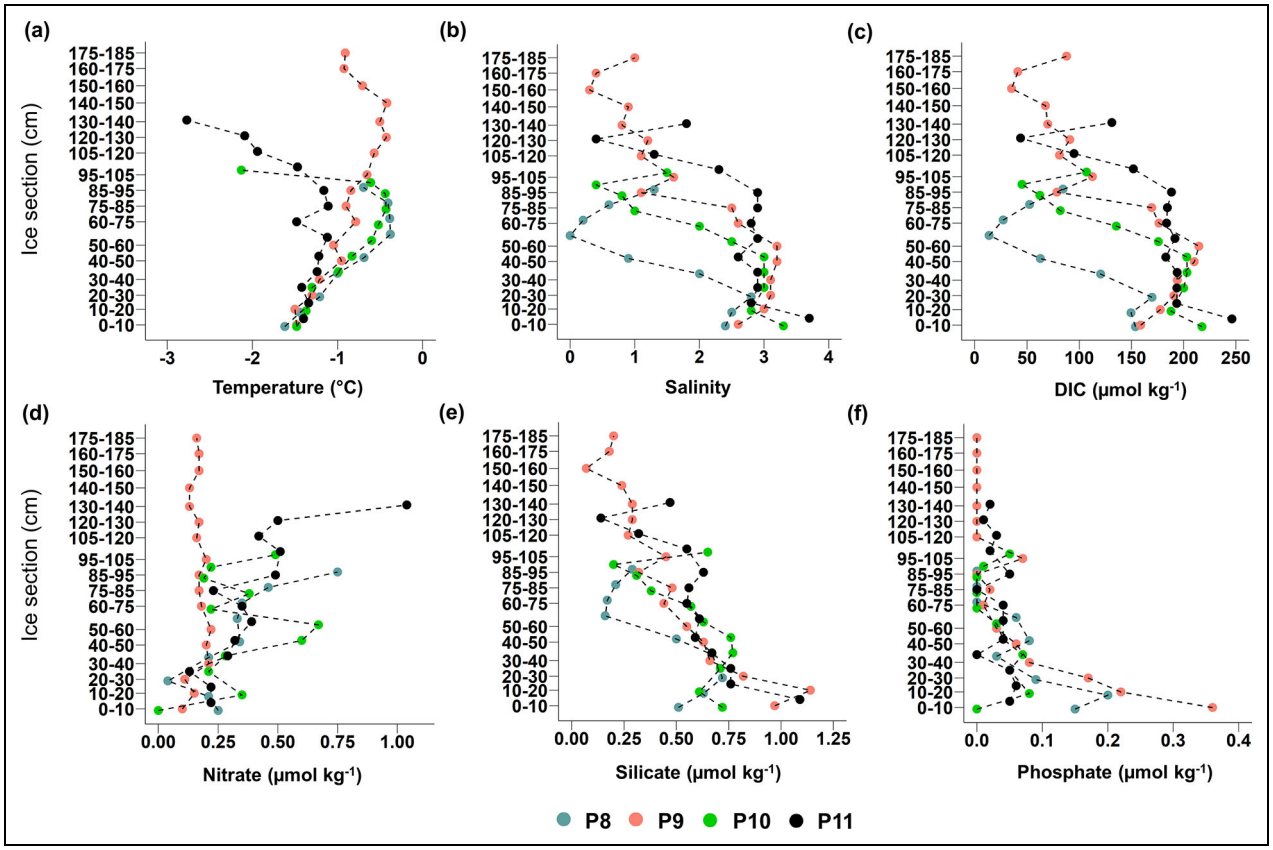

Figure 3. Vertical depth profiles of physico-chemical properties in sea ice. (a) Temperature (°C), (b) bulk salinity, (c) bulk dissolved inorganic carbon (DIC, µmol kg^{-1}), (d) nitrate (µmol kg^{-1}), (e) silicate (µmol kg^{-1}), and (f) phosphate (µmol kg^{-1}) for different sections of the sea ice (cm) collected at (color-coded) stations P8–P11. The 0–10 cm ice section indicates the ice-water interface. Lengths of the entire ice cores varied by station: 98 cm at P8, 184 cm at P9, 109 cm at P10, and 141 cm at P11. Ice section lengths varied between approximately 10 cm and 15 cm. Values in panels (d–f) are also bulk values. Sea-ice DIC data can be found in Fransson et al. (2025a) and nutrient data are published in Fransson et al. (2025b). Figure prepared in Software R (v4.1.0; R Core Team, 2021), using the ggplot2 package (Wickham, 2016).

(**Figure 3d**). [PO_4^{3-}] showed the lowest values in the top at P9 and the bottom at P10, while the highest values were found at the bottom of the ice at P9 (**Figure 3f**).

3.1.2. Water column properties

3.1.2.1. Seawater temperature and salinity

The sampled transect covered 15 CTD stations from the northern edge of the AW inflow at P7 to the AW recirculation along the Lomonosov Ridge at P11 (**Figure 4**). The upper AW boundary deepened from 60 m at P7 to 140–160 m in the Nansen Basin (P8 and P9) and to 170–180 m in the Amundsen Basin (P10 and P11), and its base was located at depths between 800 m and 900 m. The AW cooled northward across the Nansen and Amundsen basins from a mean temperature of 1.3°C at P7 to 1.0°C in the Nansen Basin at P8 and 0.6–0.7°C at P10 and P11. Its core broadened and deepened from 100–200 m depth at P7 with temperatures exceeding 2.0°C and 200–400 m depth at P8 with temperatures warmer than 1.5°C in the Nansen Basin to a core temperature just warmer than 1.0°C between 300–400 m and 200–450 m at P10 and P11, respectively, in the Amundsen Basin (**Figure 4a**).

Surface Mixed Layer salinity showed a strong decrease northward into the Amundsen Basin with a clearly discernible salinity front over the Gakkel Ridge (**Figure 4b**). The mean Surface Mixed Layer salinity in the Nansen Basin was 32.9 g kg^{-1} versus 30.3 g kg^{-1} in the Amundsen Basin. The Surface Mixed Layer was also deeper in the Amundsen Basin than in the Nansen Basin (30 m versus 20 m, respectively).

Upper ocean hydrography and stratification between the surface and AW layers showed clear differences between the basins. The southern Nansen Basin stations (P7 and NLEG26) were strongly affected by the shallow AW inflow core. There was a weak halocline above the AW core with highly variable temperatures well above the freezing point. In the northern Nansen Basin (P8), the upper water column showed signs of winter convection to 120 m depth, evidenced by an isohaline layer with a temperature close to the surface freezing point. Above this depth, our late summer profiles showed a weak warming and freshening. Below the fresh surface layer, stations in the Amundsen Basin had a Cold Halocline Layer with temperatures close to the freezing point and increasing salinity to a depth of 90–110 m.

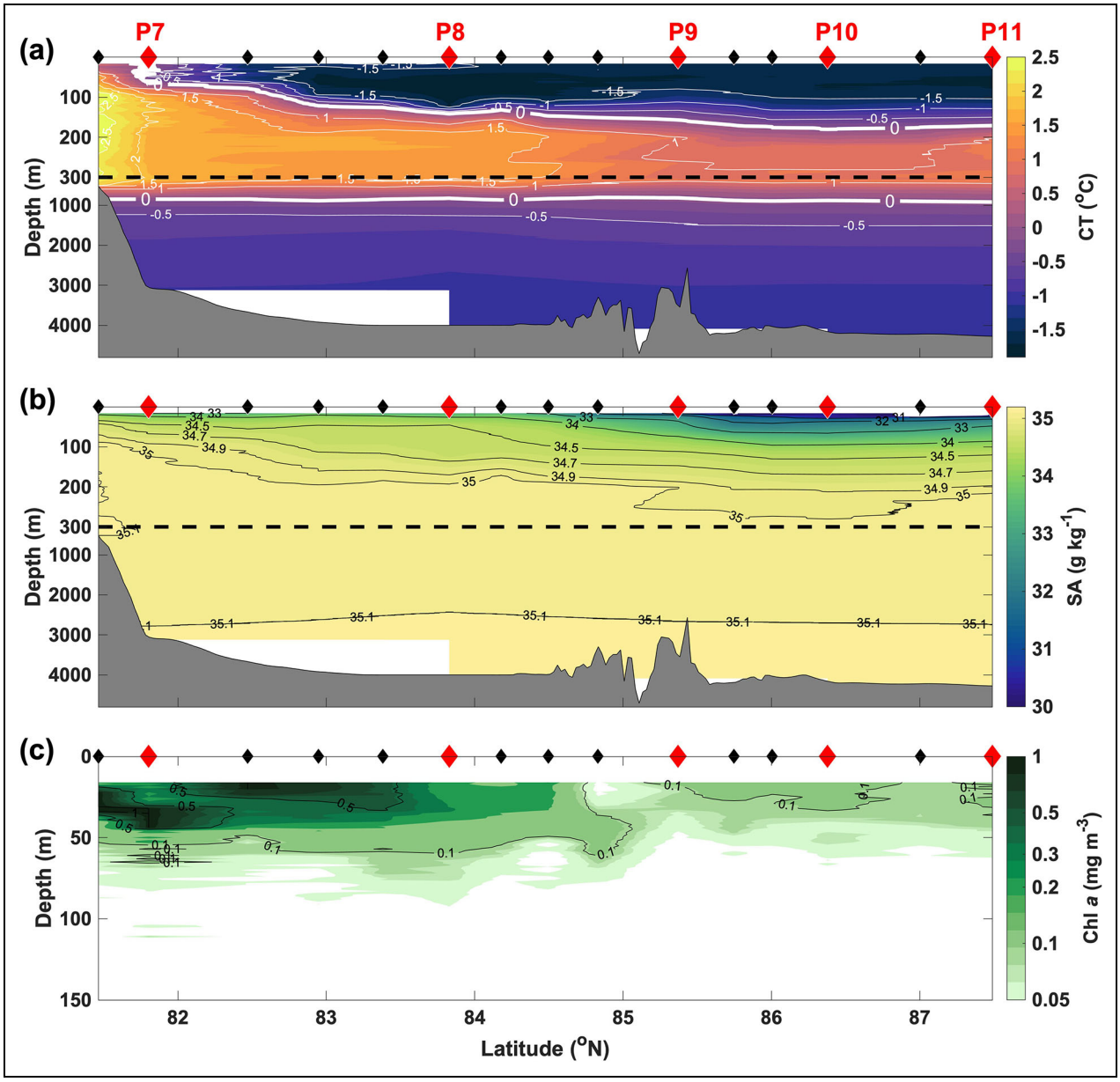

Figure 4. Distributions of water column physico-chemical properties along the JC2-2 transect. (a) Conservative temperature (CT, °C) with the 0°C isotherm in bold to highlight the Atlantic Water boundaries, (b) absolute salinity (SA, g kg^{-1}), and (c) chlorophyll *a* fluorescence (chl *a*, mg m^{-3}). In panels (a) and (b), depths below 300 m have been contracted by a factor of 10 to better represent the upper water column. In panel (c), chl *a* exceeded 1 mg m^{-3} at the southern end of the transect; values from bottle samples are given in the text (Section 3.2.2). Red diamonds indicate stations P7 to P11 (left to right; **Figure 2a**); black diamonds, NLEG stations where mostly CTD casts were taken (see **Table 1** for full list). CTD data can be found in Fransson (2022) and chl *a* data are published in Vader and Marquardt (2022). Figure created using MATLAB.

Below the AW layer, Upper Polar Deep Water was found to depths of 1,300 m in the Nansen Basin and 1,500 m in the Amundsen Basin with a mean temperature of –0.2 to –0.3°C, respectively, and a mean salinity of 35.05 g kg^{-1} (**Figure 4a** and **4b**). The bottom of both basins was filled with Deep Water with a mean temperature of –0.6 to –0.7°C and a mean salinity of 35.1 g kg^{-1}. Water mass properties below the AW layer were largely homogeneous with very weak stratification.

3.1.2.2. Seawater nutrient and DIC concentrations

The lowest NO_3^- concentrations, depleted or near depletion, were observed in the upper 20 m in both basins, whereas PO_4^{3-} concentrations were lower in the Nansen Basin than in the Amundsen Basin (**Figure 5a** and **5c**). The nutricline (largest vertical gradient in [NO_3^-]) was shallower in the Amundsen Basin than in the Nansen Basin (approximately 20 m versus 30 m depth). The nitrate concentration was higher deeper in the water column. Below 2,000 m, the highest nutrient concentrations were found in both basins, where the NO_3^- concentrations in the Nansen Basin generally were higher (approximately 15 µmol kg^{-1}) than in the Amundsen Basin (up to 14 µmol kg^{-1}). In the latter, high $Si(OH_4)$ concentrations were observed, up to >10 µmol kg^{-1}, in a layer of the upper 50–60 m (P10 and P11; **Figure 5b**). $Si(OH_4)$ concentrations below 2,000 m were

similar in both basins, with mean values of 11.4 ± 0.3 µmol kg^{-1} ($n = 8$ in Nansen Basin, $n = 5$ in Amundsen Basin; **Figure 5b**).

Nutrient ratios [$Si(OH_4)$]:[NO_3^-] and [$Si(OH_4)$]:[PO_4^{3-}] differed between basins, with higher values in the Amundsen Basin (average up to 3.8 and 14.0, respectively, including all stations; see **Table 1**) than in the Nansen Basin (average up to 1.2 and 7.5, respectively; Figure S4a and b). [NO_3^-]:[PO_4^{3-}] ratios showed an inverse pattern with substantially higher values in the Nansen Basin (average up to 8.8) than in the Amundsen Basin (average up to 4.9; Figure S4c).

At 100–200 m, DIC concentrations differed between the two basins, particularly evident in the elevated DIC (>2,170 µmol kg^{-1}) in the Amundsen Basin Cold Halocline Layer compared to lower DIC (2,150–2,160 µmol kg^{-1}) in the Nansen Basin in the same layer (**Figure 5d**). The lowest concentrations of DIC (<2,000 µmol kg^{-1}) were found in the upper 20 m, mainly in the Amundsen Basin (at stations P10 and P11). In the deeper layer at 1,000–2,000 m depth, higher DIC (>2,170 µmol kg^{-1}) was observed compared to below 2,000 m (2,160 µmol kg^{-1}), mostly evident in the Amundsen Basin.

As suggested by an NMDS ordination plot (**Figure 6a**), water column properties, including temperature, salinity, nutrients, and DIC of the uppermost 100 m, were clearly different at station P7 compared to the other stations, and also between stations in the ice-covered Nansen and Amundsen basins. This pattern was also detected for microbial abundances (**Figure 6b**), as discussed further in Section 3.2.

3.1.2.3. Turbulence and nutrient fluxes

We used basin-average profiles to highlight the differences in stratification and their consequences on vertical mixing between basins (turbulence; **Figure 7a** and **7b**). The fresher surface layer in the Amundsen Basin resulted in stronger stratification over the upper ocean than in the Nansen Basin. The upper ocean in the Nansen Basin was more susceptible to turbulence and vertical mixing than the Amundsen Basin as shown by the profiles of eddy diffusivity in **Figure 7f**. Turbulence was larger in the mixed layer, and then dropped significantly below 50 m depth. A local turbulence maximum at 70 m was found in the average profile of the Nansen Basin but was absent in the Amundsen Basin. Consequently, nitrate fluxes in the Nansen Basin were significantly larger than the fluxes in the Amundsen Basin (**Figure 7e** and **7f**). Averaged vertical turbulent fluxes of nitrate, however, were very low in both basins (about 0.2 10^{-2} µmol m^{-2} s^{-1} at highest values, representing a flux of 0.1 mmol m^{-2} d^{-1}). Fluxes were the largest around 50–70 m depth, where eddy diffusivity was the largest and where the gradient of nutrients was strong.

3.1.2.4. Seawater CDOM and FDOM

Seawater samples for CDOM and FDOM were collected only at stations in the Amundsen Basin (P10, P11, and NLEG37 which was located between P10 and P11). Here, elevated CDOM absorption (peaking at around 0.80 m^{-1} at 350 nm) was found in the upper 100 m. Intensity of the humic-like peaks (Coble, 1996) was also relatively high (about 0.05 RU). Both CDOM and FDOM had a subsurface maximum at salinity of about 32, equaling a depth of around 40–50 m.

3.1.3. Seafloor sediment properties

Sediments at all stations consisted predominantly of fine-grained sediment, that is, silt and clay particles (>95%, particles <63 µm). The highest sand content (up to 5%) was observed at Gakkel Ridge station P9. The Nansen Basin sites had very similar grain size distribution patterns in sediment cores. Slightly higher down-core variations were observed in Amundsen Basin sediments (**Figure 8a**).

TOC content (dw %) was generally low, ranging from 0.5% (P10) to 1.3% (P7) in the top 1 cm of the sediment, yet slightly higher at stations located in the Nansen Basin (P7 and P8) than Amundsen Basin (P10 and P11). As expected, the TOC content generally decreased downcore, except at P11 where it reached a minimum value at 3–4 cm core depth (**Figure 8b**). TIC showed less spatial variability in the surface sediments (0–1 cm), ranging from 0.9% (P9) to 1.4% (P10), but fluctuations in TIC were stronger and more variable than in TOC. The highest TIC content was observed at P11 at 3–4 cm core depth. While the TIC content slightly decreased downcore at P8 and P9, there was a decreasing trend in core P10, and it remained constant in the P7 core (**Figure 8b**).

TN was generally low in all sediment samples. The highest values were observed in the sediments of core P7 (>0.17%), while in all other samples, values were <0.13%. Generally, the TN content increased upcore, except at P11, where it reached the overall lowest value at 3–4 cm (**Figure 8b**). The TOC:TN ratio was highest at station P7 (ratio >6) and lowest at station P10 (ratio <5; Table S6). The sediment bulk stable carbon isotope values ($\delta^{13}C$) were less enriched and exhibited larger upcore variations in the Amundsen Basin than at other stations (Hess et al., 2024). Stable nitrogen values ($\delta^{15}N$) were highest in the surface sediments (0–1 cm) at Gakkel Ridge station P9 (>7.2‰) and ranged from 6.5‰ to 6.8‰ at the other stations (Table S6). $\delta^{15}N$ values generally increased upcore, except at P11, where the lowest values were recorded at 3–4 cm (3.2‰).

Sedimentation rates appeared to be extremely low, inferred from otolith age at Gakkel Ridge station P9. Age of fish otoliths found in the upper 2 cm of the sediment was estimated, based on ^{14}Carbon dating, at 4,100 ± 30, 5,065 ± 30, and 5,390 ± 30 years (five pooled otoliths each) for *Arctogadus glacialis* and 6,720 ± 35 years (six otoliths pooled) and 7,380 ± 40 years (five otoliths pooled) for *Boreogadus saida*.

3.2. Biological components in sympagic, pelagic, and benthic environments

3.2.1. POC and PN in sea ice and water column

As expected, POC and PN concentrations were the highest in the bottom centimeter of the ice and decreased toward the top (**Figure 9a** and **9b**). Ice cores at stations P8 (mean core length 90 cm), P10 (110 cm), and P11 (156 cm) were very similar in terms of concentrations and pattern. Averaged across the three stations, POC concentration was 1,784 mg m^{-3} and PN was 102 mg m^{-3} in the bottom 3 cm of the ice, while averaged POC in the respective top

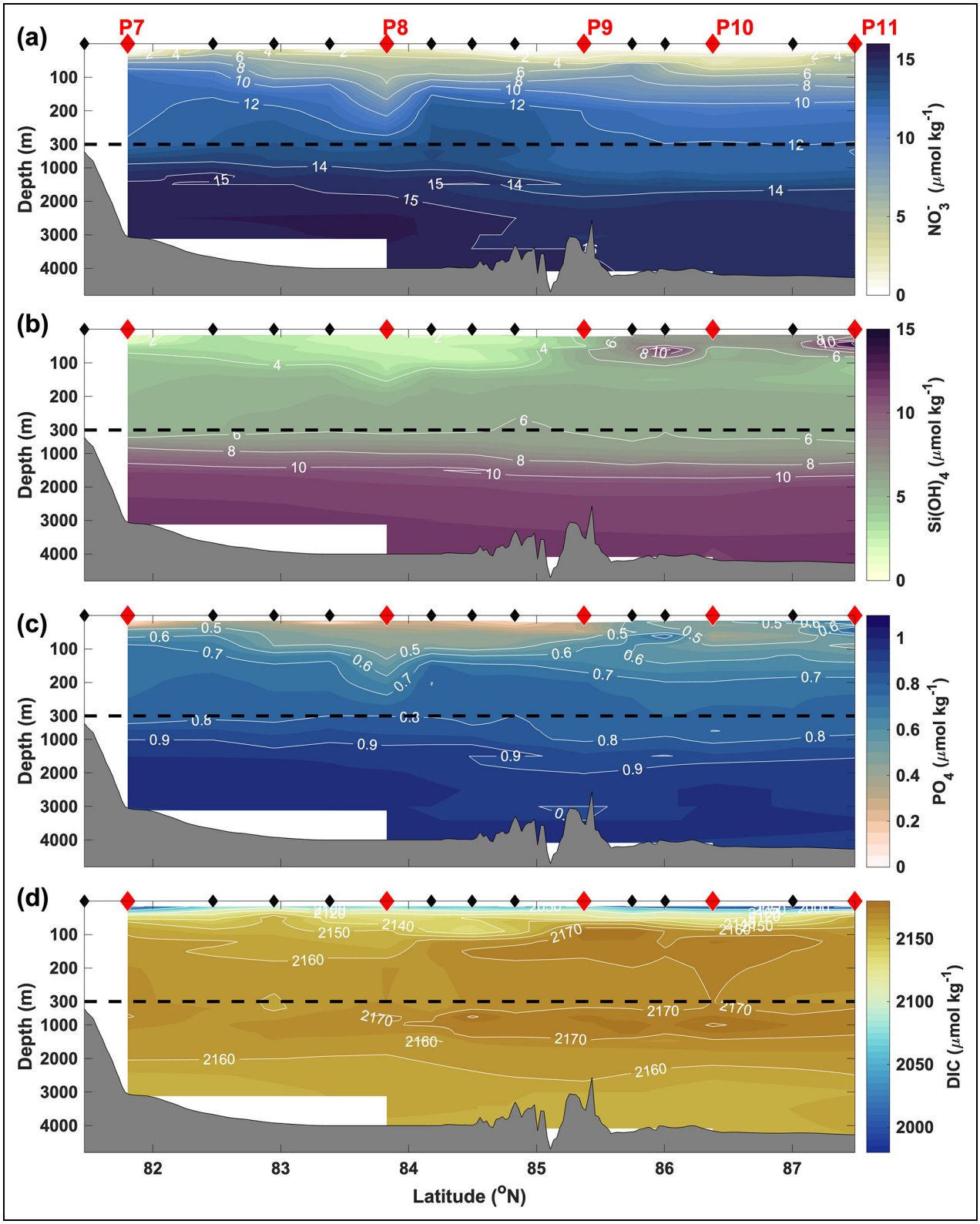

Figure 5. Distributions of water column nutrients and dissolved inorganic carbon along the JC2-2 transect. (a) Nitrate (NO_3^-, µmol kg^{-1}), (b) silicate ($Si(OH)_4$, µmol kg^{-1}), (c) phosphate (PO_4^{3-}, µmol kg^{-1}), and (d) dissolved inorganic carbon (DIC, µmol kg^{-1}). Depths below 300 m have been contracted by a factor of 10 to better represent the upper water column. Red diamonds indicate stations P7 to P11 (left to right; **Figure 2a**); black diamonds, NLEG stations where mostly CTD casts were taken (see **Table 1** for full list). Seawater DIC data can be found in Chierici and Fransson (2025) and nutrient data are published in Chierici et al. (2025). Figure created using MATLAB.

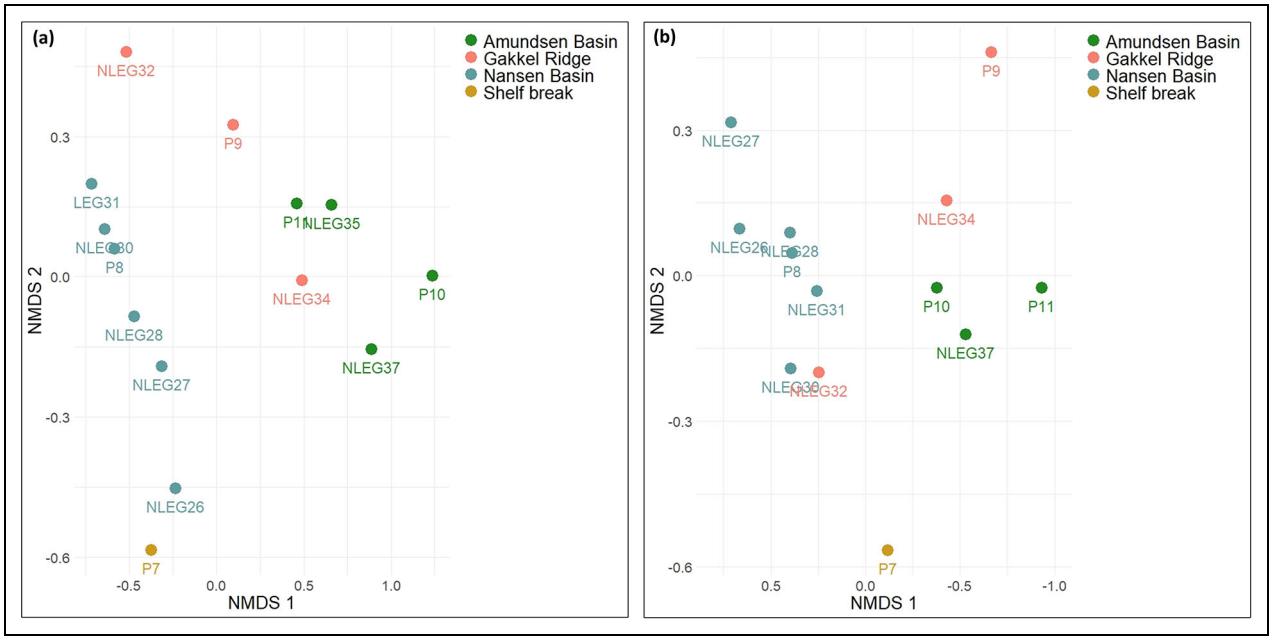

Figure 6. Non-metrical multidimensional scaling (NMDS) of physical, chemical, and biological parameters in the upper water column. NMDS plots of (a) physical-chemical parameters (temperature, salinity, nutrients, and dissolved inorganic carbon) and (b) microbial abundances (viral particles, bacteria, picophytoplankton, and nanophytoplankton) of the uppermost 100 m of the water column from samples collected in the Amundsen Basin, over the Gakkel Ridge, in the Nansen Basin, and at the shelf break (station P7). Bray-Curtis distance; stress values of 0.04 for both plots. Figure prepared in Software R (v4.2.0; R Core Team, 2021), using the vegan package (Oksanen et al., 2010).

sections was 674 mg m^{-3} and PN was 55 mg m^{-3} at these three stations. In contrast, the ice over Gakkel Ridge station P9 (core length 164 cm) had about 3-fold higher concentrations of POC (5,156 mg m^{-3}) and PN (274 mg m^{-3}) in the lowermost 3 cm of the ice, but values similar to the other stations toward the top of the ice. Atomic C:N ratios ranged from 8.8 to 24, with lowest values at P9 in the interior sections (10–30 cm) and highest values at P11 (section 10–20 cm; Table S7).

Overall, POC and PN concentrations in the water column were higher in the Nansen Basin than in the Amundsen Basin (**Figure 9c** and **9d**). Highest concentrations were measured in the surface layers (approximately 15–60 m) and decreased with depth, with values of 7–14 mg C m^{-3} and <1–2 mg N m^{-3} below 200 m depth (not presented in **Figure 9c** and **9d**). The exception was P7 closest to the shelf, where concentrations were higher even in deep layers (e.g., 28.0 ± 8.7 mg C m^{-3} at 2,000 m, $n = 3$) and the overall highest values were measured (e.g., 157 ± 17 mg C m^{-3} and 23 ± 0.3 mg N m^{-3} at 30 m). In the Nansen Basin, a sharp gradient in POC and PN occurred around 60 m, while profiles were more homogeneous in the Amundsen Basin. Atomic C:N ratios were very similar at all stations (Table S7), usually ranging between 6 and 13 (average 9), and appeared to be slightly higher in the deeper layers (approximately 11 at >200 m).

3.2.2. Chl *a* concentrations in sea ice, water column and sediments

Chl *a* values in the sea ice were overall low and variable, with no obvious geographic trend (**Figure 10d**). Sea-ice chl *a* values of nearly 4 mg m^{-3} were found at stations P9 and P11, while at P10, no section exceeded 0.4 mg m^{-3}. As expected, the vertical distribution of algal biomass within the ice cores showed maximum values in the lowermost layers of the core (0–3 cm or 3–10 cm sections); distribution was similar across stations.

Regarding characteristics of the water column and sediment, the station closest to the shelf (P7) stood out. Chl *a* concentrations in the water column peaked at ice-free station P7 with 2.1 mg m^{-3} at 37 m depth. Depth-integrated chl *a* values (15–90 m) declined >10-fold from 40.7 mg m^{-2} at P7 to 3.7 mg m^{-2} at P11. Despite generally low chl *a* values away from the slope, maximum chl *a* values were higher in the Nansen Basin (0.4 and 0.2 mg m^{-3} at P8 and P9, respectively) than in the AB (<0.15 mg m^{-3}; **Figures 4c** and **10d**). Chl *a* was the highest in the upper 70 m of the Nansen Basin and upper 50 m of the Amundsen Basin, reaching 1 mg m^{-3} in the former but only 0.1 mg m^{-3} in the latter (**Figures 4c** and **7d**). Sediment chl *a* at P7 was one order of magnitude higher compared to all other stations (**Figure 8b**). Chl *a* generally decreased downcore and showed little variation among stations P8 to P11 (<0.1 mg m^{-3}).

3.2.3. Sea-ice environment

3.2.3.1. Viral particles, bacteria and BP, pico- and nanoalgae, and heterotrophic nanoflagellates

Abundances of sympagic bacteria and nanoalgae were generally higher in sea ice sampled at stations P8 and P9 than at stations located in the Amundsen Basin (P10 and P11; **Figure 10a** and **10b**). Accurate estimates of viral abundance in the ice cores are lacking, but our flow cytometry counts (not shown) suggest that the concentration

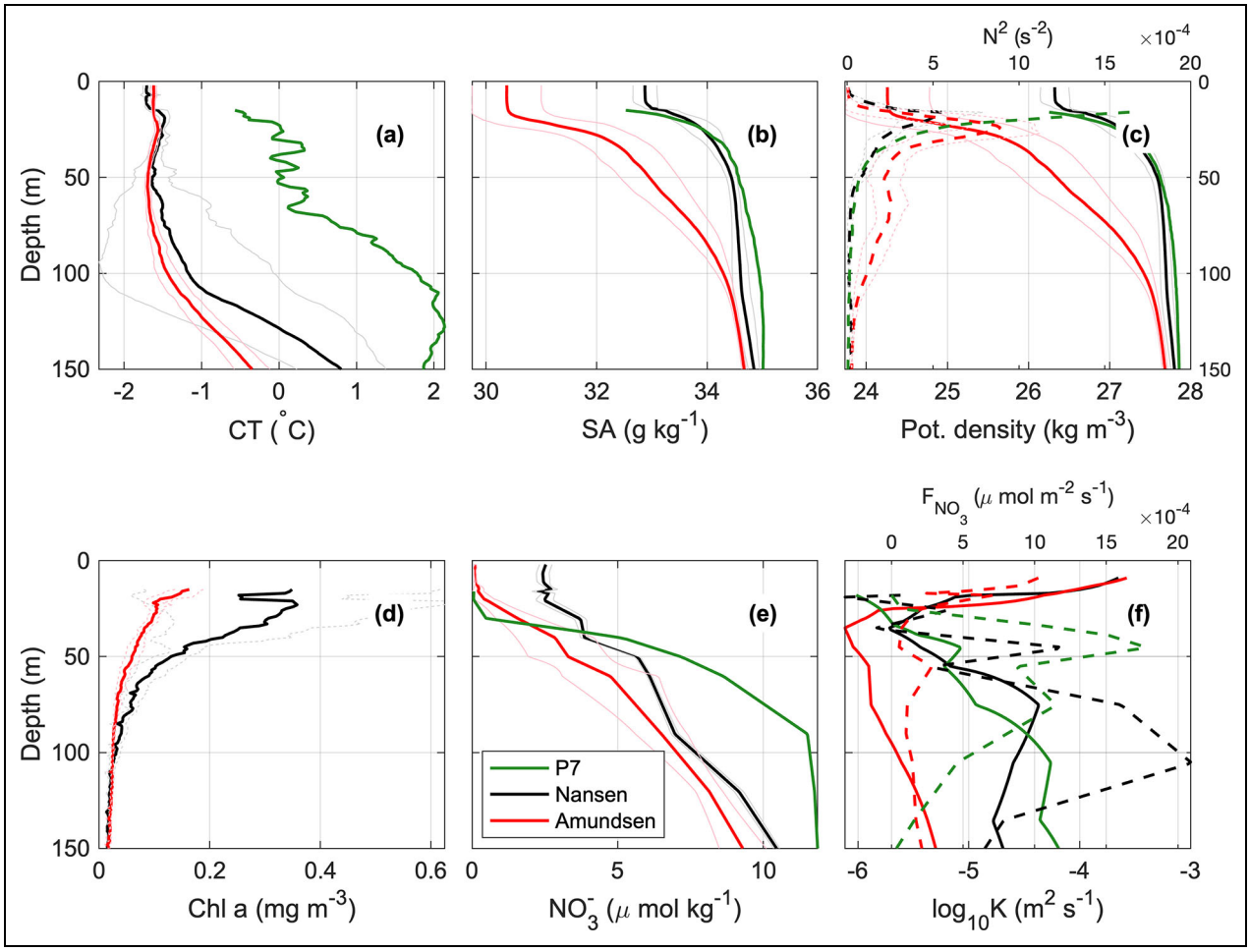

Figure 7. Depth profiles of water column physico-chemical properties. Profiles are based on 80 MSS casts: 3 at station P7, 20 in the Nansen Basin, and 57 in the Amundsen Basin: (a) conservative temperature (CT, °C), (b) absolute salinity (SA, g kg^{-1}), (c) potential density (kg m^{-3}; bottom axis, solid lines) and buoyancy frequency (Brunt-Vaisala Frequency squared, N^2, s^{-2}; top axis, dashed lines), (d) corrected chlorophyll fluorescence (chl *a,* mg m^{-3}), (e) nitrate (NO_3^-, µmol kg^{-1}) from discrete sampling, and (f) eddy diffusivity ($log_{10}K$, m^2 s^{-1}; bottom axis, solid lines) and nitrate fluxes (F_{NO3}, µmol m^{-2} s^{-1}; top axis, dashed lines). Red lines indicate average profile over the Amundsen Basin for seven stations; black lines, average profile over the Nansen Basin for five stations; and gray/pink lines, ±1 SD for average profiles in the Nansen/Amundsen basins. Figure created using MATLAB.

of viral particles in the sea ice at stations P8 and P9 was higher compared to the concentration in the water immediately below (0–5 m), while at stations P10 and P11 the viral concentration in the ice appeared lower than in the water below. Sea ice at P8 had the overall highest abundance of nanoalgae (up to 2,680 cells mL^{-1}, in the 3–10 cm section; **Figure 10b**), relatively homogeneous from the bottom to the 40–50 cm section, and this community was dominated by the smaller nanoalgae group, which was unique to this station. Similarly, bacterial abundance was high from the bottom to 70 cm, mostly due to the higher abundance of the group of larger bacteria (**Figure 10a**). Sympagic BP was overall higher than pelagic BP, and all ice cores had a generally higher ratio of large, high nucleic acid bacteria to small, low nucleic acid bacteria than seawater samples. Highest BP rates were generally measured in the 0–3 cm bottom sections ranging from 0.96 µg C L^{-1} d^{-1} at P10 to 3.8 µg C L^{-1} d^{-1} at P9, where large nanoalgae were also most abundant (**Figure 10a** and **10b**). P10 had overall the lowest microbial and algal abundances of all sea-ice cores and was very homogeneous throughout the entire ice core in terms of BP and abundances of bacteria and algae.

3.2.3.2. Sea-ice protist communities (nano- and microalgae)

Abundances of sympagic protists in the lowermost 10 cm of the sea ice were higher at stations P8 (2.3×10^6 cells L^{-1}; Nansen Basin) and P9 (4.6×10^6 cells L^{-1}; Gakkel Ridge) than at the two stations in the Amundsen Basin, P10 (0.8×10^6 cells L^{-1}) and P11 (1.4×10^6 cells L^{-1}). Abundances of microscopically identified and enumerated sympagic protists always peaked in the bottom sections (3 cm at P9–P11, or 3–10 cm at P8) and were dominated by diatoms (**Figure 10c**). Within the diatoms, *Nitzschia frigida* was generally most abundant, except at P8 where *Cylindrotheca closterium*, *Chaetoceros tenuissimus*, and *Conticribra weissflogii* dominated. Flagellates were co-dominant in some sections, particularly at P8 (predominantly

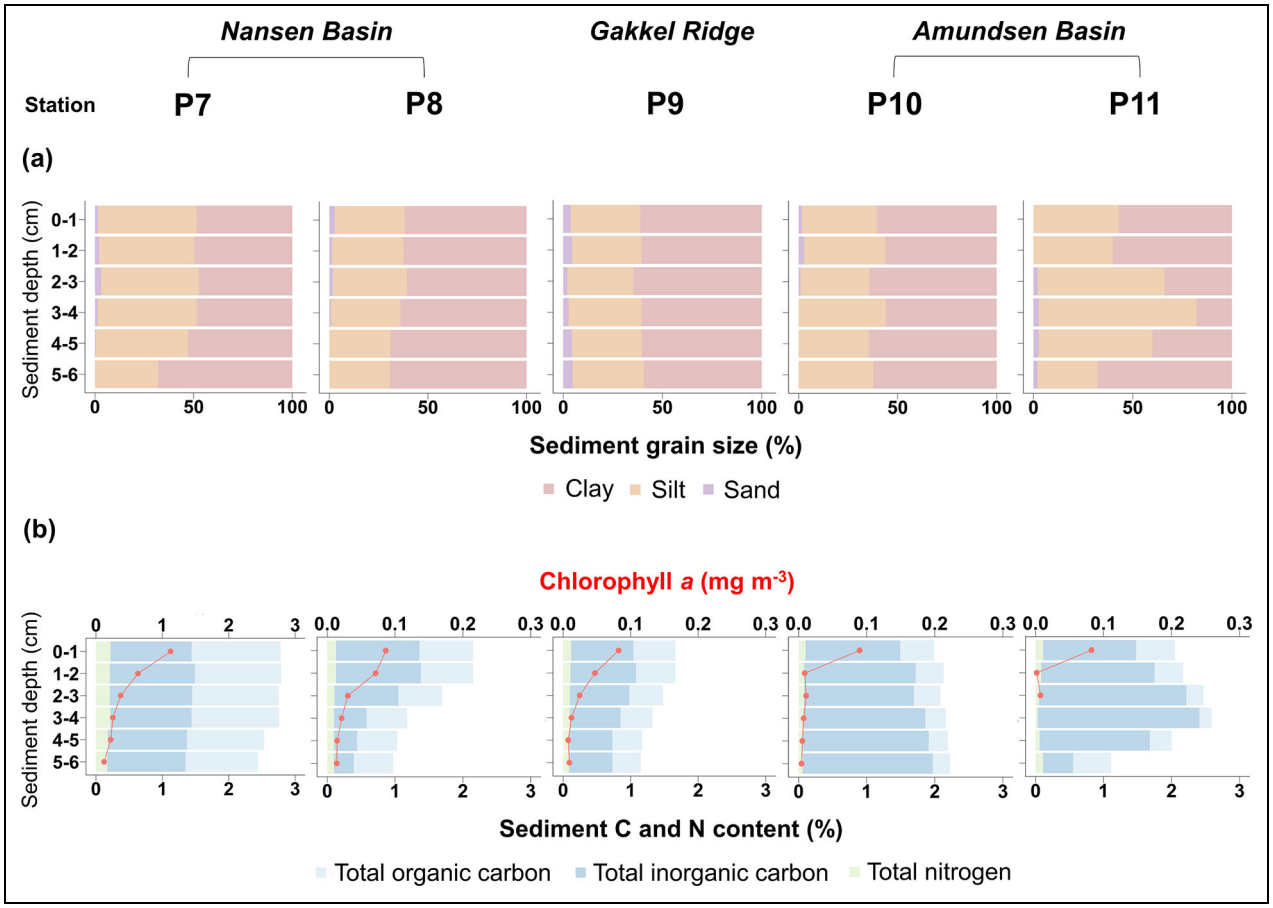

Figure 8. Seafloor sediment properties along the JC2-2 transect. (a) Relative grain size distributions (%), and (b) percentages of total organic carbon (TOC), total inorganic carbon (TIC), and total nitrogen (TN) with sediment chlorophyll (chl) *a* concentrations (mg m^{-3}; red points and line) in different sections of the benthic sediment cores collected at stations P7–P11. Note different scale for sediment chl *a* at P7. Sediment chl *a* data can be found in Akvaplan-niva (2023); sediment chemical properties (TOC, TIC, TN) are published in Hess et al. (2024). Figure prepared in Software R (v4.1.0; R Core Team, 2021), using the ggplot2 package (Wickham, 2016).

chrysophytes), while ciliates and dinoflagellates contributed little to cell abundances. Live microscopy observations onboard (Figure S5) confirmed the dominance of pennate diatoms and showed that heterotrophic dinoflagellates, nano- and pico-sized autotrophic flagellates, cryptomonads, chrysophytes (cysts in particular), and haptophytes were also frequent. A few *Melosira* assemblages with associated other diatoms, flagellates, and ciliates were observed at P9. SEM of under-ice water and ice cores from P9, P10, and P11 revealed naviculoid diatoms, *Fragilariopsis cylindrus*, *Attheya* cf. *septentrionalis*, and a *Nitzschia* cell being ingested by a thaumatoid. A naked peridinoid dinoflagellate, the choanoflagellate *Parvicorbicula*, a chrysophyte cyst, and an undescribed protist were also recorded among many other protists (Figure S6).

Chl *a* largely followed the distribution of protist abundances (driven by diatoms), except at P11 where chl *a* peaked at 3–10 cm but abundances did not (a majority of the chl *a* biomass was in the <10 µm fraction). Based on live light-microscopic observations of protists onboard the ship, the abundances in sea ice were much higher and cells larger than in the water column.

3.2.3.3. Sympagic NPP rates

The integrated sympagic NPP within the bottom 3 cm of the sea ice contributed between 1.7% (P10) and 10.3% (P8) to the total integrated NPP at the stations and was higher at the Nansen Basin station compared to the Amundsen Basin stations (**Figure 11a**). Ice algal primary productivity per unit of meltwater volume ranged from 5.4 µg C L^{-1} d^{-1} at P10 to 61.6 µg C L^{-1} d^{-1} at P8 (**Figure 11b**).

3.2.3.4. Sea-ice meiofauna

Overall, meiofaunal abundances were higher in sea ice over the Nansen Basin and Gakkel Ridge than in the Amundsen Basin when eggs were excluded, yet no distinct basin-specific difference in composition was obvious between the two basins, or in abundance when eggs were included. The range of averaged abundances of sea-ice metazoans including eggs was 2–175 ind. L^{-1}. Highest abundances of metazoans—dominated by harpacticoid copepods and metazoan eggs—were found in the bottom 0–3 cm of ice at all stations and decreased toward the interior ice sections. The ice over the Gakkel Ridge (P9) had the highest total abundances (average of 175 ind. L^{-1}

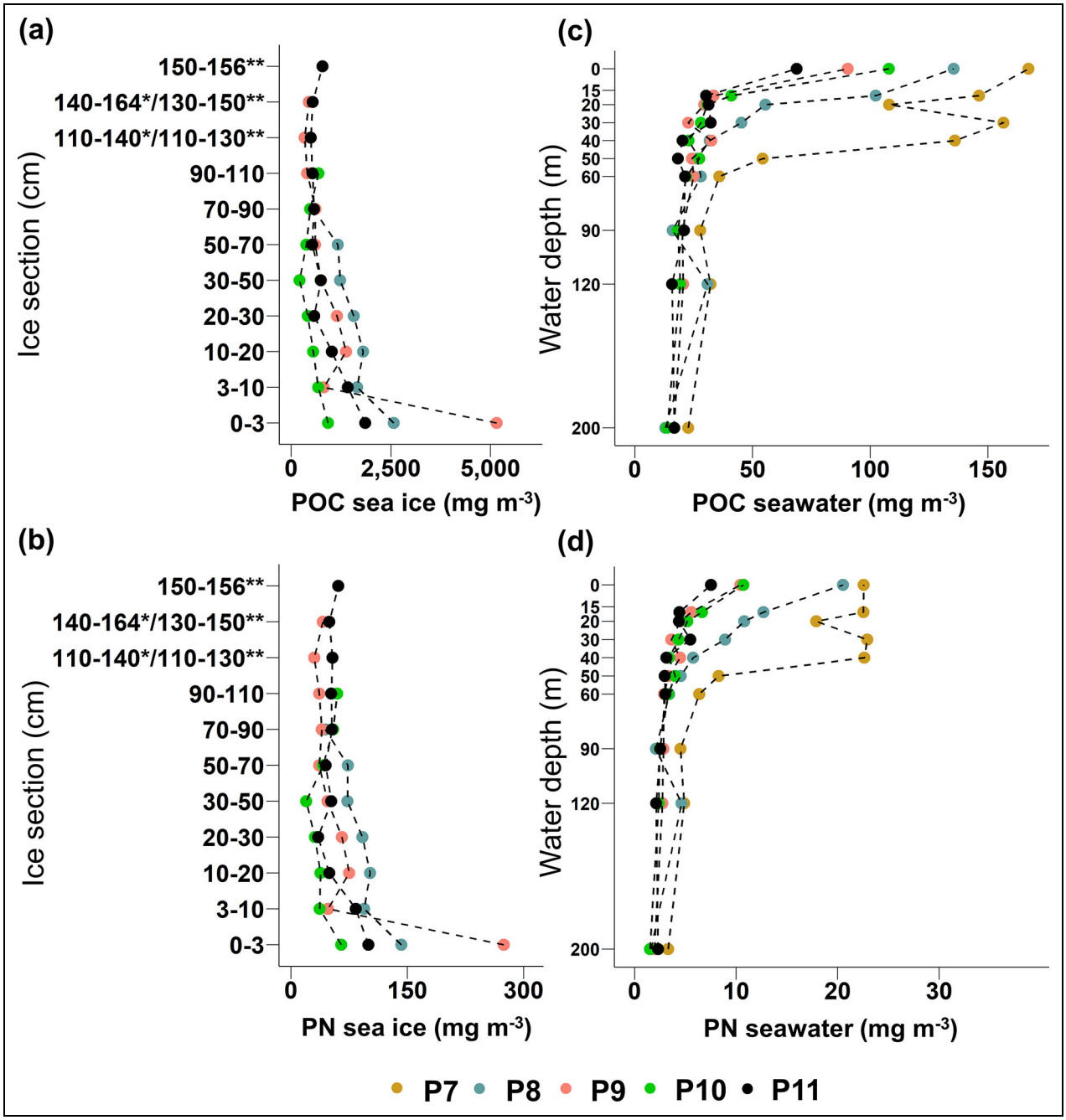

Figure 9. Depth profiles of particulate organic carbon (POC) and nitrogen (PN) in sea ice and seawater. (a) POC (mg m^{-3}) and (b) PN (mg m^{-3}) in different sections of the sea ice (cm, 0 cm indicates ice-water interface) and (c) POC and (d) PN at discrete depths of the water column (m) sampled at stations P7 (seawater only) and P8–P11. Lengths of entire ice cores varied by station (* indicates P9; **, P11). Note the different axis scales for sea-ice and seawater figures. POC and PN concentrations in sea ice were analyzed mostly on individual samples; for seawater, mean values of triplicate samples are shown. All data, including standard deviations where replicate samples were analyzed, can be found in Marquardt et al. (2022). Figure prepared in Software R (v4.1.0; R Core Team, 2021), using the ggplot2 package (Wickham, 2016).

in 0–3 cm) and highest number of large taxa among the ice stations. At P10 and P11, only few metazoans were found in the ice (average <13 ind. L^{-1}), or were even absent, but high numbers of eggs were present (e.g., average of 102 eggs L^{-1} in 0–3 cm at P10).

The sea-ice meiofaunal community was dominated by harpacticoid copepod taxa, such as *Halectinosoma* sp. and cf. *Tisbe furcata*, copepod nauplii and rotifers of the family Synchaetidae and a diverse range of metazoan eggs (**Figure 10d**). Orange Acoela (Xenacoelomorpha) and *Clione limacina* juveniles (gastropods) were occasionally found within the sea ice. Large protists are not presented in **Figure 10d** but are reported in Marquardt et al. (2023a). Ciliates in fact dominated the sea-ice meiofauna at all stations and ice sections with 80–90% relative abundances (range of 29–538 ind. L^{-1}). Pelagic foraminifers

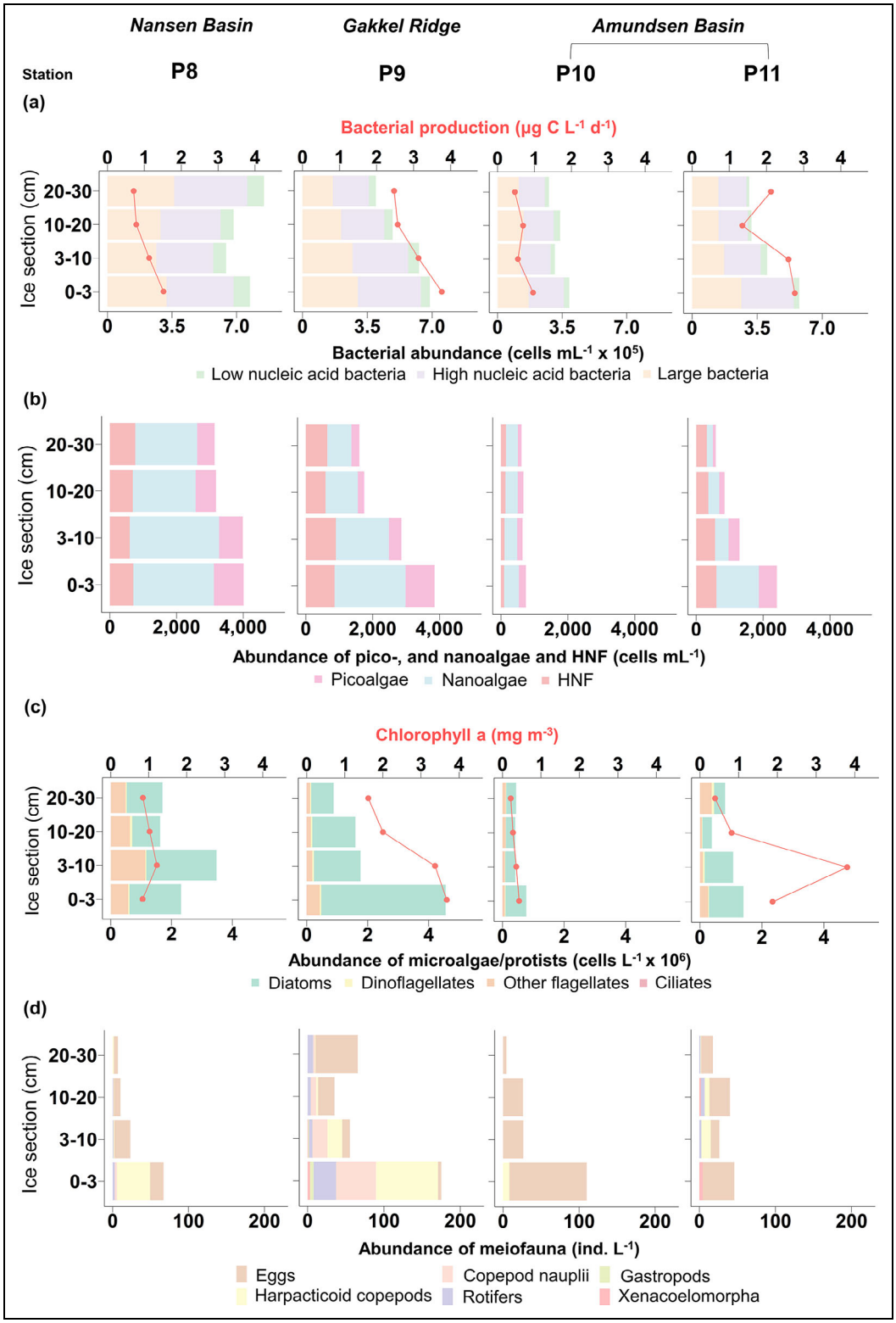

Figure 10. Abundances, composition, and production of sympagic microbial and meiofauna communities. (a) Bacterial abundance (cells mL^{-1}) and production (µg C L^{-1} d^{-1}; red points and line), (b) abundances of picoalgae, nanoalgae, and heterotrophic nanoflagellates (HNF; cells mL^{-1}), (c) abundance of microalgae/protists in different sections of the sea ice (cells L^{-1}) and sea-ice chlorophyll *a* concentrations (mg m^{-3}; red points and line), and (d) meiofaunal taxa (ind. L^{-1}; only living individuals are presented, excluding large protists) collected at stations P8–P11. The 0–10 cm ice section indicates the ice-water interface. Abundances of microalgae/protists and meiofauna represent average values of three replicates. Abundances of bacteria, pico- and nanoalgae are published in Bratbak et al. (2023), sympagic bacterial production in Müller et al. (2023b), protist community data in Assmy et al. (2022b), chlorophyll *a* data in Vader and Marquardt (2022), and sea-ice meiofauna data in Marquardt et al. (2023a). Figure prepared in Software R (v4.1.0 and v4.2.0; R Core Team, 2021), using the ggplot2 package (Wickham, 2016).

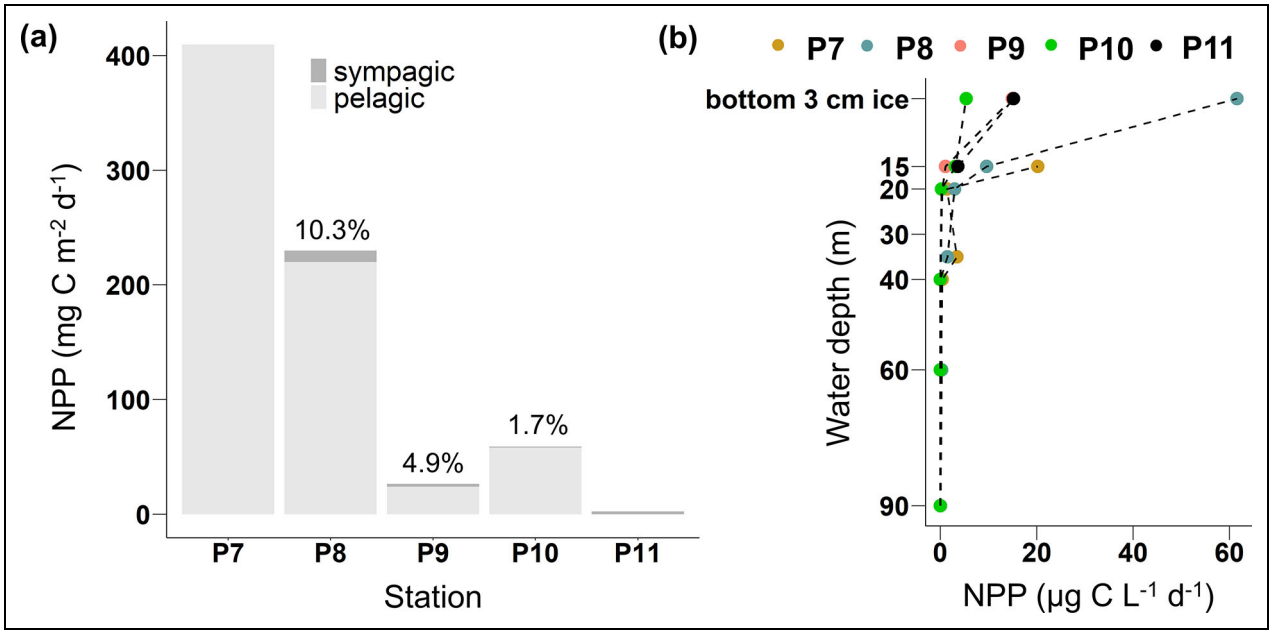

Figure 11. Sympagic and pelagic net primary production. (a) Rates of integrated net primary production (NPP; mg C m^{-2} d^{-1}) in sea ice (sympagic) and the water column (pelagic) with percentages representing the relative contribution of sea-ice NPP to total NPP for stations where both water and ice values were available (P8–P10), and (b) vertical profiles of NPP (µg C L^{-1} d^{-1}) collected at (color-coded) stations P7–P11 from the bottom 3 cm of ice to 90 m depth in the water column. In panel (a), sympagic data represent the integrated activity in the lowermost 3 cm of the ice, and pelagic data the integrated activity down to 90 m water depth except for station P11 where only data within the uppermost 15 m were available. Figure prepared in Software R (v4.1.0; R Core Team, 2021), using the ggplot2 package (Wickham, 2016).

Neogloboquadrina pachyderma were only found alive at P8 and P9 in very low abundances (average 2 ind. L^{-1}), while empty shells were also found in the ice at P11.

3.2.4. Water column

3.2.4.1. Viral particles, bacteria and BP, pico- and nanophytoplankton, and heterotrophic nanoflagellates

Considering data from all stations sampled (**Table 1** and **Figure 6b**), abundances of viral particles, bacteria, and pico- and nanophytoplankton were generally higher in surface waters (0–30 m) of the Nansen Basin than the Amundsen Basin, while there was no clear difference in the abundances of HNF and small viruses between basins (see Bratbak et al., 2023). The highest abundance of viral particles was measured at P8 (6.5×10^6 mL^{-1} at 0 m), and abundances decreased (to 3.7×10^6 mL^{-1}) from P9 northward into the AB, with the largest difference in the group of large viruses. The highest abundance of high fluorescence viral particles was detected at P8, correlating and likely associated with the higher abundance of nanoplankton cells at this station (**Figure 12a**). Total bacterial abundance followed a pattern similar to viral abundance and was the highest at station P8 (1.1×10^6 mL^{-1} at 0 m) and low at stations in the Amundsen Basin, ranging between 1.6×10^5 (15 m at P11) and 4.5×10^5 (15 m at P10) bacteria mL^{-1} in the uppermost 30 m of the water column. BP was overall low with highest values in the upper 30 m, ranging between 0.1 and 0.2 µg C L^{-1} d^{-1}. In general, BP followed the same pattern as described for bacterial abundance, with highest values at the southern stations, decreasing from P8 to P9 (**Figure 12b**).

Overall abundance of both pico- and nanophytoplankton was relatively low, with the highest abundance of picophytoplankton generally in the upper 30 m and of nanophytoplankton around 30–60 m (**Figure 12c**). Overall nanophytoplankton abundance was the highest at P8. Highest picophytoplankton abundance was measured at station P7 with 8,200 cells mL^{-1} at 0 m. There was a gradual decrease in picophytoplankton abundance from P7 to P9. Abundances of HNF were overall low, 35–212 cells mL^{-1} (for depths 0–90 m), with the highest measurement at station P7 with 400 cells mL^{-1} (20 m).

3.2.4.2. Pelagic protist communities (nano- and microplankton)

There was a gradual decrease in protist abundances (from 1.6×10^6 cells L^{-1} at P7 to 4.9×10^5 cells L^{-1} at P11, 0 m) and a shift in predominance of larger to smaller taxa from the Nansen Basin near the shelf slope toward the Amundsen Basin. This gradient was confirmed by live microscopy observations onboard. Both analysis of fixed samples and onboard observations showed that flagellates largely dominated protist abundances (80–88% of total abundances) in both basins, particularly at the surface (0 m), throughout the transect. Flagellate abundance, along with total protist abundance, peaked at the surface (0 m), and gradually declined with depth at all stations (**Figure 12d**). Both diatom abundances and chl *a* concentrations showed subsurface maxima only in the Nansen Basin and over Gakkel Ridge. Moving into the ice cover, live imaging

confirmed that larger diatom species became much scarcer and were generally in poor condition.

The live imaging at P7 showed that the protist community was characterized by high species diversity of diatoms and dinoflagellates. Among the flagellates, the chrysophyte *Dinobryon balticum* was particularly abundant, for example, at the surface at P7. *Phaeocystis pouchetii* and *D. balticum* were co-dominant at the surface at P8. Among the diatoms, *Chaetoceros* sp. was abundant at 30 m at P7 and *Fragilariopsis* sp. dominated at P8 (15 m) and P9 (30 m). Abundant dinoflagellates included different species of *Gymnodinium* at all stations and depths. Large dinoflagellates (>50 μm), such as *Tripos* spp. and *Protoperidinium* spp., were also abundant at P7. Water column communities changed with increasing ice cover in the Amundsen Basin: smaller and heterotrophic species, especially dinoflagellates became more prominent. Ciliates contributed overall little to protist abundances (0.5–1.5% of total abundances; prominent taxa were, e.g., *Lohmanniella oviformis* and *Strombidium* spp.).

3.2.4.3. Pelagic NPP rates

On average, the Nansen Basin (P7 and P8) had higher integrated pelagic NPP rates (top 90 m of water column; average 314.7 mg C m^{-2} d^{-1}) than the stations on the Gakkel Ridge (P9) and in the Amundsen Basin (only P10, because at P11 only the value from 15 m was available, averaging 41.2 mg C m^{-2} d^{-1}). Integrated pelagic NPP ranged from a maximum of 409.4 mg C m^{-2} d^{-1} at P7 to a minimum of 24.1 mg C m^{-2} d^{-1} at station P9 (**Figure 11a**). Highest pelagic NPP per unit of volume was measured at 15 m at P7 (20.2 μg C L^{-1} d^{-1}, **Figure 11b**). At all stations, highest NPP per unit of volume was found closest to the surface, decreasing with depth. At all stations, integrated values of phytoplankton NPP far exceeded the sea-ice algal productivity at the time of sampling (see Section 3.2.3.3).

3.2.4.4. Vertical flux of pelagic protists

The vertical protist flux was highest at P7 in the Nansen Basin, decreased toward the north and was distinctly lower at station P9 and the two Amundsen Basin stations (**Figure 12e**). The cell flux was dominated by flagellates, mirroring the composition of the suspended pelagic communities (**Figure 12d**). Dinoflagellates contributed more to the cell flux than to the suspended communities and were particularly high in their relative contributions at P9 and P10.

3.2.4.5. Zooplankton communities

The total abundance and biomass of mesozooplankton were considerably higher in the southern part of Nansen Basin (P7) than further north, mainly due to the contribution of Atlantic species, such as *Calanus finmarchicus* (19,000 ind. m^{-2} at P7 versus 40–400 ind. m^{-2} at stations further north), *Metridia longa* (24,000 ind. m^{-2} versus 300–3,000 ind. m^{-2}) as well as Arctic shelf species such as *Calanus glacialis* (14,000 ind. m^{-2} versus 500–2,500 ind. m^{-2}; **Figures 13a**–**13c** and S7). At all stations, small copepods and nauplii were the most numerous while *Calanus* spp. contributed the largest share to the biomass (**Figures 13a** and S7d). Among the small copepods, calanoid copepods of the genus *Microcalanus*, cyclopoid copepods of the species *Oithona similis*, and various genera of the family Oncaeidae were the most abundant at all stations, with Oncaeidae being ubiquitous and observed in consistently high abundance throughout the transect (**Figure 13a**). From the taxonomic point of view, the Oncaeidae group in this study contains various representatives of the Oncaeidae family, including the most known species *Triconia borealis*. Illustrated is the presence primarily of CI to CV developmental stages of *T. borealis* and other species of this family, mainly of the genus *Oncaea*, and the presence of adults of *Oncaea* or other Oncaeidae (among them *Atrophia glacialis* and *Homeognathia brevis*) apart from *T. borealis*. Information on the occurrence and abundance of adult females of the latter species is presented in the *T. borealis* group. Copepod nauplii were dominated by cyclopoid nauplii, whereas calanoid and harpacticoid nauplii were mainly present in the Nansen Basin. The total abundance of copepod nauplii peaked at P7 with numbers exceeding 1,000 × 10^3 ind. m^{-2}. At P8–P11, nauplii abundance was relatively stable at 350–550 × 10^3 ind. m^{-2}. All three *Calanus* species were present in the study area, but there were noteworthy differences between stations in their occurence. At P7, *C. finmarchicus* and *C. glacialis* (as identified based on prosome length measurements) constituted the bulk part of the *Calanus* fraction both in terms of abundance and biomass, whereas at the other stations, each species was less abundant and *C. glacialis* and *C. hyperboreus* had higher shares while those of *C. finmarchicus* were small (**Figures 13b** and S7d).

Regarding distribution with depth, the highest abundance of zooplankton was found at P7 within the surface layer (0–50 m), with *Calanus finmarchicus* and *C. glacialis* contributing the largest fraction (Figure S7d). At P8–P11, in contrast, the zooplankton was distributed more evenly in the water column than at P7 but different species preferring greater depths were found in various depth layers. Of the large copepods, *Metridia longa* contributed most to abundance and biomass in the Nansen Basin. Large deep-water copepods such as *Spinocalanus antarcticus*, *Scaphocalanus brevicornis*, *Scaphocalanus magnus*, or *Gaetanus brevispinus* as well as *Paraeuchaeta* spp. and *C. hyperboreus*, on the other hand, were the most abundant in the Amundsen Basin (**Figures 13c** and S7b).

Similar to mesozooplankton, the total abundance of macrozooplankton was highest in the southern Nansen Basin (P7) due to high numbers of the chaetognath *Eukrohnia* spp. (predominantly *E. hamata*; **Figure 13d**), amphipods, such as *Themisto libellula*, *T. compressa*, and *T. abyssorum,* as well as the euphausiid *Thysanoessa longicaudata* (**Figure 13e**). Euphausiids were represented by two species, *T. longicaudata* and a few individuals of *Meganyctiphanes norvegica,* north of P7. The pteropod *Clione limacina* was only present at P7. The species composition of gelatinous zooplankton also differed at P7, with presence of the ctenophore *Mertensia ovum* (but see trawl results below) and higher abundance of *Aglantha digitale*, compared to stations further north (**Figure 13f**).

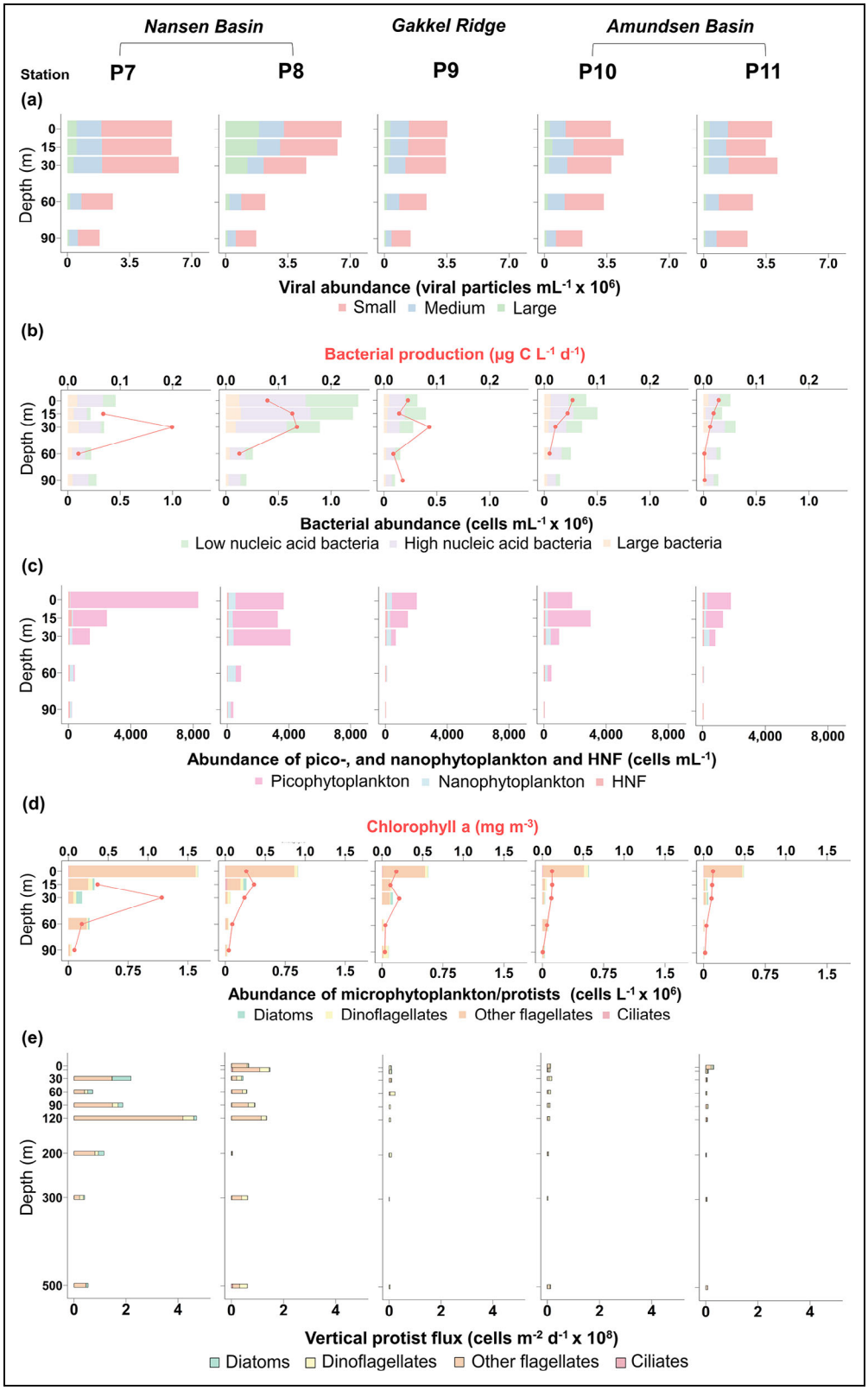

Figure 12. Abundances, composition, and production of pelagic microbial communities. (a) Viral abundance (viral particles $mL^{-1} \times 10^6$), (b) bacterial abundance (cells $mL^{-1} \times 10^5$) and production (µg C L^{-1} d^{-1}; red points and line), (c) abundances of pico-, nanophytoplankton, and heterotrophic nanoflagellates (HNF; cells mL^{-1}), (d) protist abundances (cells $L^{-1} \times 10^5$) and chlorophyll *a* concentrations (mg m^{-3}; red points and line), and (e) vertical flux of protists (cells m^{-2} $d^{-1} \times 10^8$) in samples collected at discrete depths of the water column at stations P7–P11. Additional data on viral abundance and bacterial abundance and production at stations sampled between the P stations can be found in Bratbak et al. (2023) and Müller et al. (2023b), respectively. Protist data can be found in Assmy et al. (2022a) and chl *a* data in Vader and Marquardt (2022). Figure prepared in Software R (v4.1.0; R Core Team, 2021), using the ggplot2 package (Wickham, 2016).

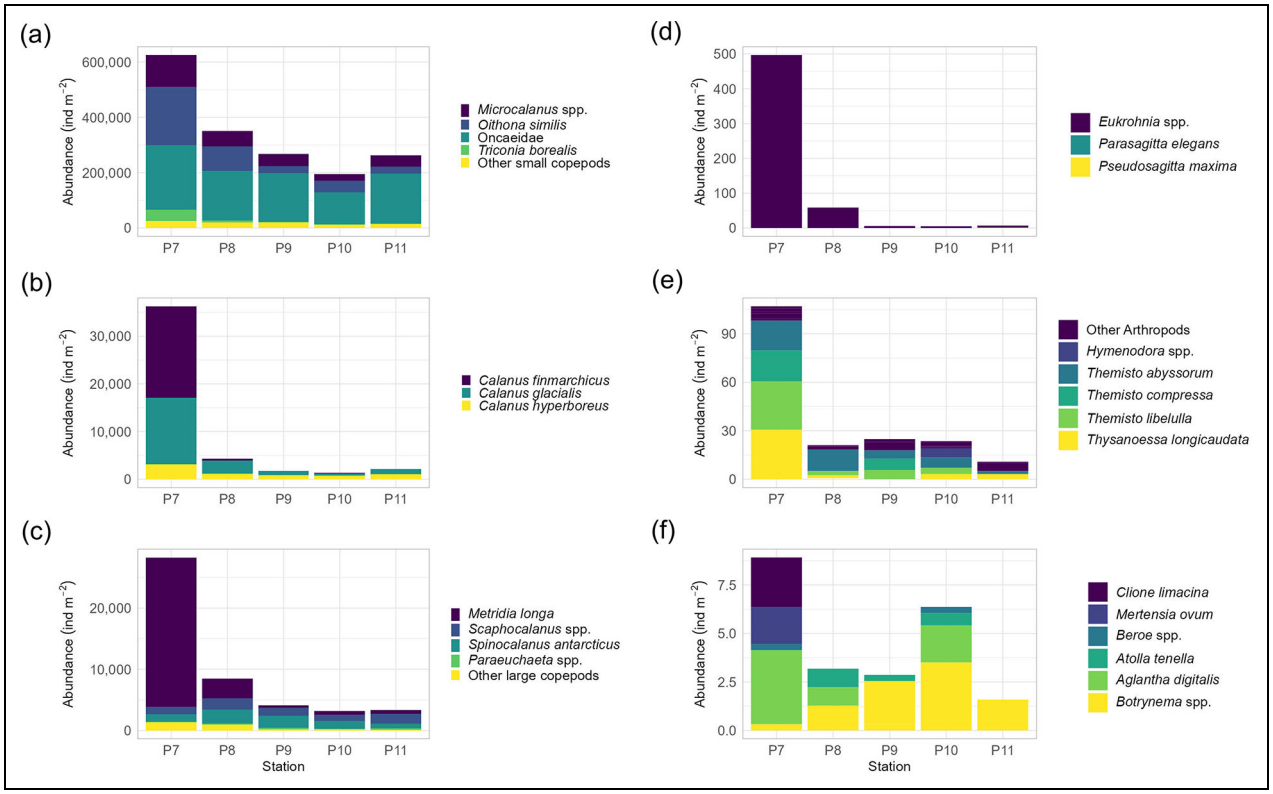

Figure 13. Abundance and composition of zooplankton communities. (a–c) Abundances of the numerically dominant species of mesozooplankton (ind. m^{-2}) based on Multinet 64 µm and 180 µm tows, separated into (a) small copepods, (b) *Calanus* spp., and (c) other large copepods. Abundances of macrozooplankton (ind. m^{-2}) based on MIK-net 1,500 µm tows are separated into (d) chaetognaths, (e) arthropods, and (f) molluscs, cnidarians, and ctenophores collected at stations P7–P11. Note the different scales for the different groups. Figure prepared in Software R (v4.2.0; R Core Team, 2021), using the ggplot2 package (Wickham, 2016).

At P8–P11, the hydromedusae *Botrynema brucei* and *B. brucei ellinorae* were the most abundant gelatinous zooplankton, with the highest numbers in the Amundsen Basin (P10). Catches from macrozooplankton and fish trawls confirmed, in part, the results from the MIK sampling but also revealed additional information on the larger macrozooplankton poorly captured by the MIK (Ingvaldsen et al., 2023). Generally, the trawling revealed a more diverse macrozooplankton fauna in the southern part of the Nansen Basin compared to further north, driven by the high abundance and diversity found at P7. In contrast to the MIK hauls, the trawl hauls showed relatively high biomass of ctenophores (*Beroe* spp. and *M. ovum*) in all regions, and these species completely dominated the wet weight biomass in the 50–500 m layer of the Amundsen Basin (no abundance data are available). Occurrences of chaetognaths matched those in the MIK hauls (**Figure 13d**) but with the highest biomass at the Gakkel Ridge station (P9). Also at this station, to our knowledge, we recorded the northernmost occurrence of the warm-water krill species *Hansarsia megalops* (previously *Nematoscelis megalops)* and, in the Nansen Basin, of the deep-water jellyfish *Periphylla periphylla.*

3.2.4.6. Fish

Three fish species were caught with the pelagic haul, but the catch was limited to seven individuals. All three species occurred in the Nansen Basin, where one individual of *Boreogadus saida*, one individual of *Reinhardtius hippoglossoides* larva, and three individuals of *Benthosema glaciale* were caught. The larva collected is, to our knowledge, the northernmost record of *R. hippoglossoides* and it was the first time it has been observed north of the shelf break in the CAO. No fish were caught at the Gakkel Ridge. In contrast, two individuals of *B. glaciale* were caught in the Amundsen Basin (Ingvaldsen et al., 2023).

In addition, 18 fish otoliths were found in the surface sediments at P9 of which 11 were identified as *Boreogadus saida*, seven as *Arctogadus glacialis*, and five as belonging to the family Gadidae but could not be further identified. Carbon dating suggested that *B. saida* was present at the Gakkel Ridge as far back as 7,380 ± 40 years ago and *A. glacialis* was present at least 5,390 ± 30 years ago.

3.2.5. Benthic environment

3.2.5.1. Macrofauna communities

The abundance of benthic macrofauna (>250 µm) was very low at all five P stations (<1,000 ind. m^{-2}) compared to the adjacent shelf. Yet, as with the pelagic ecosystem components, abundance was highest at P7 nearest the slope (despite samples here being sieved on 500 µm mesh). At this station, annelids contributed most to abundance (**Figure 14a**). All other stations were dominated by

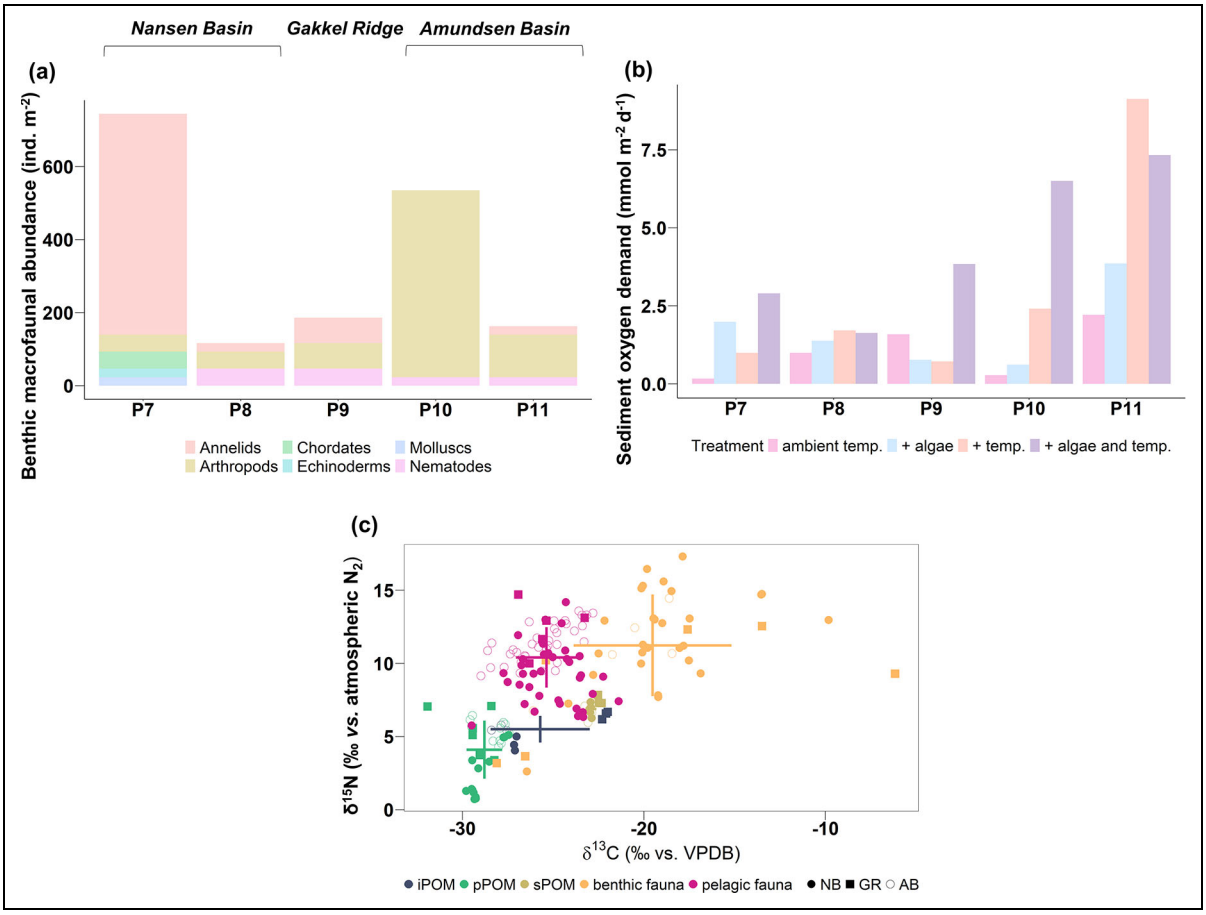

Figure 14. Biological properties of benthic communities. (a) Abundance of benthic macrofaunal taxa (ind. m^{-2}) collected at stations P7–P11 (fragments not included; sum of 4–5 subcores per station). Abundances at station P7 represent faunal composition encountered during Nansen Legacy seasonal cruise Q3 (August 5–27, 2019; Jordà-Molina et al., 2024, using mesh size of 500 µm); macrofauna data at stations P8–P11 can be found in Bluhm et al. (2023). (b) Sediment community oxygen demand (mmol m^{-2} d^{-1}), average of 3–5 replicates. The different treatments included (i) ambient temperature, no food added, (ii) 30 mg of added algae per core, run at ambient temperature, (iii) increased temperature (ambient temperature + 2°C), and (iv) the combined increase of temperature (ambient + 2°C) and food availability (30 mg of added algae). (c) Carbon ($\delta^{13}C$, ‰) and nitrogen stable isotope compositions ($\delta^{15}N$, ‰) in ice-associated particulate organic matter (iPOM; $n = 9$), pelagic POM (pPOM; $n = 30$), sediment POM (sPOM in top 0–1 cm of sediment; $n = 14$), benthic fauna ($n = 38$), and pelagic fauna ($n = 77$) sampled in the Nansen Basin (NB), at the Gakkel Ridge (GR), and in the Amundsen Basin (AB). Error bars indicate ±1 SD‰. Isotopic data of sea ice, seawater, and invertebrates are published in Ziegler et al. (2024a, 2024b, 2024c), respectively; isotopic data of sediments can be found in Hess et al. (2024). Figure prepared in Software R (v4.1.0; R Core Team, 2021), using the ggplot2 package (Wickham, 2016).

meiofaunal taxa, namely nematodes and harpacticoid copepods (arthropods), the latter of which contributed most at P10.

3.2.5.2. SOD

At all stations, SOD of ambient sediment was low and experimental treatments resulted in increases to the rates (**Figure 14b** and Table S8). Added algal food alone did not significantly alter SOD rates at any of the stations, while the temperature treatment alone significantly increased SOD rates at the Amundsen Basin stations (up to approximately 8-fold higher) but not significantly at the Nansen Basin stations. The combined increase of temperature and food resulted in higher SOD rates compared to either factor taken individually but increases were only statistically significant at one Nansen Basin station (P7, approximately 15-fold higher) and one Amundsen Basin station (P10, approximately 22-fold higher).

3.2.6. Food-web structure

The $\delta^{13}C$ and $\delta^{15}N$ values of carbon sources (iPOM, pPOM) clearly differed from each other. Both mean $\delta^{13}C$ and $\delta^{15}N$ values as well as C:N ratios were higher in iPOM ($\delta^{13}C = -25.7 \pm 2.7$‰, $\delta^{15}N = 5.5 \pm 0.9$‰, C:N = 24.2 ± 1.9) than in pPOM ($\delta^{13}C = -28.8 \pm 1.0$‰, $\delta^{15}N = 4.1 \pm 2.0$‰, C:N = 13.7 ± 5.0; **Figure 14c**). This difference was driven in part by iPOM samples from P9 that had higher $\delta^{13}C$ and $\delta^{15}N$ values than the other ice samples (Table S6). In pPOM, $\delta^{13}C$ values at P7 and P11 were higher, and C:N ratios lower, compared to the other stations, while $\delta^{15}N$ was lower at P8. Particularly at P9, both $\delta^{13}C$ and $\delta^{15}N$ values showed large variation. Overall,

pPOM $\delta^{15}N$ values were higher at the Gakkel Ridge and Amundsen Basin stations than in the Nansen Basin. Mean $\delta^{13}C$ of sPOM was by far higher than mean values of iPOM and pPOM, suggesting substantial microbial reworking during sedimentation of POM from the surface. There was very little variation among individual sPOM values. Notably, at P9, sPOM isotopic composition was very similar to that of iPOM (**Figure 14c** and Table S6).

The $\delta^{13}C$ values in zooplankton (average of –25.4 ± 1.7‰) varied relatively little among the different taxa, with averages ranging from –26.3 ± 2.5‰ in molluscs to –24.3 ± 1.6‰ in cnidarians (Figure S8a). Average $\delta^{15}N$ values (10.4 ± 2.1‰) varied from 8.7 ± 1.3‰ in chaetognaths to 11.0 ± 2.1‰ in cnidarians (Figure S8a) and were higher in animals from the Gakkel Ridge and the two Amundsen Basin stations compared to station P7 (Figure S8b). Zooplankton at P7 had distinctly higher $\delta^{13}C$ values (average of –23.5 ± 1.3‰) with lower $\delta^{15}N$ values (average of 7.2 ± 0.9‰) compared to the other stations (Figure S8b), but we could not identify a clear basin-specific pattern.

As expected, benthic fauna had on average the highest $\delta^{13}C$ (–19.5 ± 4.3‰) and $\delta^{15}N$ (11.1 ± 3.6‰) values among all investigated sample types, though interestingly $\delta^{15}N$ largely overlapped with those of zooplankton taxa (**Figure 14c**). Among the benthic taxa (Figure S8c), foraminifers showed the lowest $\delta^{13}C$ values (–25.9 ± 1.6‰) and echinoderms the highest $\delta^{13}C$ values (–11.7 ± 2.6‰; possibly as a result of consuming strongly reworked sediment), while the remaining three taxa showed little variation in their $\delta^{13}C$ composition. The $\delta^{15}N$ values were higher in porifers (14.6 ± 1.7‰) and echinoderms (13.8 ± 1.2‰) than in other taxa (averages of 5.2–10.9‰). There was no difference in average $\delta^{13}C$ of the benthic macrofauna between the Nansen Basin, Gakkel Ridge, and Amundsen Basin, though $\delta^{15}N$ values were overall slightly lower at the Gakkel Ridge (Figure S8d).

4. Discussion

During our sampling campaign, we observed distinct differences between the Nansen and Amundsen basins in hydrographic and various chemical and biological characteristics of the water column (**Table 2**) which largely confirmed observations from studies going back to the 1980s (syntheses in Bluhm et al., 2011; Kosobokova et al., 2011; Bluhm et al., 2015; Nöthig et al., 2020a; Wiedmann et al., 2020; Skjoldal, 2022; Vedenin et al., 2022). Physico-chemical differences were reflected to some degree in biological stocks, taxon composition, and biological activity, primarily in the water column and partly at the seafloor. Stocks and rates were generally highest nearest to the AW inflow at the southernmost open-water station P7 and declined with increasing distance from the advective inputs northward into the Amundsen

Table 2. Main similarities and differences in sea ice and upper ocean physical, chemical, and biological properties between the Nansen Basin (NB) and Amundsen Basin (AB) in this study

	Basin Comparison	
Properties	**Similarities[a]**	**Differences[b]**
Sea-ice conditions	Mixture of ice types (FYI, MYI, ridged floes)	Heavily deformed ridged ice in AB; larger snow depth and ice thickness in AB and GR
Water-mass characteristics	Cold and fresher surface layer above warmer and saltier intermediate and deep waters	Southern NB: AW inflow; NB warmer, saltier, more turbulent than AB; TPD and river inflow signal in AB
Nutrient concentrations	Sea ice: Large variability among stations rather than between basins; water column: highest concentrations >2,000 m	Sea ice: no clear basin-specific differences; water column: nitrate concentrations higher in NB, silicate concentrations higher in AB
Primary production	Generally low levels	Sea ice: higher productivity at P8 versus AB stations; water column: higher productivity in NB (particularly P7)
Protist communities	Sea ice: dominated by diatoms; water column: dominated by flagellates	Sea ice: no clear basin-specific differences, but abundances higher at P8 than AB; water column: abundances higher in NB
Sea-ice meiofauna	Dominance of pelagic taxa (ciliates, rotifers); high abundance of eggs	No clear basin-specific differences, but higher abundance and diversity at GR than both basins
Zooplankton communities	Overall low abundances; low taxonomic diversity in upper ocean; few taxa dominant by abundance or biomass; species range expansion	Higher abundance and biomass of Atlantic species in NB but virtually absent in AB; more diverse macrozooplankton fauna in NB
Benthic communities	Generally low abundances; dominance of small, meiofaunal taxa at P8–P11	Higher abundance and diversity at P7 (NB)
Food-web structure	Typical trophic structure yet strong overlap of pelagic and benthic taxa	Zooplankton: differences in food-source use at P7 (NB); benthic fauna: generally no clear basin-specific differences
Sediment properties	TOC and TN generally low	High TOC and chl *a* concentrations at P7 (NB)

[a]First-year ice (FYI), multiyear ice (MYI), total organic carbon (TOC), total nitrogen (TN).

[b]Atlantic Water (AW), Gakkel Ridge (GR), Transpolar Drift (TPD).

Basin, where instead, distinct signals of the TPD were observed at the surface. A number of ecosystem differences between the two basins persisted, however, when excluding the area of the southern Nansen Basin (**Figure 6**). Ice-associated chemical and biological properties, in contrast, differed among stations, likely as a result of differences in ice-drift trajectories and history and/or differences in bottom-ice melt stages with subsequent loss of biomass; they did not show a clear latitudinal or basin-related pattern. The general sea-ice situation, however, was typical for the area for the time of year with open water in the southern Nansen Basin and increasingly heavy ice cover in the Amundsen Basin.

Multidisciplinary studies like ours are the first step toward an overarching assessment of ecosystem structure and functioning in the Eurasian Basin of the CAO to improve predictions of future changes to these ecosystems (e.g., Fong et al., 2024). Information about physical conditions and climate change-driven changes in the sea-ice and pelagic environments of the CAO are increasingly available (e.g., Lei et al., 2018; Krumpen et al., 2019; Polyakov et al., 2020; Nicolaus et. al, 2022; Rabe et al., 2022). They point toward a slight increase in salinity and temperature in the Eurasian Basin leading to a reduced stratification in this previously considered "quiescent" basin (Polyakov et al., 2020). A notable decline in ice extent and thickness in the CAO is now well documented, associated in particular with a loss of MYI (Polyakov et al., 2012; Stroeve and Notz, 2018) and pronounced variations in the strength of the TPD for sea ice (Krumpen et al., 2019). However, data about biological community compositions and activities, driven by environmental conditions and impacts of environmental change on the distribution and structure of these faunal communities are more limited in overall spatial coverage. Collectively, however, they have provided a basic understanding of system functioning based on markedly lower stocks and productivity compared to adjacent shelves (e.g., Kröncke, 1994; Melnikov, 1997; Kröncke, 1998; Mumm et al., 1998; Kosobokova et al., 2011; David et al., 2015; Snoeijs-Leijonmalm et al., 2021; Fong et al., 2024). Our results largely confirmed the general physico-chemical as well as biological features of the study region at this time of year (approximately July to September), though a few indicator species may suggest an increasing presence of boreal taxa in the water column.

4.1. The Nansen Basin: Shaped by AW inflow especially at its southern margin

Our hydrographic observations across the western Nansen and Amundsen basins covered the known different oceanographic regimes of the two basins (**Table 2**; Rudels et al., 2013; Timmermans and Marshall, 2020; Rudels and Carmack, 2022). The southern part of the Nansen Basin at the open-water station P7 was most strongly characterized by the influence of the AW inflow with comparatively high temperature and salinity and elevated nitrate concentrations (**Figures 4** and **5**), consistent with, for example, Polyakov et al. (2020) and Renner et al. (2023). Toward the Gakkel Ridge, the AW layer became colder and fresher, but along with the surface layer, remained warmer and more saline than in the Amundsen Basin, which is consistent with the previously reported recirculation of the Fram Strait branch of the AW inflow (Schauer et al., 2002; Rudels et al., 2013). The higher nitrate concentrations in the AW layer and the weaker stratification also beyond P7 enabled an order of magnitude higher vertical nitrate fluxes in the Nansen Basin (up to 2×10^{-3} µmol m^{-2} s^{-1}) than in the AB (0.3×10^{-3} µmol m^{-2} s^{-1}; **Figure 7e** and **7f**), comparable to estimates by Randelhoff et al. (2020), leading to more efficient replenishment of mixed layer nitrate in the Nansen Basin than in the Amundsen Basin.

The hydrographic conditions combined with the quasi-continuous advective supply of nitrate, particles, and heat in the AW inflow region were reflected in the biological patterns of the water column with somewhat higher stocks and rates at Nansen Basin stations (with noteworthy exceptions) that were driven by the core of the AW inflow at P7. Pelagic primary production and surface algal biomass were higher in the AW inflow region at P7 compared to the Gakkel Ridge and Amundsen Basin sites, which was also reflected in the lower DIC values due to biological CO_2 drawdown. While our measured primary productivity level would have been somewhat exaggerated by seasonally decreasing light levels over the course of the expedition and were too few to establish a region-wide pattern, our findings are in agreement with previously established patterns of higher production along the AW inflow path at the perimeter of the Nansen Basin (Slagstad et al., 2011; 2015), which keeps this area ice-free much longer and comparatively irradiance-richer than the remaining transect. Our data and earlier studies indicate higher algal production and biomass at the southern Nansen Basin perimeter being linked to higher stocks and/or biological activity of pelagic consumers in that region (Kosobokova et al., 2011; Wassmann et al., 2015; Basedow et al., 2018; Hop et al., 2019; Ehrlich et al., 2021). This pattern suggests differences in ecosystem carrying capacity between the southern Nansen Basin and the Amundsen Basin, and also stresses that the inflow area around P7 is not representative of the Nansen Basin proper. In addition to affecting pelagic stocks, the strong influence of AW in this region is also reflected in taxonomic composition with particular AW indicator taxa, again consistent with previous observations as will be discussed below in this section.

Regarding the microbial components, both abundances and process rates were generally higher in the Nansen Basin than in the Amundsen Basin (for bacterial counts, see Bratbak et al., 2023), agreeing with previous literature (e.g., Ulfsbo et al., 2014; Lalande et al., 2019; Piontek et al., 2021). Specifically, abundances of bacteria, pico- and nanophytoplankton, cryptophytes and large viruses, as well as BP in surface waters (0–30 m), were on average two to five times higher in the Nansen Basin compared to the Amundsen Basin (**Figure 12a**–**12c**; datasets, also including NLEG stations, in Bratbak et al., 2023; Müller et al., 2023b) and comparable to values that have been reported before (August 2014) further south (around 82°N) at the West Spitsbergen Current southern branch into the Arctic Ocean (Paulsen et al., 2016; 2017). The abundances of HNF and small viruses, however, did not

show the same trend as the other microbial components, as they were not clearly different between basins. Different water masses having different origins and "biological history" may be the simplest explanation, but speculation that larger viruses, presumably infecting phytoplankton, play a more prominent role in the microbial food web of the Nansen Basin is tempting. Consistent with the earlier assignment of *Synechococcus* as an indicator of AW advection (Paulsen et al., 2016; Schmidt et al., 2020), abundance of this cyanobacterium was highest at P7 (37 m, 10 cells mL^{-1}), though overall very low compared to previous reports further south, while concentrations were below the detection limit (<5 cells mL^{-1}) at most other stations. Picophytoplankton generally exhibited highest abundances in the upper 30 m, while nanophytoplankton showed deeper maxima, similar to reports from ice-covered areas in the Canadian Arctic (Ribeiro et al., 2022).

Overall, pelagic protist communities showed a numerical dominance of flagellates at all stations and had distinct abundance maxima at the surface (**Figure 12d**; consistent with Gosselin et al., 1997; Sherr et al., 2003; Schanke et al., 2021). While this situation is interpreted as a summer stage in shelf regions (Assmy et al., 2023; Kohlbach et al., 2023), the phenology of bloom stages in the CAO is not well established. Though diatoms were generally low in abundance, their relatively higher contribution at P7 was indicative of contributions from the adjacent productive shelf and the vicinity to the AW inflow. Despite the overall low diatom abundance, chl *a* concentrations largely followed the vertical distribution of diatoms, and not that of total protist abundances, suggesting that a relatively large fraction of the protists belonged to heterotrophic taxa. In agreement with higher nitrate concentrations and fluxes and the slightly elevated contribution of diatoms at P7, pelagic NPP was highest at this station near the AW inflow (**Figure 11b**). Though NPP estimates based on in situ incubations depend on light availability during the incubations, limiting comparability, maximum integrated NPP values were on the same order of magnitude as reported earlier for roughly the same time of year (July–August) from the Nansen Basin (409 mg C m^{-2} d^{-1} in the present study versus 521 mg C m^{-2} d^{-1} by Gosselin et al., 1997). The absence of ice at P7 (as is typical for that region in fall) and thinner ice cover at P8 compared to Amundsen Basin stations resulted in lower or no light limitation, also reflected in patterns of POC, PN, and chl *a* concentrations as well as vertical flux rates (**Figures 9** and **12d** and **12e**). While ice conditions are a temporal snapshot, the prevalent conditions do reflect the ice conditions typical of the region in today's Arctic, namely of open water in the southern Nansen Basin and a seasonal, thinner ice cover in much of the Nansen Basin than the region of the Amundsen Basin north of Greenland that we studied (Meier and Stroeve, 2022; Sumata et al., 2023).

For both meso- and macrozooplankton, their peaks in abundance nearest to the AW inflow at station P7 (**Figure 13**) reflect the well-established effects of advection of zooplankton with AW masses and higher levels of phytoplankton (for herbivorous/omnivorous species) and prey (for carnivorous species) in the water column (e.g., Kosobokova et al., 2011; Wassmann et al., 2015; Basedow et al., 2018; Ehrlich et al., 2021). In agreement with the literature, *Calanus* copepods, *Metridia longa*, chaetognaths, cnidarians, ctenophores, and amphipods were abundant taxa in the slope region that, again, is characterized by long periods of open water (Mumm et al., 1998; Blachowiak-Samolyk et al., 2008; Kosobokova and Hirche, 2009). While the Atlantic *C. finmarchicus* was only abundant at P7, *C. glacialis* and *C. hyperboreus* were found at all stations but decreased in abundance from the Nansen Basin to the Amundsen Basin (**Figure 13b**). The basin-wide importance of small copepod species as well as the role of *C. finmarchicus* being restricted to slope regions has been described since the 1980s (Hirche and Mumm, 1992; Mumm, 1993; Thibault et al., 1999; Auel and Hagen, 2002). However, the numerical predominance of small copepod species such as *Oithona similis*, *Triconia borealis*, and other Oncaeidae species could only be well evaluated since plankton nets with finer mesh size were used in the study area (Groendahl and Hernroth, 1986; Svensen et al., 2019; Barth-Jensen et al., 2022; this study). Macrozooplankton trawls yielded basin-specific differences in macrozooplankton compositions: euphausiids, amphipods, and gelatinous zooplankton dominated the catch in the Nansen Basin, while euphausiids were virtually absent and ctenophores (*Mertensia ovum* and *Beroe* spp.) were numerically important in the Amundsen Basin (**Figure 13d**–**13f**; see Ingvaldsen et al., 2023, for details). Observations of a few, yet noteworthy, Atlantic and/or boreal species in the Nansen Basin possibly give support, albeit meager, to the predicted poleward range extension of temperate species (Ingvaldsen et al., 2023): the northernmost records of (i) the warm-water associated (sub-tropical temperate) krill species *Hansarsia megalops* (= *Nematoscelis megalops*; over Gakkel Ridge), whose changes in biogeography have also been described previously (Zhukova et al., 2009; Huenerlage and Buchholz, 2015); (ii) a young Greenland halibut *Reinhardtius hippoglossoides*; and (iii) the cosmopolitan deep-water jellyfish *Periphylla periphylla*, which has been speculated to expand its distribution northward (Geoffroy et al., 2018). Many of these species are understudied, with their distributions largely unknown; therefore, a more extensive study is essential to unveil their current distribution patterns and potential changes in them.

Due to the challenges of operating fishing gear in the CAO, the historical data for comparison of possible pelagic fish stocks, including fish larvae, is very limited. Yet, the few existing studies are in agreement with our finding that the density of pelagic fishes is apparently (very) low in both basins (Gradinger and Bluhm, 2004; David et al., 2016, Snoeijs-Leijonmalm et al., 2021) beyond the AW inflow area just north of Svalbard. We caught only a total of seven individuals of three species, namely the endemic polar cod *Boreogadus saida*, the single species for which the distribution in the Eurasian Basin is comparatively better studied (David et al., 2016), the glacier lantern fish *Benthosema glaciale*, and the perhaps northward-expanding Greenland halibut *R. hippoglossoides* (Ingvaldsen et al., 2023). Previously, young Greenland halibut have been observed to concentrate in the AW core closer to the

continental slope as far east as the St. Anna and Voronin Troughs, where they fed primarily on polar cod (Dolgov and Benzik, 2017). Modeling suggests possible suitable habitat around the Arctic and northward expansion of this species related to ice decline and changes in productivity, but depth limitation makes it unlikely that the basins per se will be populated, though larvae may drift into the basins (Vihtakari et al., 2021).

At the seafloor, the most distinct difference between stations was that the maximum TOC and sediment chl *a* concentrations were observed at P7 (**Figure 8b**), which were similar to concentrations observed during four other seasons at this and nearby stations (Ricardo de Freitas et al., 2024). These elevated values indicate higher food availability for the benthic community under the AW inflow, also evident in the highest vertical carbon flux (**Figure 12e**) and reflected by the higher abundance of macrofaunal organisms at this site (**Figure 14a**), though being distinctly lower than on the adjacent shelf (Jordà-Molina et al., 2023). The increased $\delta^{13}C$ values of sPOM compared to iPOM and pPOM reflected earlier findings that particles are substantially degraded and remineralized during sinking through the water column to great depths (Wassmann et al., 1991; Iken et al., 2005; Zhulay et al., 2023). Whereas annelids numerically dominated (in spring co-dominating with molluscs) both shelf communities and P7 year-round (Jordà-Molina et al., 2023), their abundance dropped by an order of magnitude away from the shelf break in both basins. On the other hand, the numerical importance of nematodes today and in the past (Pfannkuche and Thiel, 1987; Soltwedel et al., 2000; Vanreusel et al., 2000; Schewe, 2001) indicates stability in benthic community structure in the central Arctic at a coarse level. While our benthic dataset is too small to compare taxonomic specificities between basins, earlier compilations have shown that seafloor ridges in the CAO do not generally appear to prevent benthic taxa from dispersing into a neighboring basin (Bluhm et al., 2011; Vedenin et al., 2022; Ramirez-Llodra et al., 2024).

Isotopic compositions indicated a typical food-web structure found in Arctic ecosystems: decreasing $\delta^{13}C$ values from sPOM *via* iPOM to pPOM and generally higher $\delta^{13}C$ values in benthic compared to pelagic fauna as a result of the highly reworked organic material at the seafloor (e.g., Iken et al., 2001; Hobson et al., 2002; Iken et al., 2005; Tamelander et al., 2006; Bergmann et al., 2009; Zhulay et al., 2023; **Figure 14c**). Largely overlapping $\delta^{13}C$ signatures among different zooplankton taxa and across multiple trophic levels suggest similarities in food-source use between different taxonomic groups, which was also robust across the ice-covered stations in both basins (Figure S8a and b). While zooplankton $\delta^{13}C$ values at stations P8–P11 were relatively similar, zooplankton (and pPOM) in the southern Nansen Basin (P7) exhibited, on average, higher $\delta^{13}C$ values in comparison to the other stations, carrying the (pelagic) signal of a different dietary composition than animals further north at the ice-covered stations. Interestingly, this signal did not seem to be transferred to the seafloor, as neither sPOM nor the benthic fauna had clearly different isotopic compositions in the southern Nansen Basin compared to farther north. Despite highest vertical cell flux rates at P7, these decoupled isotopic signatures indicate weak pelagic-benthic coupling at this station, likely as a result of the high biological interception at P7 due to higher grazer stocks, allowing only a small portion of organic material to reach the seabed. Events of fast sinking material (e.g., sea-ice associated *Melosira arctica*), however, have been documented in the CAO (Boetius et al., 2013) but are generally rather ephemeral and were likely not captured by our sediment traps. The overall lowest, albeit highly variable, $\delta^{13}C$ values among the zooplankton were observed in *Clione limacina* (sea butterfly), pointing to a larger pelagic component in its diet in comparison to other taxa. The $\delta^{13}C$ values were more closely resembling that of pPOM, consistent with previous findings for these pteropods in the CAO (Kohlbach et al., 2016). *C. limacina* from the seasonally ice-covered Barents Sea, however, was found to also utilize sympagic food (Kohlbach et al., 2021), and juveniles of this species were in fact present in the ice in our study, suggesting a general dietary plasticity and opportunistic feeding behavior for this species. Pronounced differences in carbon and nitrogen isotopic values among the benthic taxa (Figure S8c) mirrored their more diverse trophic pathways and feeding strategies compared to pelagic species (Iken et al., 2005; Bergmann et al., 2009).

4.2. The Amundsen Basin: Signals of the TPD and weaker AW influence

Amundsen Basin stations showed both signals of the TPD and a weakened influence of AW, confirming observations reported by Schulz et al. (2024). The AW layer was colder and fresher than in the Nansen Basin, indicating that the AW was mostly sourced from the Barents Sea branch of the AW inflow as suggested by, for example, Rudels et al. (2013) and Schulz et al. (2024), and transformed along its path to the Amundsen Basin. Above the AW layer in the upper 50–100 m, the low surface salinity and higher silicate concentrations (**Figures 4b** and **5b**) as well as higher silicate:nitrate and silicate:phosphate ratios (Figure S4) in the Amundsen Basin compared to the Nansen Basin were consistent with the river-influenced TPD containing high concentrations of silicate (Olsson and Anderson, 1997; Flores et al., 2019; Tank et al., 2023). Indeed, upper ocean samples (upper approximately 100 m) for CDOM and FDOM in the Amundsen Basin (only from stations NLEG35, P10, and P11) showed elevated levels of CDOM absorption and humic-like FDOM, indicative of a distinct terrestrial/riverine signal (compared to Charette et al., 2020; Stedmon et al., 2021). The CDOM and FDOM levels in the Amundsen Basin (about 0.8 m^{-1} and 0.05 RU, respectively) were on par with what has been found in the Arctic outflow in western Fram Strait (East Greenland Current), and distinctively higher-than-typical values of 0.15 m^{-1} and 0.02 RU found in the AW dominated parts in the Nansen Basin and eastern Fram Strait (Pavlov et al., 2015; Kowalczuk et al., 2017; Stedmon et al., 2021). At the stations in the Amundsen Basin, the very surface concentrations had also apparently been diluted by sea-ice

meltwater, which, on average, had lower concentrations of these constituents than the TPD waters.

Basin-scale nitrate gradients seen in our dataset, while perhaps somewhat biased by a two-week time lag in sampling, have previously been interpreted as being driven by advection of relatively nitrate-rich AW in the Nansen Basin and strong and increasing haline stratification toward the Amundsen Basin (Bluhm et al., 2015; Randelhoff and Guthrie, 2016; Randelhoff et al., 2020). These settings may explain biological stocks and rates being somewhat lower in the Amundsen Basin than Nansen Basin (**Figures 11** and **12**), consistent with, for example, Ulfsbo et al. (2014), with these patterns likely being either responses to weakening AW influence and direct or indirect effects of riverine and terrestrial footprints related to the TPD. Unfortunately (for lack of sequencing data), we were unable to reveal distinct TPD signals in viral and bacterial communities based solely on abundance data.

We attribute the decline in pelagic protist abundance (**Figure 12d**), depth-integrated chl *a* standing stocks (factor of 3–10 lower 90 m-depth-integrated chl *a* in Amundsen Basin than Nansen Basin), and change in pelagic protist community composition from larger-sized diatoms toward smaller-sized flagellates largely to declining nutrient (nitrate) inventories from the shelf-slope station P7 toward the Amundsen Basin. The seasonal decline in light levels from August to September will have likely played an additional role. However, similar basin gradients in nutrient levels, phytoplankton production, biomass, and composition observed earlier in summer (July–August) 30 years ago (Gosselin et al., 1997) suggests that basin-scale nutrient status is likely one of the main drivers of pelagic ecosystem structure and has not changed dramatically over the era of rapid climate change. Nitrate concentrations are generally low in surface waters of the CAO (Bluhm et al., 2015; Ardyna et al., 2017) and in particular in the Amundsen Basin, where nitrate concentrations remain low (around 1 μM) during the winter (Fong et al., 2024). Hence, we consider that the oligotrophic conditions found in the Amundsen Basin are unlikely to be explained by the time of sampling (summer). Small-sized phytoplankton with a larger surface-to-volume ratio as well as taxa with mixo- or heterotrophic feeding modes are favored under such oligotrophic conditions (Litchman et al., 2007; Zhang et al., 2015; 2016; Wang et al., 2019), reflected in the increasing dominance of flagellates and mixo- and heterotrophic dinoflagellates toward the Amundsen Basin (**Figure 12d**). Accordingly, despite the overall decrease in phytoplankton abundance from the Nansen Basin to the Amundsen Basin, the proportion of flagellates relative to large-sized diatoms increased toward the Amundsen Basin (**Figure 12d**).

In line with the base of the food web, zooplankton densities also generally decreased with latitude toward the Amundsen Basin and species composition changed along the transect (**Figure 13**). Specifically, *Calanus finmarchicus* was virtually absent from the Amundsen Basin stations, although that species does track the Arctic Circumpolar Boundary Current all the way to the East Siberian Sea (Ershova et al., 2021). In previous investigations, *Oithona similis*, *Triconia borealis*, and *Microcalanus* spp. have been reported as the most abundant species in the CAO (Auel and Hagen, 2002; Kosobokova et al., 2011). However, in the present study, the family Oncaeidae had high and persistent abundances stretching into the Amundsen Basin. Whether this new observation is due to environmental factors or because we sampled with a smaller mesh size than what has been used in earlier investigations is not clear. Fish densities were too low to detect any clear patterns, yet visual observations of overturned ice floes along the cruise track, also in the Nansen Basin, indicated that *Boreogadus saida* was regularly present, albeit not numerous, immediately under the sea ice, the known habitat for young fish age classes (Gradinger and Bluhm, 2004; David et al., 2016; Geoffroy et al., 2023). This habitat is notoriously difficult to sample with nets, though an under-ice trawl has successfully produced estimates of young *B. saida* under the ice across the Eurasian Basin where they were encountered at virtually all sample locations (David et al., 2016). These findings and our anecdotal evidence are consistent with our observations of a handful of seals, prominent predators of *B. saida*, in leads across the study region.

At the seafloor, both the surface sediment TOC and chl *a* concentrations were considerably lower at station P8 and in the Amundsen Basin compared to P7 closer to the shelf break (**Figure 8b**), consistent with previous observations in the region (Stein et al., 1994; Boetius et al., 1996). This low amount of available organic matter in the sediments was no surprise given the low sympagic and pelagic algal biomass and production in the Amundsen Basin and the consequently low quantity of food reaching the seafloor. The somewhat higher pelagic stocks at P8 than in the Amundsen Basin did not translate into higher biomass, but too few stations do not allow establishing a pattern. Benthic macrofaunal abundance was low, away from the slope (consistent with Oleszczuk et al., 2021), and in both basins outside P7 small meiofaunal taxa dominated (**Figure 14a**); this relatively increasing role of small taxa is a general feature of the global deep sea (Rex et al., 2006; Wei et al., 2010). The overall low benthic faunal biomass was further corroborated by the basin-wide low SOD under ambient conditions (**Figure 14b**) compared to shallower and more productive shelf regions (Bourgeois et al., 2017, and references therein), which was further in agreement with the absence of enhanced flux events over the Amundsen Basin. In both basins, respiration rates increased with experimentally increased temperature, added food, and both combined; however, the increases were in most cases not significantly different from ambient rates. The lack of a stronger response to food addition was likely the result of the overall low benthic biomass; even if the animals responded, overall rates were not much higher because so little faunal biomass was present at the start.

4.3. Sea-ice characteristics follow a different non basin-specific pattern

Sea-ice back trajectories suggest that the origin of ice floes sampled at stations P8, P10, and P11 differed from the

origin of the floe at P9 (**Figure 2b**). Whether this difference in origin is true or a consequence of the high uncertainty of the backtracking method is unclear, because calculated trajectories do not necessarily represent the correct or precise behavior and drift history of a sampled ice floe, but rather a single possible realization of the floe path within a large probability space (Down et al., 2023). Regardless, the shorter trajectory is in contradiction to the ice thickness of the floe at P9 (approximately 1.8 m) exceeding that of all other stations (<1.4 m; Table S1) and may explain its different physico-chemical and biological properties. Sympagic protists and meiofauna were more abundant and compositionally different at P9 compared to the other stations in both basins (**Figure 10c** and **10d**). Concentrations of nitrate and phosphate at P9 were lower in the top ice than in the ice cores at other stations, and nitrate was homogeneously distributed throughout the ice, which was not observed elsewhere (**Figure 3d** and **3f**). These described differences in sea-ice related biological properties were not likely caused by the presence of the Gakkel Ridge, given that we did not observe any enhanced biological stocks or rates in the water column or the benthic environment at the ridge. These results indicate different drivers of variability for the sea ice versus pelagic and benthic environments observed in our study (i.e., ice history versus water-mass characteristics).

In contrast to the water column, at all four ice stations, diatoms were the most abundant protist taxa within the sea ice, confirming known sympagic protist community compositions from the CAO and other Arctic regions (Booth and Horner, 1997; Gosselin et al., 1997; Poulin et al., 2011; Hardge et al., 2017). There was a generally positive relationship between chl *a* concentration and diatom abundance, indicating that auto- and mixotrophic non-diatom taxa contributed little to the algal biomass. The centric sub-ice diatom *Melosira arctica*, previously described as a dominant ice-associated species in the CAO (Gosselin et al., 1997; Boetius et al., 2013), occurred infrequently in our samples, but their known patchy distribution could explain their low contribution.

Besides diatoms, flagellates, predominantly chrysophytes, also contributed substantially to the sympagic protist community at P8 and in a previous CAO study (Hardge et al., 2017). The lower protist abundance and algal biomass in the ice at P8 compared to P9 (**Figure 10c**) could be related to enhanced melting processes at this station consistent with the more southern location and with the lower sea-ice salinity in the thinner ice (<1 m) compared to all other locations (>1 m; Table S1). The lower $\delta^{13}C$ values of iPOM could be indicative of a pelagic signal as the result of enhanced mixing with the underlying water column (Loose et al., 2011) and, hence, phytoplankton, at this station. The dominance of the centric diatoms *Chaetoceros tenuissimus* and *Conticribra weissflogii*, both atypical sea-ice diatoms, at station P8 further agrees with documented changes in sea-ice protist community composition observed over the last 30 years from ice specialists toward more cryo-pelagic species as a result of the transition from a MYI- toward a FYI-dominated ice habitat (Hop et al., 2020). Protist taxon richness has been found to be higher in older than younger sea ice, associated with a decreasing uniqueness of ice protist communities relative to pelagic communities in today's Arctic compared to the past (Hop et al., 2020). Our limited sea-ice sample size, however, precludes confident assessment of these described trends.

The contribution of ice algal NPP to total NPP (<15%, decreasing from south to north) was much lower than from previous studies in the area at the end of the productive season (up to approximately 60%; Gosselin et al., 1997; Fernandez-Mendez et al., 2015). This difference from previous studies could be attributed to the use of different methodologies. Other possible explanations for the lower ice algal production fraction could be the early onset of sea-ice melt and retreat in the Laptev Sea in spring 2020 and 2021 (Perovich et al., 2020; Meier et al., 2021), the area where most of the ice from this study presumably originated, which might have triggered early melt-out of ice algae. These findings could be further indication for the recent suggestions that intensified melt in the CAO interrupts the TPD (Krumpen et al., 2019) and may decrease Arctic-wide connectivity in ice-associated ecosystems (Ehrlich et al., 2021). We caution, however, that different sample treatments could also be at least partly responsible for the large discrepancy between sympagic production contributions in this study and previous studies (e.g., Fernandez-Mendez et al., 2015).

Sea-ice meiofaunal communities were generally dominated by taxa of pelagic origin, namely large ciliates and rotifers, as described previously for recent Arctic meiofaunal communities (Bluhm et al., 2018, and references within; Ehrlich et al., 2020; Marquardt et al., 2023b). In addition, high numbers of metazoan eggs, nauplii, and juveniles of *Clione limacina* support the notion that sea ice is a nursery ground for early life stages of pelagic organisms (Schnack-Schiel, 2003; Bluhm et al., 2010). Orange Acoela (yet unidentified but called by that name since the 1990s), one of the few taxa of benthic origin and so far considered ice-obligate, were found in low numbers. These flatworms were a frequent contributor to Arctic sea-ice meiofauna several decades ago (Gradinger, 1999), but were absent or rare in more recent studies. One could speculate that this pattern is due to ongoing changes and loss of thick and old MYI with which they prefer to associate (Bluhm et al., 2018; Ehrlich et al., 2020; 2021). A similar pattern applies to another benthic taxon, the nematodes, which occur in high numbers in seasonally ice-covered Arctic regions (Gradinger, 1999; Nozais et al., 2001; Gradinger et al., 2005; 2010; Marquardt et al., 2011; Pitusi et al., 2023). Their virtual absence in more recent studies of offshore pack ice (Bluhm et al., 2018; Ehrlich et al., 2020; Marquardt et al., 2023b) again may indicate a shift in ice-faunal community structure with the transition from perennial to seasonal sea-ice cover. A link to the interruption of the TPD (Krumpen et al., 2019) has been suggested previously (Kiko et al., 2017; Ehrlich et al., 2020).

4.4. Outlook

The dramatic reduction of the sea-ice cover has already made the western Nansen and Amundsen basins

accessible for increased human activity. This development gives new prospects for shipping, resource extraction (fishery, deep-sea mining), and tourism in the region (Stevenson et al., 2019). The region is already influenced by fisheries along the continental slope (Misund et al., 2016; Haug et al., 2017) and ship traffic associated with tourism, military operations, and research activity (Stocker et al., 2020; Müller et al., 2023a). Furthermore, being in or near the Arctic gateway, the region is exposed to northward range expansions of boreal and/or invasive species (e.g., Brandt et al., 2023) and global (long-transported) impacts from stressors such as pollutants (e.g., Ross et al., 2021). Progressing ocean acidification due to increased ice loss represents an additional stressor for the ecosystem, in particular for calcifying organisms (Ericson et al., 2023). These changes clearly increase the pressures on vulnerable Arctic Ocean ecosystems and impose new challenges for their sustainable management (Huntington et al., 2022). The Central Arctic Ocean Fisheries Agreement prohibits commercial fisheries in the areas beyond national jurisdiction of the CAO until 2037 (Vylegzhanin et al., 2020). However, it also commits to the establishment of a Joint Program of Scientific Research and Monitoring to improve the understanding of the ecosystems (Balton, 2022). Our results contribute to building this knowledge. We show, consistent with earlier studies, that under current environmental conditions, that is, perennial ice cover, strong stratification, and limited nutrient availability, the production in the CAO is very low in comparison to slope regions and continental shelves (e.g., Snoeijs-Leijonmalm et al., 2021; Ingvaldsen et al., 2023). Other studies conclude that the predicted modest increase in primary and secondary production (Slagstad et al., 2015) also will be too low to sustain commercial fisheries in the future (Haug et al., 2017; Polyakov et al., 2020). Our results suggest further that basin-specific approaches for successful and sustainable management are required for this region. The distinctly higher biological activity at the AW-influenced station P7 compared to the rest of the sampling area provides evidence that monitoring stations located just north of Svalbard fall short of representing the ecosystem status and processes or responses to environmental change in the Eurasian Basin in its entity.

Data accessibility statement

The following datasets were generated:

- Abundances of viral particles, bacteria, pico- and nanoalgae in sea ice and water column: Bratbak et al. (2023). DOI: https://doi.org/10.21335/nmdc-911461071.
- Bacterial production in sea ice and water column: Müller et al. (2023b). DOI: https://doi.org/10.21335/NMDC-1815353537-2021710.
- Benthic communities: Bluhm et al. (2023). DOI: https://doi.org/10.15468/twumu2.
- Bulk stable isotopes of pelagic and benthic invertebrate fauna: Ziegler et al. (2024c). DOI: https://doi.org/10.21335/NMDC-1888717245.
- Chlorophyll *a* in sea ice and water column: Vader and Marquardt (2022). DOI: https://doi.org/10.21335/NMDC-1635641464.
- Chlorophyll *a* in sea-bottom sediments: Akvaplan-niva (2023). DOI: https://doi.org/10.11582/2023.00027.
- CTD data: Fransson (2022). DOI: https://doi.org/10.21335/NMDC-1814168447.
- Dissolved inorganic carbon (DIC) in (bulk) sea ice: Fransson et al. (2025a). DOI: https://doi.org/10.21334/npolar.2025.71dbfe18.
- Dissolved inorganic carbon (DIC) in water column: Chierici and Fransson (2025). DOI: https://doi.org/10.21334/npolar.2025.67b3ecbf.
- Dissolved inorganic nutrients in (bulk) sea ice: Fransson et al. (2025b). DOI: https://doi.org/10.21334/npolar.2025.96853520.
- Dissolved inorganic nutrients in water column: Chierici et al. (2025). DOI: https://doi.org/10.21334/npolar.2025.3b80fac9.
- Ice algal abundance and biodiversity: Assmy et al. (2022b). DOI: https://doi.org/10.21334/npolar.2022.5c2738dd.
- Microstructure profiler (MSS) profiles: Koenig et al. (2023a). DOI: https://doi.org/10.21334/npolar.2023.f09a8062.
- Particulate organic carbon and nitrogen (POC/PN) concentrations in sea ice and water column: Marquardt et al. (2022). DOI: https://doi.org/10.11582/2022.00051.
- Pelagic bulk stable isotopes (pPOM): Ziegler et al. (2024b). DOI: https://doi.org/10.21335/NMDC-1380716613.
- Phytoplankton abundances and biodiversity: Assmy et al. (2022a). DOI: https://doi.org/10.21334/npolar.2022.b7aae0e9.
- Sea-bottom sediment properties: Hess et al. (2024). DOI: https://doi.org/10.21335/NMDC-962959866.
- Sea-ice bulk stable isotopes (iPOM): Ziegler et al. (2024a). DOI: https://doi.org/10.21335/NMDC-245429765.
- Sea-ice concentrations: Steer and Divine (2023). DOI: https://doi.org/10.21334/npolar.2023.24f2939c.
- Sea-ice meiofauna communities: Marquardt et al. (2023a). DOI: https://doi.org/10.15468/dfz5gb.

Supplemental files

The supplemental files for this article can be found as follows:

Figures S1–S8. Tables S1–S8. Text S1. Docx

Acknowledgments

The authors would like to thank the captain and the crew of RV *Kronprins Haakon* for their excellent support at sea during the Nansen Legacy expedition JC2-2. We would like to thank NPI logistics in Longyearbyen, Marius Bratrein (NPI), Eirik Hellerud (NPI), and Kunuk Lennert (UiT) for logistics, safety courses, field support, and safety on the sea ice. We thank the helicopter crew (Airlift) for the flights to obtain large-scale ice observations. We further would

like to thank Adam Steer (then NPI) for his help with the sea-ice characterization, Signe Aaboe (Meteorological Institute) for support with the ice-floe tracking, and Irina Zhulay (then UiT) for sorting macrobenthos samples. Thanks are due to Antje Hofgaard and the electron microscopy unit at the Department of Biosciences at the University of Oslo for their assistance with the preparation and imaging of specimens. MAG acknowledges support from the Hanse-Wissenschaftskolleg (Delmenhorst, Germany). We thank the editor and the three reviewers for their helpful comments and suggestions during the review process. The publication charges for this article have been funded by a grant from the publication fund of UiT, The Arctic University of Norway.

Funding

This work was funded by the Research Council of Norway through the project The Nansen Legacy (RCN # 276730). DK is currently funded by the German Helmholtz Association Initiative and Networking Fund (Helmholtz Young Investigator Group Double-Trouble).

Competing interests

The authors declare that the research was conducted in the absence of any commercial or financial relationships that could be construed as a potential conflict of interest.

Author contributions

Contributed to conception and design (alphabetical order): AF, BAB, DK, KMA, MAG.
Contributed to acquisition of data (alphabetical order): AC, AF, AS, AV, AW, AZ, BAB, BR, CS, DVD, IVN, JG, KMA, MAA, MC, MM, MO, MZ, OM, ØF, RBI, RRG, SM, SV, TRdF, WE, ZK, ZS.
Contributed to analysis and interpretation of data (alphabetical order): AC, AF, AHHR, AS, AV, AW, AZ, BAB, CS, DVD, DK, ED, GB, KMA, MAA, MAG, MC, MM, OM, ØF, PA, PR, RBI, RRG, SH, SK, TRdF, WE, ZK, ZS.
Drafted and/or revised the article: All authors.
Approved the submitted version for publication: All authors.

References

Ahme, A, **Von Jackowski, A**, **McPherson, RA**, **Wolf, KK**, **Hoppmann, M**, **Neuhaus, S**, **John, U.** 2023. Winners and losers of Atlantification: The degree of ocean warming affects the structure of Arctic microbial communities. *Genes* **14**(3): 623. DOI: http://dx.doi.org/10.3390/genes14030623.

Aksenov, PV, **Ivanov, VV.** 2018. "Atlantification" as a possible cause for reducing of the sea-ice cover in the Nansen Basin in winter. *Arctic and Antarctic Research* **64**(1): 42–54. DOI: http://dx.doi.org/10.30758/0555-2648-2018-64-1-42-54.

Akvaplan-niva**.** 2023. Nansen Legacy sediment pigment data JC2-2 [dataset]. Norstore. DOI: https://doi.org/10.11582/2023.00027.

Ardyna, M, **Babin, M**, **Devred, E**, **Forest, A**, **Gosselin, M**, **Raimbault, P**, **Tremblay, J-É.** 2017. Shelf-basin gradients shape ecological phytoplankton niches and community composition in the coastal Arctic Ocean (Beaufort Sea). *Limnology and Oceanography* **62**(5): 2113–2132. DOI: http://dx.doi.org/10.1002/lno.10554.

Assmy, P, **Gradinger, R**, **Edvardsen, B**, **Wold, A**, **Wiktor, J**, **Tatarek, A**, **Smola, Z**, **Goraguer, L.** 2022a. Phytoplankton biodiversity Nansen Legacy JC2-2 [dataset]. Norwegian Polar Institute. DOI: https://doi.org/10.21334/npolar.2022.b7aae0e9.

Assmy, P, **Kvernvik, AC**, **Hop, H**, **Hoppe, CJ**, **Chierici, M**, **Duarte, P**, **Fransson, A**, **García, LM**, **Patuła, W**, **Kwaśniewski, S**, **Maturilli, M**, **Pavlova, O**, **Tatarek, A**, **Wiktor, JM**, **Wold, A**, **Wolf, KKE**, **Bailey, A.** 2023. Seasonal plankton dynamics in Kongsfjorden during two years of contrasting environmental conditions. *Progress in Oceanography* **213**: 102996. DOI: http://dx.doi.org/10.1016/j.pocean.2023.102996.

Assmy, P, **Wold, A**, **Gradinger, R**, **Edvardsen, B**, **Wiktor, J**, **Tatarek, A**, **Goraguer, L.** 2022b. Ice algae biodiversity Nansen Legacy JC2-2 [dataset]. Norwegian Polar Institute. DOI: https://doi.org/10.21334/npolar.2022.5c2738dd.

Auel, H, **Hagen, W.** 2002. Mesozooplankton community structure, abundance and biomass in the central Arctic Ocean. *Marine Biology* **140**: 1013–1021. DOI: http://dx.doi.org/10.1007/s00227-001-0775-4.

Backstrom, LG, **Eicken, H.** 2006. Capacitance probe measurements of brine volume and bulk salinity in first-year sea ice. *Cold Regions Science and Technology* **46**(3): 167–180. DOI: http://dx.doi.org/10.1016/j.coldregions.2006.08.018.

Balton, D. 2022. What will the BBNJ agreement mean for the Arctic fisheries agreement? *Marine Policy* **142**: 103745. DOI: http://dx.doi.org/10.1016/j.marpol.2019.103745.

Barth-Jensen, C, **Daase, M**, **Ormańczyk, MR**, **Varpe, Ø**, **Kwaśniewski, S**, **Svensen, C.** 2022. High abundances of small copepods early developmental stages and nauplii strengthen the perception of a non-dormant Arctic winter. *Polar Biology* **45**: 675–690. DOI: http://dx.doi.org/10.1007/s00300-022-03025-4.

Basedow, SL, **Sundfjord, A**, **von Appen, W-J**, **Halvorsen, E**, **Kwasniewski, S**, **Reigstad, M.** 2018. Seasonal variation in transport of zooplankton into the Arctic Basin through the Atlantic Gateway, Fram Strait. *Frontiers in Marine Science* **5**: 194. DOI: http://dx.doi.org/10.3389/fmars.2018.00194.

Bergmann, M, **Dannheim, J**, **Bauerfeind, E**, **Klages, M.** 2009. Trophic relationships along a bathymetric gradient at the deep-sea observatory HAUSGARTEN. *Deep Sea Research Part I: Oceanographic Research Papers* **56**(3): 408–424. DOI: http://dx.doi.org/10.1016/j.dsr.2008.10.004.

Blachowiak-Samolyk, K, **Søreide, JE**, **Kwasniewski, S**, **Sundfjord, A**, **Hop, H**, **Falk-Petersen, S**, **Hegseth, EN.** 2008. Hydrodynamic control of mesozooplankton abundance and biomass in northern Svalbard waters (79–81°N). *Deep Sea Research Part II: Topical Studies in Oceanography* **55**(20–21): 2210–2224. DOI: http://dx.doi.org/10.1016/j.dsr2.2008.05.018.

Bluhm, B, **Ambrose, WG**, **Bergmann, M**, **Clough, LM**, **Gebruk, AV**, **Hasemann, C**, **Iken, K**, **Klages, M**, **MacDonald, IR**, **Renaud, PE**, **Schewe, I**, **Soltwedel, T**, **Włodarska-Kowalczuk, M.** 2011. Diversity of the Arctic deep-sea benthos. *Marine Biodiversity* **41**: 87–107. DOI: http://dx.doi.org/10.1007/s12526-010-0078-4.

Bluhm, BA, **Gradinger, RR**, **Schnack-Schiel, SB.** 2010. Sea ice meio- and macrofauna, in Thomas, DN, Dieckmann, GS eds., *Sea ice*. West Sussex, UK: Wiley-Blackwell: 357–393.

Bluhm, BA, **Hop, H**, **Vihtakari, M**, **Gradinger, RR**, **Iken, K**, **Melnikov, IA**, **Søreide, JE.** 2018. Sea ice meiofauna distribution on local to pan-Arctic scales. *Ecology and Evolution* **8**(4): 2350–2364. DOI: http://dx.doi.org/10.1002/ece3.3797.

Bluhm, BA, **Kosobokova, KN**, **Carmack, EC.** 2015. A tale of two basins: An integrated physical and biological perspective of the deep Arctic Ocean. *Progress in Oceanography* **139**: 89–121. DOI: http://dx.doi.org/10.1016/j.pocean.2015.07.011.

Bluhm, BA, **Legezynska, J**, **Oleszczuk, B**, **Sen, A**, **Schuppe, B**, **Ziegler, A**, **Zhulay, I**, **Wlodarska-Kowalczuk, M.** 2023. Macrobenthos of the Nansen and Amundsen Basins from the Nansen Legacy joint cruise JC2-2 in Aug/Sept 2021. Version 1.7. The Nansen Legacy Project. DOI: https://doi.org/10.15468/twumu2.

Boetius, A, **Albrecht, S**, **Bakker, K**, **Bienhold, C**, **Felden, J**, **Fernández-Méndez, M**, **Hendricks, S**, **Katlein, C**, **Lalande, C**, **Krumpen, T**, **Nicolaus, M**, **Peeken, I**, **Rabe, B**, **Rogacheva, A**, **Rybakova, E**, **Somavilla, R**, **Wenzhöfer, F**; **RV *Polarstern* ARK27-3-Shipboard Science Party**. 2013. Export of algal biomass from the melting Arctic sea ice. *Science* **339**(6126): 1430–1432. DOI: http://dx.doi.org/10.1126/science.1231346.

Boetius, A, **Grahl, C**, **Kroencke, I**, **Liebezeit, G**, **Nöthig, EM.** 1996. Distribution of plant pigments in surface sediments of the eastern Arctic, in Stein, R, Ivanov, GI, Levitan, MA, Fahl, K eds., *Surface-sediment composition and sedimentary processes in the central Arctic Ocean and along the Eurasian Continental Margin: Berichte Zur Polarforschung*. Bremerhaven, Germany: Alfred Wegener Institute for Polar and Marine Research: 213–218.

Booth, BC, **Horner, RA.** 1997. Microalgae on the Arctic Ocean section, 1994: Species abundance and biomass. *Deep Sea Research Part II: Topical Studies in Oceanography* **44**(8): 1607–1622. DOI: http://dx.doi.org/10.1016/S0967-0645(97)00057-X.

Bourgain, P, **Gascard, JC.** 2011. The Arctic Ocean halocline and its interannual variability from 1997 to 2008. *Deep Sea Research Part I: Oceanographic Research Papers* **58**(7): 745–756. DOI: http://dx.doi.org/10.1016/j.dsr.2011.05.001.

Bourgeois, S, **Archambault, P**, **Witte, U.** 2017. Organic matter remineralization in marine sediments: A Pan-Arctic synthesis. *Global Biogeochemical Cycles* **31**(1): 190–213. DOI: http://dx.doi.org/10.1002/2016GB005378.

Brandt, S, **Wassmann, P**, **Piepenburg, D.** 2023. Revisiting the footprints of climate change in Arctic marine food webs: An assessment of knowledge gained since 2010. *Frontiers in Marine Science* **10**: 1096222. DOI: http://dx.doi.org/10.3389/fmars.2023.1096222.

Bratbak, G, **Müller, O**, **Petelenz, E**, **Tsagkaraki, T**, **Langvad, M**, **Våge, S**, **Ntinou, I.** 2023. Flow cytometry measurements (abundance of virus, bacteria and small protists (primarily <20μm)) during Nansen Legacy cruise 2021710 (from August 23rd to September 25th in 2021) in the Arctic Ocean. Norwegian Marine Data Centre. DOI: https://doi.org/10.21335/nmdc-911461071.

Castellani, G, **Schaafsma, FL**, **Arndt, S**, **Lange, BA**, **Peeken, I**, **Ehrlich, J**, **David, C**, **Ricker, R**, **Krumpen, T**, **Hendricks, S**, **Schwegmann, S**, **Massicotte, P**, **Flores, H.** 2020. Large-scale variability of physical and biological sea-ice properties in polar oceans. *Frontiers in Marine Science* **7**: 536. DOI: http://dx.doi.org/10.3389/fmars.2020.00536.

Charette, MA, **Kipp, LE**, **Jensen, LT**, **Dabrowski, JS**, **Whitmore, LM**, **Fitzsimmons, JN**, **Williford, T**, **Ulfsbo, A**, **Jones, E**, **Bundy, RM**, **Vivancos, SM**, **Pahnke, K**, **John, SG**, **Xiang, Y**, **Hatta, M**, **Petrova, MV**, **Heimbürger-Boavida, L-E**, **Bauch, D**, **Newton, R**, **Pasqualini, A**, **Agather, AM**, **Amon, RMW**, **Anderson, RF**, **Andersson, PS**, **Benner, R**, **Bowman, KL**, **Edwards, RL**, **Gdaniec, S**, **Gerringa, LJA**, **González, AG**, **Granskog, M**, **Haley, B**, **Hammerschmidt, CR**, **Hansell, DA**, **Henderson, PB**, **Kadko, DC**, **Kaiser, K**, **Laan, P**, **Lam, PJ**, **Lamborg, CH**, **Levier, M**, **Li, X**, **Margolin, AR**, **Measures, C**, **Middag, R**, **Millero, FJ**, **Moore, WS**, **Paffrath, R**, **Planquette, H**, **Rabe, B**, **Reader, H**, **Rember, R**, **Rijkenberg, MJA**, **Roy-Barman, M**, **van der Loeff, MR**, **Saito, M**, **Schauer, U**, **Schlosser, P**, **Sherrell, RM**, **Shiller, AM**, **Slagter, H**, **Sonke, JE**, **Stedmon, C**, **Woosley, RJ**, **Valk, O**, **van Ooijen, J**, **Zhang, R.** 2020. The transpolar drift as a source of riverine and shelf-derived trace elements to the central Arctic Ocean. *Journal of Geophysical Research: Oceans* **125**(5): e2019JC015920. DOI: http://dx.doi.org/10.1029/2019JC015920.

Chierici, M, **Fransson, A**. 2025. Water column data on dissolved inorganic carbon (DIC) in the central Arctic Ocean, from the Nansen LEGACY Joint Cruise 2-2, 2021710, with R/V *Kronprins Haakon*, 26 August–22 September 2021 [dataset]. Norwegian Polar Institute. DOI: https://doi.org/10.21334/npolar.2025.67b3ecbf.

Chierici, M, **Fransson, A**, **Raffel, B**. 2025. Water column data on dissolved inorganic nutrients in the central Arctic Ocean, from the Nansen LEGACY Joint Cruise 2-2, 2021710, with R/V *Kronprins Haakon*, 26 August–22 September 2021 [dataset]. Norwegian Polar Institute. DOI: https://doi.org/10.21334/npolar.2025.3b80fac9.

Coble, PG. 1996. Characterization of marine and terrestrial DOM in seawater using excitation-emission

matrix spectroscopy. *Marine Chemistry* **51**(4): 325–346. DOI: http://dx.doi.org/10.1016/0304-4203(95)00062-3.

Craig, H. 1957. Isotopic standards for carbon and oxygen and correction factors for mass-spectrometric analysis of carbon dioxide. *Geochimica et Cosmochimica Acta* **12**(1–2): 133–149. DOI: http://dx.doi.org/10.1016/0016-7037(57)90024-8.

David, C, **Lange, B**, **Krumpen, T**, **Schaafsma, F**, **van Franeker, JA**, **Flores, H.** 2016. Under-ice distribution of polar cod *Boreogadus saida* in the central Arctic Ocean and their association with sea-ice habitat properties. *Polar Biology* **39**: 981–994. DOI: http://dx.doi.org/10.1007/s00300-015-1774-0.

David, C, **Lange, BA**, **Rabe, B**, **Flores, H.** 2015. Community structure of under-ice fauna in the Eurasian central Arctic Ocean in relation to environmental properties of sea-ice habitats. *Marine Ecology Progress Series* **522**: 15–32. DOI: http://dx.doi.org/10.3354/meps11156.

Dickson, AG, **Sabine, CL**, **Christian, JR**, **ed.** 2007. Guide to best practices for ocean CO_2 measurement (PICES Special Publication 3; IOCCP Report 8). Sidney, British Columbia: North Pacific Marine Science Organization: 191. DOI: http://dx.doi.org/10.25607/OBP-1342.

Dolgov, AV, **Benzik, AN.** 2017. Feeding of Greenland halibut *Reinhardtius hippoglossoides* (Pleuronectidae) in the Kara Sea. *Journal of Ichthyology* **57**: 402–409. DOI: http://dx.doi.org/10.1134/S0032945217030043.

Dore, JE, **Houlihan, T**, **Hebel, DV**, **Tien, G**, **Tupas, L**, **Karl, DM.** 1996. Freezing as a method of sample preservation for the analysis of dissolved inorganic nutrients in seawater. *Marine Chemistry* **53**(3–4): 173–185. DOI: http://dx.doi.org/10.1016/0304-4203(96)00004-7.

Down, EJ, **Aaboe, S**, **Divine, DV.** 2023. Sea ice drift backtrajectories of Nansen Legacy cruises sea ice stations [dataset]. Norwegian Polar Institute. DOI: http://dx.doi.org/10.21334/npolar.2023.0c7cbaa2.

Edler, L, **Elbrächter, M.** 2010. The Utermöhl method for quantitative phytoplankton analysis, in Karlson, B, Cusack, C, Bresnan, E eds., *Microscopic and molecular methods for quantitative phytoplankton analysis*. Paris, France: UNESCO: 13–20.

Ehrlich, J, **Bluhm, BA**, **Peeken, I**, **Massicotte, P**, **Schaafsma, F**, **Castellani, G**, **Brandt, A**, **Flores, H.** 2021. Sea-ice associated carbon flux in Arctic spring. *Elementa: Science of the Anthropocene* **9**(1): 00169. DOI: http://dx.doi.org/10.1525/elementa.2020.00169.

Ehrlich, J, **Schaafsma, FL**, **Bluhm, BA**, **Peeken, I**, **Castellani, G**, **Brandt, A**, **Flores, H.** 2020. Sympagic fauna in and under Arctic pack ice in the annual sea-ice system of the new Arctic. *Frontiers in Marine Science* **7**: 452. DOI: http://dx.doi.org/10.3389/fmars.2020.00452.

Ericson, Y, **Fransson, A**, **Chierici, M**, **Jones, EM**, **Skjelvan, I**, **Omar, A**, **Olsen, A**, **Becker, M.** 2023. Rapid fCO_2 rise in the northern Barents Sea and Nansen Basin. *Progress in Oceanography* **217**: 103079. DOI: http://dx.doi.org/10.1016/j.pocean.2023.103079.

Ershova, EA, **Kosobokova, KN**, **Banas, NS**, **Ellingsen, I**, **Niehoff, B**, **Hildebrandt, N**, **Hirche, HJ.** 2021. Sea ice decline drives biogeographical shifts of key *Calanus* species in the central Arctic Ocean. *Global Change Biology* **27**(10): 2128–2143. DOI: http://dx.doi.org/10.1111/gcb.15562.

Fer, I. 2014. Near-inertial mixing in the central Arctic Ocean. *Journal of Physical Oceanography* **44**(8): 2031–2049. DOI: http://dx.doi.org/10.1175/JPO-D-13-0133.1.

Fernández-Méndez, M, **Katlein, C**, **Rabe, B**, **Nicolaus, M**, **Peeken, I**, **Bakker, K**, **Flores, H**, **Boetius, A.** 2015. Photosynthetic production in the central Arctic Ocean during the record sea-ice minimum in 2012. *Biogeosciences* **12**(11): 3525–3549. DOI: http://dx.doi.org/10.5194/bg-12-3525-2015.

Flores, H, **David, C**, **Ehrlich, J**, **Hardge, K**, **Kohlbach, D**, **Lange, BA**, **Niehoff, B**, **Nöthig, E-M**, **Peeken, I**, **Metfies, K.** 2019. Sea-ice properties and nutrient concentration as drivers of the taxonomic and trophic structure of high-Arctic protist and metazoan communities. *Polar Biology* **42**: 1377–1395. DOI: http://dx.doi.org/10.1007/s00300-019-02526-z.

Fong, AA, **Hoppe, CJ**, **Aberle, N**, **Ashjian, CJ**, **Assmy, P**, **Bai, Y**, **Bakker, DCE**, **Balmonte, JP**, **Barry, KR**, **Bertilsson, S**, **Boulton, W**, **Bowman, J**, **Bozzato, D**, **Bratbak, G**, **Buck, M**, **Campbell, RG**, **Castellani, G**, **Chamberlain, EC**, **Chen, J**, **Chierici, M**, **Cornils, A**, **Creamean, JM**, **Damm, E**, **Dethloff, K**, **Droste, ES**, **Ebenhöh, O**, **Eggers, SL**, **Engel, A**, **Flores, H**, **Fransson, A**, **Frickenhaus, S**, **Gardner, J**, **Gelfman, CE**, **Granskog, MA**, **Graeve, M**, **Havermans, C**, **Heuzé, C**, **Hildebrandt, N**, **Hill, TCJ**, **Hoppema, M**, **Immerz, A**, **Jin, H**, **Koch, BP**, **Kong, X**, **Kraberg, A**, **Lan, M**, **Lange, BA**, **Larsen, A**, **Lebreton, B**, **Leu, E**, **Loose, B**, **Maslowski, W**, **Mavis, C**, **Metfies, K**, **Mock, T**, **Müller, O**, **Nicolaus, M**, **Niehoff, B**, **Nomura, D**, **Nöthig, E-M**, **Oggier, M**, **Oldenburg, E**, **Olsen, LM**, **Peeken, I**, **Perovich, DK**, **Popa, O**, **Rabe, B**, **Ren, J**, **Rex, M**, **Rinke, A**, **Rokitta, S**, **Rost, B**, **Sakinan, S**, **Salganik, E**, **Schaafsma, FL**, **Schäfer, H**, **Schmidt, K**, **Shoemaker, KM**, **Shupe, MD**, **Snoeijs-Leijonmalm, P**, **Stefels, J**, **Svenson, A**, **Tao, R**, **Torres-Valdés, S**, **Torstensson, A**, **Toseland, A**, **Ulfsbo, A**, **van Leeuwe, MA**, **Vortkamp, M**, **Webb, AL**, **Zhuang, Y**, **Gradinger, RR.** 2024. Overview of the MOSAiC expedition: Ecosystem. *Elementa: Science of the Anthropocene* **12**(1): 00135. DOI: http://dx.doi.org/10.1525/elementa.2023.00135.

Fossheim, M, **Primicerio, R**, **Johannesen, E**, **Ingvaldsen, RB**, **Aschan, MM**, **Dolgov, AV.** 2015. Recent warming leads to a rapid borealization of fish communities in the Arctic. *Nature Climate Change* **5**: 673–677. DOI: http://dx.doi.org/10.1038/nclimate2647.

Fransson, A. 2022. CTD data from Nansen Legacy Cruise—Arctic Basin joint cruise 2–2. Norwegian

Marine Data Centre. DOI: https://doi.org/10.21335/NMDC-1814168447.

Fransson, A, **Bluhm, B**, **Amargant-Arumi, M**, **Assmann, K**, **Bårnås Gravelle, AM**, **Bratrein, M**, **Buvik, K**, **Chierici, M**, **Ciesielski, T**, **Cristea, A**, **Eikrem, W**, **Espinel, N**, **Gardner, J**, **Gawinski, C**, **Hellerud, E**, **Koenig, Z**, **Lennert, K**, **Lockwood-Ireland, C**, **Lundesgaard, Ø**, **Marquardt, M**, **Ntinou, IV**, **Ortiz, G**, **Palmesen, M**, **Raffel, B**, **Sanchez, N**, **Schuppe, BK**, **Sen, A**, **Sletteng Garvang, E**, **Steer, A**, **Svensen, C**, **Vader, A**, **Våge, S**, **Van Dihn, K**, **Wold, A**, **Ziegler, A.** 2022. Joint cruise 2–2 2021: Cruise report. The Nansen Legacy Report Series 30/2022. DOI: https://doi.org/10.7557/nlrs.6413.

Fransson, A, **Chierici, M**, **Raffel, B**. 2025a. Sea-ice bulk data on dissolved inorganic carbon (DIC) in the central Arctic Ocean, from the Nansen LEGACY Joint Cruise 2-2, 2021710, with R/V *Kronprins Haakon*, 26 August–22 September 2021 [dataset]. Norwegian Polar Institute. DOI: https://doi.org/10.21334/npolar.2025.71dbfe18.

Fransson, A, **Chierici, M**, **Raffel, B**. 2025b. Sea-ice bulk data on inorganic nutrients in the central Arctic Ocean, from the Nansen LEGACY Joint Cruise 2-2, 2021710, with R/V *Kronprins Haakon*, 26 August–22 September 2021 [dataset]. Norwegian Polar Institute. DOI: https://doi.org/10.21334/npolar.2025.96853520.

Geoffroy, M, **Berge, J**, **Majaneva, S**, **Johnsen, G**, **Langbehn, TJ**, **Cottier, F**, **Mogstad, AA**, **Zolich, A**, **Last, K.** 2018. Increased occurrence of the Jellyfish *Periphylla periphylla* in the European high Arctic. *Polar Biology* **41**: 2615–2619. DOI: http://dx.doi.org/10.1007/s00300-018-2368-4.

Geoffroy, M, **Bouchard, C**, **Flores, H**, **Robert, D**, **Gjøsæter, H**, **Hoover, C**, **Hop, H**, **Hussey, NE**, **Nahrgang, J**, **Steiner, N**, **Bender, M**, **Berge, J**, **Castellani, G**, **Chernova, N**, **Copeman, L**, **David, CL**, **Deary, A**, **Divoky, G**, **Dolgov, AV**, **Duffy-Anderson, J**, **Dupont, N**, **Durant, JM**, **Elliott, K**, **Gauthier, S**, **Goldstein, ED**, **Gradinger, R**, **Hedges, K**, **Herbig, J**, **Laurel, B**, **Loseto, L**, **Maes, S**, **Mark, FC**, **Mosbech, A**, **Pedro, S**, **Pettitt-Wade, H**, **Prokopchuk, I**, **Renaud, PE**, **Schembri, S**, **Vestfals, C**, **Walkusz, W.** 2023. The circumpolar impacts of climate change and anthropogenic stressors on Arctic cod (*Boreogadus saida*) and its ecosystem. *Elementa: Science of the Anthropocene* **11**(1): 00097. DOI: http://dx.doi.org/10.1525/elementa.2022.00097.

Godø, O, **Valdemarsen, J**, **Engås, A.** 1993. Comparison of efficiency of standard and experimental juvenile gadoid sampling trawls. *ICES Journal of Marine Science* **196**: 196–201.

Gosselin, M, **Levasseur, M**, **Wheeler, PA**, **Horner, RA**, **Booth, BC.** 1997. New measurements of phytoplankton and ice algal production in the Arctic Ocean. *Deep Sea Research Part II: Topical Studies in Oceanography* **44**(8): 1623–1644. DOI: http://dx.doi.org/10.1016/S0967-0645(97)00054-4.

Gradinger, R. 1999. Integrated abundance and biomass of sympagic meiofauna in Arctic and Antarctic pack ice. *Polar Biology* **22**: 169–177. DOI: http://dx.doi.org/10.1007/s003000050407.

Gradinger, RR, **Bluhm, B**, **Iken, K.** 2010. Arctic sea-ice ridges—Safe heavens for sea-ice fauna during periods of extreme ice melt? *Deep Sea Research Part II: Topical Studies in Oceanography* **57**(1–2): 86–95. DOI: http://dx.doi.org/10.1016/j.dsr2.2009.08.008.

Gradinger, RR, **Bluhm, BA.** 2004. In-situ observations on the distribution and behavior of amphipods and Arctic cod (*Boreogadus saida*) under the sea ice of the high Arctic Canada Basin. *Polar Biology* **27**: 595–603. DOI: http://dx.doi.org/10.1007/s00300-004-0630-4.

Gradinger, RR, **Meiners, K**, **Plumley, G**, **Zhang, Q**, **Bluhm, BA.** 2005. Abundance and composition of the sea-ice meiofauna in off-shore pack ice of the Beaufort Gyre in summer 2002 and 2003. *Polar Biology* **28**: 171–181. DOI: http://dx.doi.org/10.1007/s00300-004-0674-5.

Grasshoff, K, **Kremling, K**, **Ehrhardt, M.** 2009. *Methods of seawater analysis*. Hoboken, NJ: John Wiley & Sons.

Gregg, MC, **D'Asaro, EA**, **Riley, JJ**, **Kunze, E.** 2018. Mixing efficiency in the ocean. *Annual Review of Marine Science* **10**: 443–473. DOI: http://dx.doi.org/10.1146/annurev-marine-121916-063643.

Groendahl, F, **Hernroth, L.** 1986. Vertical distribution of copepods in the Eurasian part of the Nansen Basin, Arctic Ocean, in Schriever, G, Schminke, HK, Shih, C-T eds., *Proceedings of the second international conference on Copepoda, Ottawa, Canada, August 13–17, 1984. Syllogeus No. 58*. Ottawa, Canada: National Museums of Canada: 311–320.

Guarino, M-V, **Sime, LC**, **Schröeder, D**, **Malmierca-Vallet, I**, **Rosenblum, E**, **Ringer, M**, **Ridley, J**, **Feltham, D**, **Bitz, C**, **Steig, EJ**, **Wolff, E**, **Stroeve, J**, **Sellar, A.** 2020. Sea-ice-free Arctic during the Last Interglacial supports fast future loss. *Nature Climate Change* **10**: 928–932. DOI: http://dx.doi.org/10.1038/s41558-020-0865-2.

Gundersen, K, **Møgster, JS**, **Lien, VS**, **Ershova, E**, **Lunde, LF**, **Arnesen, H**, **Olsen, A-K.** 2022. Thirty years of nutrient biogeochemistry in the Barents Sea and the adjoining Arctic Ocean, 1990–2019. *Scientific Data* **9**: 649. DOI: http://dx.doi.org/10.1038/s41597-022-01781-w.

Haas, C, **Lobach, J**, **Hendricks, S**, **Rabenstein, L**, **Pfaffling, A.** 2009. Helicopter-borne measurements of sea ice thickness, using a small and lightweight, digital EM system. *Journal of Applied Geophysics* **67**(3): 234–241. DOI: http://dx.doi.org/10.1016/j.jappgeo.2008.05.005.

Hammes, F, **Egli, T.** 2010. Cytometric methods for measuring bacteria in water: Advantages, pitfalls and applications. *Analytical and Bioanalytical Chemistry* **397**: 1083–1095. DOI: http://dx.doi.org/10.1007/s00216-010-3646-3.

Hardge, K, **Peeken, I**, **Neuhaus, S**, **Lange, BA**, **Stock, A**, **Stoeck, T**, **Weinisch, L**, **Metfies, K.** 2017. The importance of sea ice for exchange of habitat-specific protist communities in the Central Arctic Ocean. *Journal of Marine Systems* **165**: 124–138. DOI: http://dx.doi.org/10.1016/j.jmarsys.2016.10.004.

Haug, T, **Bogstad, B**, **Chierici, M**, **Gjøsæter, H**, **Hallfredsson, EH**, **Høines, ÅS**, **Hoel, AH**, **Ingvaldsen, RB**, **Jørgensen, LL**, **Knutsen, T**, **Loeng, H**, **Naustvoll, L-J**, **Røttingen, I**, **Sunnanå, K.** 2017. Future harvest of living resources in the Arctic Ocean north of the Nordic and Barents Seas: A review of possibilities and constraints. *Fisheries Research* **188**: 38–57. DOI: http://dx.doi.org/10.1016/j.fishres.2016.12.002.

Hess, S, **Ricardo de Freitas, TR**, **Alve, E**, **Bluhm, B**, **Jorda Molina, E**, **Reiss, H**, **Renaud, PE**, **Sen, A**, **Ziegler, A.** 2024. Sediment property data (0–6 cm) from the Nansen Legacy Joint Cruise 2–2, cruise 2021710 (JC2-2). Norwegian Marine Data Centre. DOI: https://doi.org/10.21335/NMDC-962959866.

Hirche, HJ, **Mumm, N.** 1992. Distribution of dominant copepods in the Nansen Basin, Arctic Ocean, in summer. *Deep Sea Research Part A. Oceanographic Research Papers* **39**(2): S485–S505. DOI: http://dx.doi.org/10.1016/S0198-0149(06)80017-8.

Hobson, KA, **Fisk, A**, **Karnovsky, N**, **Holst, M**, **Gagnon, JM**, **Fortier, M**. 2002. A stable isotope ($\delta^{13}C$, $\delta^{15}N$) model for the North Water food web: Implications for evaluating trophodynamics and the flow of energy and contaminants. *Deep Sea Research Part II: Topical Studies in Oceanography* **49** (22–23): 5131–5150. DOI: https://doi.org/10.1016/S0967-0645(02)00182-0.

Holm-Hansen, O, **Riemann, B.** 1978. Chlorophyll *a* determination: Improvements in methodology. *Oikos* **30**(3): 438–447. DOI: http://dx.doi.org/10.2307/3543338.

Hop, H, **Assmy, P**, **Wold, A**, **Sundfjord, A**, **Daase, M**, **Duarte, P**, **Kwasniewski, S**, **Gluchowska, M**, **Wiktor, JM**, **Tatarek, A**, **Wiktor, J Jr**, **Kristiansen, S**, **Fransson, A**, **Chierici, M**, **Vihtakari, M.** 2019. Pelagic ecosystem characteristics across the Atlantic water boundary current from Rijpfjorden, Svalbard, to the Arctic Ocean during summer (2010–2014). *Frontiers in Marine Science* **6**: 181. DOI: http://dx.doi.org/10.3389/fmars.2019.00181.

Hop, H, **Vihtakari, M**, **Bluhm, B**, **Assmy, P**, **Poulin, M**, **Gradinger, R**, **Peeken, I**, **von Quillfeldt, C**, **Olsen, LM**, **Zhitina, L**, **Melnikov, IA.** 2020. Changes in sea-ice protist diversity with declining sea ice in the Arctic Ocean from the 1980s to 2010s. *Frontiers in Marine Science* **7**: 243. DOI: http://dx.doi.org/10.3389/fmars.2020.00243.

Hordoir, R, **Skagseth, Ø**, **Ingvaldsen, RB**, **Sandø, AB**, **Löptien, U**, **Dietze, H**, **Gierisch, AMU**, **Assmann, KM**, **Lundesgaard, Ø**, **Lind, S.** 2022. Changes in Arctic stratification and mixed layer depth cycle: A modeling analysis. *Journal of Geophysical Research: Oceans* **127**(1): e2021JC017270. DOI: http://dx.doi.org/10.1029/2021JC017270.

Huenerlage, K, **Buchholz, F.** 2015. Thermal limits of krill species from the high-Arctic Kongsfjord (Spitsbergen). *Marine Ecology Progress Series* **535**: 89–98. DOI: http://dx.doi.org/10.3354/meps11408.

Huntington, HP, **Zagorsky, A**, **Kaltenborn, BP**, **Shin, HC**, **Dawson, J**, **Lukin, M**, **Dahl, PE**, **Guo, P**, **Thomas, DN.** 2022. Societal implications of a changing Arctic Ocean. *Ambio* **51**: 298–306. DOI: http://dx.doi.org/10.1007/s13280-021-01601-2.

Iken, K, **Bluhm, BA**, **Gradinger, RR.** 2005. Food web structure in the high Arctic Canada Basin: Evidence from $\delta^{13}C$ and $\delta^{15}N$ analysis. *Polar Biology* **28**: 238–249. DOI: http://dx.doi.org/10.1007/s00300-004-0669-2.

Iken, K, **Brey, T**, **Wand, U**, **Voigt, J**, **Junghans, P**. 2001. Food web structure of the benthic community at the Porcupine Abyssal Plain (NE Atlantic): A stable isotope analysis. *Progress in Oceanography* **50**(1–4): 383–405. DOI: https://doi.org/10.1016/S0079-6611(01)00062-3.

Ingvaldsen, RB, **Assmann, KM**, **Primicerio, R**, **Fossheim, M**, **Polyakov, IV**, **Dolgov, A.** 2021. Physical manifestations and ecological implications of Arctic Atlantification. *Nature Reviews Earth and Environment* **2**: 874–889. DOI: http://dx.doi.org/10.1038/s43017-021-00228-x.

Ingvaldsen, RB, **Eriksen, E**, **Gjøsæter, H**, **Engås, A**, **Schuppe, BK**, **Assmann, KM**, **Cannaby, H**, **Dalpadado, P**, **Bluhm, BA.** 2023. Under-ice observations by trawls and multi-frequency acoustics in the Central Arctic Ocean reveals abundance and composition of pelagic fauna. *Scientific Reports* **13**: 1000. DOI: http://dx.doi.org/10.1038/s41598-023-27957-x.

IPCC. 2019. IPCC special report on the ocean and cryosphere in a changing climate [Poürtner, H-O, Roberts, DC, Masson-Delmotte, V, Zhai, P, Tignor, M, Poloczanska, E, Mintenbeck, K, Alegría, A, Nicolai, M, Okem, A, Petzold, J, Rama, B, Weyer, NM (eds.)]. Geneva, Switzerland: IPCC.

Itkin, P, **Hendricks, S**, **Webster, M**, **von Albedyll, L**, **Arndt, S**, **Divine, D**, **Jaggi, M**, **Oggier, M**, **Raphael, I**, **Ricker, R**, **Rohde, J**, **Schneebeli, M**, **Liston, GE.** 2023. Sea ice and snow characteristics from year-long transects at the MOSAiC Central Observatory. *Elementa: Science of the Anthropocene* **11**(1): 00048. DOI: http://dx.doi.org/10.1525/elementa.2022.00048.

JCOMM Expert Team on Sea Ice. 2014. Sea-Ice Nomenclature: Snapshot of the WMO Sea Ice Nomenclature (WMO No. 259, Vol. 1—Terminology and Codes; Vol. II—Illustrated Glossary; and Vol. III—International System of Sea-Ice Symbols). Geneva, Switzerland: WMO-JCOMM: 121. DOI: http://dx.doi.org/10.25607/OBP-1515.

Johnson, KM, **King, AE**, **Sieburth, J.** 1985. Coulometric TCO_2 analyses for marine studies; an introduction.

Marine Chemistry **16**(1): 61–82. DOI: http://dx.doi.org/10.1016/0304-4203(85)90028-3.

Jordà-Molina, È, **Sen, A**, **Bluhm, BA**, **Renaud, PE**, **Włodarska-Kowalczuk, M**, **Legeżyńska, J**, **Oleszczuk, B**, **Reiss, H.** 2023. Lack of strong seasonality in macrobenthic communities from the northern Barents Sea shelf and Nansen Basin. *Progress in Oceanography* **219**: 103150. DOI: http://dx.doi.org/10.1016/j.pocean.2023.103150.

Jordà-Molina, E, **Sen, A**, **Reiss, H**, **Renaud, PE**, **Bluhm, BA**, **Włodarska-Kowalczuk, M**, **Legeżyńska, J**, **Oleszczuk, B**, **Górska, B**, **Ricardo de Freitas, T**, **Hess, S**, **Ziegler, A**, **Vàzquez Alonso, M**, **Mannvik, HP**, **Hansen, J**, **Hansen, T.** 2024. Benthic macrofauna community from the Northwestern Barents Sea from seasonal cruises (Q3-August 2019; Q4-December 2019; Q1-March 2021; Q2-May 2021)—The Nansen Legacy project (Arven Etter Nansen). Norwegian Marine Data Centre. DOI: http://dx.doi.org/10.21335/NMDC-1152502405.

Kędra, M, **Moritz, C**, **Choy, ES**, **David, C**, **Degen, R**, **Duerksen, S**, **Ellingsen, I**, **Górska, B**, **Grebemeier, JM**, **Kirievskaya, D**, **van Oevelen, D**, **Piwosz, K**, **Samuelsen, A**, **Węsławski, JM.** 2015. Status and trends in the structure of Arctic benthic food webs. *Polar Research* **34**(1): 23775. DOI: http://dx.doi.org/10.3402/polar.v34.23775.

Kiko, R, **Kern, S**, **Kramer, M**, **Mütze, H.** 2017. Colonization of newly forming Arctic Sea ice by meiofauna: A case study for the future Arctic? *Polar Biology* **40**: 1277–1288. DOI: http://dx.doi.org/10.1007/s00300-016-2052-5.

Kim, Y-H, **Min, S-K**, **Gillett, NP**, **Notz, D**, **Malinina, E.** 2023. Observationally-constrained projections of an ice-free Arctic even under a low emission scenario. *Nature Communications* **14**: 3139. DOI: http://dx.doi.org/10.1038/s41467-023-38511-8.

Kirchman, DL, **Hill, V**, **Cottrell, MT**, **Gradinger, R**, **Malmstrom, RR**, **Parker, A.** 2009. Standing stocks, production, and respiration of phytoplankton and heterotrophic bacteria in the western Arctic Ocean. *Deep Sea Research Part II: Topical Studies in Oceanography* **56**: 1237–1248. DOI: http://dx.doi.org/10.1016/j.dsr2.2008.10.018.

Klevjer, T, **Melle, W**, **Knutsen, T**, **Strand, E**, **Korneliussen, R**, **Dupont, N**, **Salvanes, AGV**, **Wiebe, PH.** 2020. Micronekton biomass distribution, improved estimates across four north Atlantic basins. *Deep Sea Research Part II: Topical Studies in Oceanography* **180**: 104691. DOI: http://dx.doi.org/10.1016/j.dsr2.2019.104691.

Koenig, Z, **Assmann, K**, **Lundesgaard, Ø**, **Sundfjord, A.** 2023a. Microstructure profiler (MSS) profiles from Nansen Legacy cruise KH2021710 across the Nansen and Amundsen Basins of the Arctic Ocean [dataset]. Norwegian Polar Institute. DOI: https://doi.org/10.21334/npolar.2023.f09a8062.

Koenig, Z, **Fer, I**, **Chierici, M**, **Fransson, A**, **Jones, E**, **Kolås, EH.** 2023b. Diffusive and advective cross-frontal fluxes of inorganic nutrients and dissolved inorganic carbon in the Barents Sea in autumn. *Progress in Oceanography* **219**: 103161. DOI: http://dx.doi.org/10.1016/j.pocean.2023.103161.

Kohlbach, D, **Goraguer, L**, **Bodur, YV**, **Müller, O**, **Amargant-Arumí, M**, **Blix, K**, **Bratbak, G**, **Chierici, M**, **Dąbrowska, AM**, **Dietrich, U**, **Edvardsen, B**, **García, LM**, **Gradinger, R**, **Hop, H**, **Jones, E**, **Lundesgaard, Ø**, **Olsen, LM**, **Reigstad, M**, **Saubrekka, K**, **Tatarek, A**, **Wiktor, JM**, **Wold, A**, **Assmy, P.** 2023. Earlier sea-ice melt extends the oligotrophic summer period in the Barents Sea with low algal biomass and associated low vertical flux. *Progress in Oceanography* **213**: 103018. DOI: http://dx.doi.org/10.1016/j.pocean.2023.103018.

Kohlbach, D, **Graeve, M**, **Lange, B**, **David, C**, **Peeken, I**, **Flores, H.** 2016. The importance of ice algae-produced carbon in the central Arctic Ocean ecosystem: Food web relationships revealed by lipid and stable isotope analyses. *Limnology and Oceanography* **6**(6): 2027–2044. DOI: http://dx.doi.org/10.1002/lno.10351.

Kohlbach, D, **Hop, H**, **Wold, A**, **Schmidt, K**, **Smik, L**, **Belt, ST**, **Keck Al-Habahbeh, A**, **Woll, M**, **Graeve, M**, **Dąbrowska, AM**, **Tatarek, A**, **Atkinson, A**, **Assmy, P.** 2021. Multiple trophic markers trace dietary carbon sources in Barents Sea zooplankton during late summer. *Frontiers in Marine Science* **7**: 610248. DOI: http://dx.doi.org/10.3389/fmars.2020.610248.

Kosobokova, K, **Hirche, H-J.** 2009. Biomass of zooplankton in the eastern Arctic Ocean—A base line study. *Progress in Oceanography* **82**(4): 265–280. DOI: http://dx.doi.org/10.1016/j.pocean.2009.07.006.

Kosobokova, KN, **Hopcroft, RR**, **Hirche, HJ.** 2011. Patterns of zooplankton diversity through the depths of the Arctic's central basins. *Marine Biodiversity* **41**(4): 29–50. DOI: http://dx.doi.org/10.1007/s12526-010-0057-9.

Kowalczuk, P, **Meler, J**, **Kauko, HM**, **Pavlov, AK**, **Zabłocka, M**, **Peeken, I**, **Dybwad, C**, **Castellani, G**, **Granskog, MA.** 2017. Bio-optical properties of Arctic drift ice and surface waters north of Svalbard from winter to spring. *Journal of Geophysical Research: Oceans* **122**(6): 4634–4660. DOI: http://dx.doi.org/10.1002/2016JC012589.

Krafft, BA, **Melle, W**, **Knutsen, T**, **Bagøien, E**, **Broms, C**, **Ellertsen, B**, **Siegel, V.** 2010. Distribution and demography of Antarctic krill in the Southeast Atlantic sector of the Southern Ocean during the austral summer 2008. *Polar Biology* **33**: 957–968. DOI: http://dx.doi.org/10.1007/s00300-010-0774-3.

Kröncke, I. 1994. Macrobenthos composition, abundance and biomass in the Arctic Ocean along a transect between Svalbard and the Makarov Basin. *Polar Biology* **14**: 519–529. DOI: http://dx.doi.org/10.1007/BF00238221.

Kröncke, I. 1998. Macrofauna communities in the Amundsen Basin, at the Morris Jesup rise and at the Yermak Plateau (Eurasian Arctic Ocean). *Polar*

Biology **19**: 383–392. DOI: http://dx.doi.org/10.1007/s003000050263.

Krumpen, T, **Belter, HJ**, **Boetius, A**, **Damm, E**, **Haas, C**, **Hendricks, S**, **Nicolaus, M**, **Nöthig, E-M**, **Paul, S**, **Peeken, I**, **Ricker, R**, **Stein, R.** 2019. Arctic warming interrupts the Transpolar Drift and affects long-range transport of sea ice and ice-rafted matter. *Scientific Reports* **9**: 5459. DOI: http://dx.doi.org/10.1038/s41598-019-41456-y.

Kwasniewski, S, **Hop, H**, **Falk-Petersen, S**, **Pedersen, G.** 2003. Distribution of *Calanus* species in Kongsfjorden, a glacial fjord in Svalbard. *Journal of Plankton Research* **25**(1): 1–20. DOI: http://dx.doi.org/10.1093/plankt/25.1.1.

Kwok, R. 2018. Arctic sea ice thickness, volume, and multiyear ice coverage: Losses and coupled variability (1958–2018). *Environmental Research Letters* **13**(10): 105005. DOI: http://dx.doi.org/10.1088/1748-9326/aae3ec.

Lalande, C, **Nöthig, EM**, **Fortier, L.** 2019. Algal export in the Arctic Ocean in times of global warming. *Geophysical Research Letters* **46**(1): 5959–5967. DOI: http://dx.doi.org/10.1029/2019GL083167.

Laliberté, F, **Howell, SEL**, **Kushner, PJ.** 2016. Regional variability of a projected sea ice-free Arctic during the summer months. *Geophysical Research Letters* **43**(1): 256–263. DOI: http://dx.doi.org/10.1002/2015GL066855.

Lannuzel, D, **Tedesco, L**, **van Leeuwe, M**, **Campbell, K**, **Flores, H**, **Delille, B**, **Miller, L**, **Stefels, J**, **Assmy, P**, **Bowman, J**, **Brown, K**, **Castellani, G**, **Chierici, M**, **Crabeck, O**, **Damm, E**, **Else, B**, **Fransson, A**, **Fripiat, F**, **Geilfus, N-X**, **Jacques, C**, **Jones, E**, **Kaartokallio, H**, **Kotovitch, M**, **Meiners, K**, **Moreau, S**, **Nomura, D**, **Peeken, I**, **Rintala, J-M**, **Steiner, N**, **Tison, J-L**, **Vancoppenolle, M**, **van der Linden, F**, **Vichi, M**, **Wongpan, P.** 2020. The future of Arctic sea-ice biogeochemistry and ice-associated ecosystems. *Nature Climate Change* **10**: 983–992. DOI: http://dx.doi.org/10.1038/s41558-020-00940-4.

Lavergne, T, **Down, E.** 2023. A climate data record of year-round global sea ice drift from the EUMETSAT Ocean and Sea Ice Satellite Application Facility (OSI SAF). *Earth System Science Data Discussions* **15**(12): 1–38. DOI: http://dx.doi.org/10.5194/essd-15-5807-2023.

Lebaron, P, **Servais, P**, **Baudoux, AC**, **Bourrain, M**, **Courties, C**, **Parthuisot, N.** 2002. Variations of bacterial-specific activity with cell size and nucleic acid content assessed by flow cytometry. *Aquatic Microbial Ecology* **28**(2): 131–140. DOI: http://dx.doi.org/10.3354/ame028131.

Lei, R, **Cheng, B**, **Heil, P**, **Vihma, T**, **Wang, J**, **Ji, Q**, **Zhang, Z.** 2018. Seasonal and interannual variations of sea ice mass balance from the Central Arctic to the Greenland Sea. *Journal of Geophysical Research: Oceans* **123**(4): 2422–2439. DOI: http://dx.doi.org/10.1002/2017JC013548.

Li, WK, **Carmack, EC**, **McLaughlin, FA**, **Nelson, RJ**, **Williams, WJ**. 2013. Space-for-time substitution in predicting the state of picoplankton and nanoplankton in a changing Arctic Ocean. *Journal of Geophysical Research: Oceans* **118**(10): 5750–5759. DOI: https://doi.org/10.1002/jgrc.20417.

Li, WK, **McLaughlin, FA**, **Lovejoy, C**, **Carmack, EC.** 2009. Smallest algae thrive as the Arctic Ocean freshens. *Science* **326**(5952): 539–539. DOI: http://dx.doi.org/10.1126/science.1179798.

Liguori, BT, **Ehlert, C**, **Nöthig, EM**, **van Ooijen, JC**, **Pahnke, K**. 2021. The transpolar drift influence on the Arctic Ocean silicon cycle. *Journal of Geophysical Research: Oceans* **126**(11): e2021JC017352. DOI: https://doi.org/10.1029/2021JC017352.

Litchman, E, **Klausmeier, CA**, **Schofield, OM**, **Falkowski, PG.** 2007. The role of functional traits and trade-offs in structuring phytoplankton communities: Scaling from cellular to ecosystem level. *Ecology Letters* **10**(12): 1170–1181. DOI: http://dx.doi.org/10.1111/j.1461-0248.2007.01117.x.

Loose, B, **Schlosser, P**, **Perovich, D**, **Ringelberg, D**, **Ho, DT**, **Takahashi, T**, **Richter-Menge, J**, **Reynolds, CM**, **McGillis, WR**, **Tison, J-L.** 2011. Gas diffusion through columnar laboratory sea ice: Implications for mixed-layer ventilation of CO_2 in the seasonal ice zone. *Tellus B* **63**: 23–39. DOI: http://dx.doi.org/10.1111/j.1600-0889.2010.00506.x.

Malmgren, F. 1927. On the properties of sea ice: The Norwegian north polar expedition with the "Maud", 1918–1925. *Scientific Research* **1**: 1–67.

Marie, D, **Partensky, F**, **Vaulot, D**, **Brussaard, C.** 1999. Enumeration of phytoplankton, bacteria, and viruses in marine samples. *Current Protocols in Cytometry* **10**(1): 11.11.1–11.11.15. DOI: http://dx.doi.org/10.1002/0471142956.cy1111s10.

Mariotti, A. 1983. Atmospheric nitrogen is a reliable standard for natural ^{15}N abundance measurements. *Nature* **303**: 685–687. DOI: http://dx.doi.org/10.1038/303685a0.

Marquardt, M, **Bluhm, BA**, **Gradinger, RR.** 2023a. Sea-ice meiofauna biodiversity from the Nansen Legacy joint cruise JC2–2 (cruise number: 2021710) [dataset]. Norstore. DOI: https://doi.org/10.15468/dfz5gb.

Marquardt, M, **Dubourg, P**, **Reigstad, M.** 2022. Concentration of Particulate Organic Carbon (POC) and Particulate Organic Nitrogen (PON) from the sea water and sea ice in the northern Barents Sea as part of the Nansen Legacy project, Cruise 2021710, JC2-2 [dataset]. Norstore. DOI: https://doi.org/10.11582/2022.00051.

Marquardt, M, **Goraguer, L**, **Assmy, P**, **Bluhm, BA**, **Aaboe, S**, **Down, E**, **Patrohay, E**, **Edvardsen, B**, **Tatarek, A**, **Smoła, Z**, **Wiktor, J**, **Gradinger, RR.** 2023b. Seasonal dynamics of sea-ice protist and meiofauna in the northwestern Barents Sea. *Progress in Oceanography* **218**: 103128. DOI: http://dx.doi.org/10.1016/j.pocean.2023.103128.

Marquardt, M, **Kramer, M**, **Carnat, G**, **Werner, I.** 2011. Vertical distribution of sympagic meiofauna in sea ice in the Canadian Beaufort Sea. *Polar Biology* **34**:

1887–1900. DOI: http://dx.doi.org/10.1007/s00300-011-1078-y.

Mason, JG, **Bryndum-Buchholz, A**, **Palacios-Abrantes, J**, **Badhe, R**, **Morgante, I**, **Bianchi, D**, **Blanchard, JL**, **Everett, JD**, **Harrison, CS**, **Heneghan, RF**, **Novaglio, C**, **Petrik, CM.** 2024. Key uncertainties and modeling needs for managing living marine resources in the future Arctic Ocean. *Earth's Future* **12**(8): e2023EF004393. DOI: http://dx.doi.org/10.1029/2023EF004393.

McDougall, TJ, **Barker, PM.** 2011. Getting started with TEOS-10 and the Gibbs Seawater (GSW) oceanographic toolbox. SCOR/IAPSO Working Group 127: 1–28.

Meier, WN, **Perovich, D**, **Farrell, S**, **Haas, C**, **Hendricks, S**, **Petty, AA**, **Webster, M**, **Divine, D**, **Gerland, S**, **Kaleschke, L**, **Ricker, R**, **Steer, A**, **Tian-Kunze, X**, **Tschudi, M**, **Wood, K**. 2021. Sea Ice. Series: NOAA technical report OAR ARC; 21-05. DOI: http://dx.doi.org/10.25923/y2wd-fn85.

Meier, WN, **Stroeve, J.** 2022. An updated assessment of the changing Arctic sea ice cover. *Oceanography* **35**(3–4): 10–19. DOI: http://dx.doi.org/10.5670/oceanog.2022.114.

Melnikov, A. 1997. *Arctic sea ice ecosystem*. Amsterdam, the Netherlands: CRC Press: 221.

Misund, OA, **Heggland, K**, **Skogseth, R**, **Falck, E**, **Gjøsæter, H**, **Sundet, J**, **Watne, J**, **Lønne, OJ**. 2016. Norwegian fisheries in the Svalbard zone since 1980. Regulations, profitability and warming waters affect landings. *Polar Science* **10**(3): 312–322. DOI: http://dx.doi.org/10.1016/j.polar.2016.02.001.

Montanaro, J, **Gruber, D**, **Leisch, N.** 2016. Improved ultrastructure of marine invertebrates using non-toxic buffers. *PeerJ* **4**: e1860. DOI: http://dx.doi.org/10.7717/peerj.1860.

Monterey, G, **Levitus, S.** 1997. NOAA Atlas NESDIS 14. Washington, DC: U.S. Gov, Printing Office.

Muilwijk, M, **Nummelin, A**, **Heuzé, C**, **Polyakov, IV**, **Zanowski, H**, **Smedsrud, LH.** 2023. Divergence in climate model projections of future Arctic Atlantification. *Journal of Climate* **36**(6): 1727–1748. DOI: http://dx.doi.org/10.1175/JCLI-D-22-0349.1.

Müller, M, **Knol-Kauffman, M**, **Jeuring, J**, **Palerme, C.** 2023a. Arctic shipping trends during hazardous weather and sea-ice conditions and the Polar Code's effectiveness. Research Square Platform LLC. DOI: http://dx.doi.org/10.21203/rs.3.rs-2970431/v1.

Müller, O, **Våge, S**, **Skjøldal, E**, **Bratbak, G.** 2023b. Bacterial production measurements (rate of production of biomass expressed as carbon by prokaryotes [bacteria and archaea]) during Nansen Legacy cruise 2021710. Norwegian Marine Data Centre. DOI: https://doi.org/10.21335/NMDC-1815353537-2021710.

Mumm, N. 1993. Composition and distribution of mesozooplankton in the Nansen Basin, Arctic Ocean, during summer. *Polar Biology* **13**: 451–461. DOI: http://dx.doi.org/10.1007/BF00233136.

Mumm, N, **Auel, H**, **Hanssen, H**, **Hagen, W**, **Richter, C**, **Hirche, H-J.** 1998. Breaking the ice: Large-scale distribution of mesozooplankton after a decade of Arctic and transpolar cruises. *Polar Biology* **20**: 189–197. DOI: http://dx.doi.org/10.1007/s003000050295.

Nasmyth, PW. 1970. *Oceanic turbulence*. Vancouver, BC: University of British Columbia.

Neukermans, G, **Oziel, L**, **Babin, M.** 2018. Increased intrusion of warming Atlantic water leads to rapid expansion of temperate phytoplankton in the Arctic. *Global Change Biology* **24**(6): 2545–2553. DOI: http://dx.doi.org/10.1111/gcb.14075.

Nicolaus, M, **Perovich, DK**, **Spreen, G**, **Granskog, MA**, **von Albedyll, L**, **Angelopoulos, M**, **Anhaus, P**, **Arndt, S**, **Belter, HJ**, **Bessonov, V**, **Birnbaum, G**, **Brauchle, J**, **Calmer, R**, **Cardellach, E**, **Cheng, B**, **Clemens-Sewall, D**, **Dadic, R**, **Damm, E**, **de Boer, G**, **Demir, O**, **Dethloff, K**, **Divine, DV**, **Fong, AA**, **Fons, S**, **Frey, MM**, **Fuchs, N**, **Gabarró, C**, **Gerland, S**, **Goessling, HF**, **Gradinger, R**, **Haapala, J**, **Haas, C**, **Hamilton, J**, **Hannula, H-R**, **Hendricks, S**, **Herber, A**, **Heuzé, C**, **Hoppmann, M**, **Høyland, KV**, **Huntemann, M**, **Hutchings, JK**, **Hwang, B**, **Itkin, P**, **Jacobi, H-W**, **Jaggi, M**, **Jutila, A**, **Kaleschke, L**, **Katlein, C**, **Kolabutin, N**, **Krampe, D**, **Kristensen, SS**, **Krumpen, T**, **Kurtz, N**, **Lampert, A**, **Lange, BA**, **Lei, R**, **Light, B**, **Linhardt, F**, **Liston, GE**, **Loose, B**, **Macfarlane, AR**, **Mahmud, M**, **Matero, IO**, **Maus, S**, **Morgenstern, A**, **Naderpour, R**, **Nandan, V**, **Niubom, A**, **Oggier, M**, **Oppelt, N**, **Pätzold, F**, **Perron, C**, **Petrovsky, T**, **Pirazzini, R**, **Polashenski, C**, **Rabe, B**, **Raphael, IA**, **Regnery, J**, **Rex, M**, **Ricker, R**, **Riemann-Campe, K**, **Rinke, A**, **Rohde, J**, **Salganik, E**, **Scharien, RK**, **Schiller, M**, **Schneebeli, M**, **Semmling, M**, **Shimanchuk, E**, **Shupe, MD**, **Smith, MM**, **Smolyanitsky, V**, **Sokolov, V**, **Stanton, T**, **Stroeve, J**, **Thielke, L**, **Timofeeva, A**, **Tonboe, RT**, **Tavri, A**, **Tsamados, M**, **Wagner, DN**, **Watkins, D**, **Webster, M**, **Wendisch, M**. 2022. Overview of the MOSAiC expedition: Snow and sea ice. *Elementa: Science of the Anthropocene* **10**(1): 000046. DOI: http://dx.doi.org/10.1525/elementa.2021.000046.

Nöthig, E-M, **Lalande, C**, **Fahl, K**, **Metfies, K**, **Salter, I**, **Bauerfeind, E.** 2020a. Annual cycle of downward particle fluxes on each side of the Gakkel Ridge in the central Arctic Ocean. *Philosophical Transaction of the Royal Society A: Mathematical, Physical and Engineering Sciences* **378**: 20190368. DOI: http://dx.doi.org/10.1098/rsta.2019.0368.

Nöthig, E-M, **Ramondenc, S**, **Haas, A**, **Hehemann, L**, **Walter, A**, **Bracher, A**, **Lalande, C**, **Metfies, K**, **Peeken, I**, **Bauerfeind, E**, **Boetius, A.** 2020b. Summertime chlorophyll *a* and particulate organic carbon standing stocks in surface waters of the Fram Strait and the Arctic Ocean (1991–2015). *Frontiers in Marine Science* **7**: 350. DOI: http://dx.doi.org/10.3389/fmars.2020.00350.

Nozais, C, **Gosselin, M**, **Michel, C**, **Tita, G.** 2001. Abundance, biomass, composition and grazing impact of

the sea-ice meiofauna in the North Water, northern Baffin Bay. *Marine Ecology Progress Series* **217**: 235–250. DOI: http://dx.doi.org/10.3354/meps217235.

Oksanen, J. 2010. Vegan: Community ecology package. Available at http://vegan.r-forge.r-project.org/. Accessed September 4, 2024.

Oleszczuk, B, **Grzelak, K**, **Kędra, M.** 2021. Community structure and productivity of Arctic benthic fauna across depth gradients during springtime. *Deep Sea Research Part I: Oceanographic Research Papers* **170**: 103457. DOI: http://dx.doi.org/10.1016/j.dsr.2020.103457.

Olsson, K, **Anderson, LG.** 1997. Input and biogeochemical transformation of dissolved carbon in the Siberian shelf seas. *Continental Shelf Research* **17**(7): 819–833. DOI: http://dx.doi.org/10.1016/S0278-4343(96)00059-3.

OSI SAF. 2010. OSI SAF Global Low Resolution Sea Ice Drift, OSI-405-c, EUMETSAT Ocean and Sea Ice Satellite Application Facility. Data extracted from OSI SAF FTP server October 2023. DOI: http://dx.doi.org/10.15770/EUM_SAF_OSI_NRT_2007.

OSI SAF. 2022a. OSI SAF Global Low Resolution Sea Ice Drift data record 1991-2020 (v1, 2022), OSI-455, EUMETSAT Ocean and Sea Ice Satellite Application Facility. Data extracted from OSI SAF FTP server October 2023. DOI: http://dx.doi.org/10.15770/EUM_SAF_OSI_0012.

OSI SAF. 2022b. OSI SAF Global sea ice concentration climate data record 1978-2020 (v3.0, 2022), OSI-450-a. EUMETSAT Ocean and Sea Ice Satellite Application Facility. Data extracted from OSI SAF FTP server October 2023. DOI: http://dx.doi.org/10.15770/EUM_SAF_OSI_0013.

OSI SAF. 2022c. OSI SAF Global sea ice concentration interim climate data record (v3.0, 2022), OSI-430-a, EUMETSAT Ocean and Sea Ice Satellite Application Facility. Data extracted from OSI SAF FTP server October 2023. DOI: http://dx.doi.org/10.15770/EUM_SAF_OSI_0014.

Oziel, L, **Baudena, A**, **Ardyna, M**, **Massicotte, P**, **Randelhoff, A**, **Sallée, JB**, **Ingvaldsen, RB**, **Devred, E**, **Babin, M.** 2020. Faster Atlantic currents drive poleward expansion of temperate phytoplankton in the Arctic Ocean. *Nature Communications* **11**: 1705. DOI: http://dx.doi.org/10.1038/s41467-020-15485-5.

Paulsen, ML, **Bratbak, G**, **Larsen, A**, **Seuthe, L**, **Egge, JK**, **Erga, SR**. 2017. CarbonBridge 2014: Physical oceanography and microorganism composition during 5 cruises (Jan, March, May, August, Nov 2014) on and off the shelf northwest of Svalbard in 2014. PANGAEA. DOI: http://dx.doi.org/10.1594/PANGAEA.884255.

Paulsen, ML, **Dore, H**, **Garczarek, L**, **Seuthe, L**, **Mueller, O**, **Sandaa, R-A**, **Bratbak, G**, **Larsen, A.** 2016. *Synechococcus* in the Atlantic gateway to the Arctic Ocean. *Frontiers in Marine Science* **3**: 191. DOI: http://dx.doi.org/10.3389/fmars.2016.00191.

Pavlov, AK, **Granskog, MA**, **Stedmon, CA**, **Ivanov, BV**, **Hudson, SR**, **Falk-Petersen, S.** 2015. Contrasting optical properties of surface waters across the Fram Strait and its potential biological implications. *Journal of Marine Systems* **143**: 62–72. DOI: http://dx.doi.org/10.1016/j.jmarsys.2014.11.001.

Perovich, D, **Meier, W**, **Tschudi, M**, **Hendricks, S**, **Petty, AA**, **Divine, D**, **Farrell, S**, **Gerland, S**, **Haas, C**, **Kaleschke, L**, **Pavlova, O**, **Ricker, R**, **Tian-Kunze, X**, **Webster, M**, **Wood, K.** 2020. Arctic Report Card 2020: Sea Ice. DOI: http://dx.doi.org/10.25923/n170-9h57.

Pfannkuche, O, **Thiel, H.** 1987. Meiobenthic stocks and benthic activity on the NE-Svalbard Shelf and in the Nansen Basin. *Polar Biology* **7**: 253–266. DOI: http://dx.doi.org/10.1007/BF00443943.

Piontek, J, **Galgani, L**, **Nöthig, EM**, **Peeken, I**, **Engel, A.** 2021. Organic matter composition and heterotrophic bacterial activity at declining summer sea ice in the central Arctic Ocean. *Limnology and Oceanography* **66**(S1): S343–S362. DOI: http://dx.doi.org/10.1002/lno.11639.

Pitusi, V, **Gradinger, R**, **Søreide, JE.** 2023. Temporal and spatial variability of sympagic metazoans in a high-Arctic fjord, Svalbard. *Frontiers in Marine Science* **10**: 1201359. DOI: http://dx.doi.org/10.3389/fmars.2023.1201359.

Pnyushkov, AV, **Polyakov, IV.** 2022. Nansen And Amundsen Basins Observational System (NABOS). *Oceanography* **35**(3–4): 90–93.

Polyakov, IV, **Alkire, MB**, **Bluhm, BA**, **Brown, KA**, **Carmack, EC**, **Chierici, M**, **Danielson, SL**, **Ellingsen, I**, **Ershova, EA**, **Gardfeldt, K**, **Ingvaldsen, RB**, **Pnyushkov, AV**, **Slagstad, D**, **Wassmann, P.** 2020. Borealization of the Arctic Ocean in response to anomalous advection from sub-Arctic seas. *Frontiers in Marine Science* **7**: 491. DOI: http://dx.doi.org/10.3389/fmars.2020.00491.

Polyakov, IV, **Ingvaldsen, RB**, **Pnyushkov, AV**, **Bhatt, US**, **Francis, JA**, **Janout, M**, **Kwok, R**, **Skagseth, Ø.** 2023. Fluctuating Atlantic inflows modulate Arctic atlantification. *Science* **381**(6661): 972–979. DOI: http://dx.doi.org/10.1126/science.adh5158.

Polyakov, IV, **Pnyushkov, AV**, **Alkire, MB**, **Ashik, IM**, **Baumann, TM**, **Carmack, EC**, **Goszczko, I**, **Guthrie, J**, **Ivanov, VV**, **Kanzow, T**, **Krishfield, R**, **Kwok, R**, **Sundfjord, A**, **Morison, J**, **Rember, R**, **Zulin, A.** 2017. Greater role for Atlantic inflows on sea-ice loss in the Eurasian Basin of the Arctic Ocean. *Science* **356**(6335): 285–291. DOI: http://dx.doi.org/10.1126/science.aai8204.

Polyakov, IV, **Walsh, JE**, **Kwok, R.** 2012. Recent changes of Arctic multiyear sea ice coverage and the likely causes. *Bulletin of the American Meteorological Society* **93**: 145–151.

Postel, L, **Fock, H**, **Hagen, W.** 2000. Biomass and abundance, in Harris, RP, Wiebe, PH, Lenz, J, Skjoldal, HR, Huntley, M eds., *ICES zooplankton methodology manual*. London, UK: Academic Press: 83–192.

Poulin, M, **Daugbjerg, N**, **Gradinger, R**, **Ilyash, L**, **Ratkova, T**, **von Quillfeldt, C.** 2011. The pan-Arctic biodiversity of marine pelagic and sea-ice unicellular eukaryotes: A first-attempt assessment. *Marine Biodiversity* **41**: 13–28. DOI: http://dx.doi.org/10.1007/s12526-010-0058-8.

Prandke, H, **Stips, A.** 1998. Test measurements with an operational microstructure-turbulence profiler: Detection limit of dissipation rates. *Aquatic Sciences* **60**: 191–209. DOI: http://dx.doi.org/10.1007/s000270050036.

R Core Team. 2021. R: A language and environment for statistical computing. Vienna, Austria: R Foundation for Statistical Computing. Available at http://www.R-project.org/. Accessed October 1, 2023.

Rabe, B, **Heuzé, C**, **Regnery, J**, **Aksenov, Y**, **Allerholt, J**, **Athanase, M**, **Bai, Y**, **Basque, C**, **Bauch, D**, **Baumann, TM**, **Chen, D**, **Cole, ST**, **Craw, L**, **Davies, A**, **Damm, E**, **Dethloff, K**, **Divine, DV**, **Doglioni, F**, **Ebert, F**, **Fang, Y-C**, **Fer, I**, **Fong, AA**, **Gradinger, R**, **Granskog, MA**, **Graupner, R**, **Haas, C**, **He, H**, **He, Y**, **Hoppmann, M**, **Janout, M**, **Kadko, D**, **Kanzow, T**, **Karam, S**, **Kawaguchi, Y**, **Koenig, Z**, **Kong, B**, **Krishfield, RA**, **Krumpen, T**, **Kuhlmey, D**, **Kuznetsov, I**, **Lan, M**, **Laukert, G**, **Lei, R**, **Li, T**, **Torres-Valdés, S**, **Lin, L**, **Lin, L**, **Liu, H**, **Liu, N**, **Loose, B**, **Ma, X**, **MacKay, R**, **Mallet, M**, **Mallett, RDC**, **Maslowski, W**, **Mertens, C**, **Mohrholz, V**, **Muilwijk, M**, **Nicolaus, M**, **O'Brien, JK**, **Perovich, D**, **Ren, J**, **Rex, M**, **Ribeiro, N**, **Rinke, A**, **Schaffer, J**, **Schuffenhauer, I**, **Schulz, K**, **Shupe, MD**, **Shaw, W**, **Sokolov, V**, **Sommerfeld, A**, **Spreen, G**, **Stanton, T**, **Stephens, M**, **Su, J**, **Sukhikh, N**, **Sundfjord, A**, **Thomisch, K**, **Tippenhauer, S**, **Toole, JM**, **Vredenborg, M**, **Walter, M**, **Wang, H**, **Wang, L**, **Wang, Y**, **Wendisch, M**, **Zhao, J**, **Zhou, M**, **Zhu, J.** 2022. Overview of the MOSAiC expedition: Physical oceanography. *Elementa: Science of the Anthropocene* **10**(1): 00062. DOI: http://dx.doi.org/10.1525/elementa.2021.00062.

Ramirez-Llodra, E, **Meyer, HK**, **Bluhm, BA**, **Brix, S**, **Brandt, A**, **Dannheim, J**, **Downey, RV**, **Egilsdóttir, H**, **Eilertsen, HM**, **Gaudron, SM**, **Gebruk, A**, **Golikov, A**, **Hasemann, C**, **Hilario, A**, **Jørgensen, LL**, **Kaiser, S**, **Korfhage, SA**, **Kürzel, K**, **Lörz, A-N**, **Buhl-Mortensen, P**, **Olafsdóttir, SH**, **Piepenburg, D**, **Purser, A**, **Ribeiro, PA**, **Sen, A**, **Soltwedel, T**, **Stratmann, T**, **Steger, J**, **Svavarsson, J**, **Tandberg, AHS**, **Taylor, J**, **Theising, FI**, **Uhlir, C**, **Waller, RG**, **Xavier, JR**, **Zhulay, I**, **Saaedi, H.** 2024. The emerging picture of a diverse deep Arctic Ocean seafloor: From habitats to ecosystem. *Elementa: Science of the Anthropocene* **12**(1): 00140. DOI: http://dx.doi.org/10.1525/elementa.2023.00140.

Randelhoff, A, **Guthrie, JD.** 2016. Regional patterns in current and future export production in the central Arctic Ocean quantified from nitrate fluxes. *Geophysical Research Letters* **43**(16): 8600–8608. DOI: http://dx.doi.org/10.1002/2016GL070252.

Randelhoff, A, **Holding, J**, **Janout, M**, **Sejr, MK**, **Babin, M**, **Tremblay, JÉ**, **Alkire, MB.** 2020. Pan-Arctic Ocean primary production constrained by turbulent nitrate fluxes. *Frontiers in Marine Science* **7**: 150. DOI: http://dx.doi.org/10.3389/fmars.2020.00150.

Reigstad, M, **Riser, CW**, **Wassmann, P**, **Ratkova, T.** 2008. Vertical export of particulate organic carbon: Attenuation, composition and loss rates in the northern Barents Sea. *Deep Sea Research Part II: Topical Studies in Oceanography* **55**(21–22): 2308–2319. DOI: http://dx.doi.org/10.1016/j.dsr2.2008.05.007.

Renner, AH, **Bailey, A**, **Reigstad, M**, **Sundfjord, A**, **Chierici, M**, **Jones, EM.** 2023. Hydrography, inorganic nutrients and chlorophyll *a* linked to sea ice cover in the Atlantic Water inflow region north of Svalbard. *Progress in Oceanography* **219**: 103162. DOI: http://dx.doi.org/10.1016/j.pocean.2023.103162.

Rex, MA, **Etter, RJ**, **Morris, JS**, **Crouse, J**, **McClain, CR**, **Johnson, NA**, **Stuart, CT**, **Deming, JW**, **Thies, R**, **Avery, R.** 2006. Global bathymetric patterns of standing stock and body size in the deep-sea benthos. *Marine Ecology Progress Series* **317**: 1–8. DOI: http://dx.doi.org/10.3354/meps317001.

Ribeiro, CG, **dos Santos, AL**, **Trefault, N**, **Marie, D**, **Lovejoy, C**, **Vaulot, D.** 2022. Arctic phytoplankton spring bloom diversity across the marginal ice zone in Baffin Bay. BioRxiv. DOI: http://dx.doi.org/10.1101/2022.03.14.484350.

Ricardo de Freitas, T, **Hess, S**, **Renaud, PE**, **Appleby, P**, **Alve, E.** 2024. Drivers of organic carbon distribution and accumulation in the northern Barents Sea. *Progress in Oceanography* **225**: 103286. DOI: http://dx.doi.org/10.1016/j.pocean.2024.103286.

Roesler, C, **Uitz, J**, **Claustre, H**, **Boss, E**, **Xing, X**, **Organelli, E**, **Briggs, N**, **Bricaud, A**, **Schmechtig, C**, **Poteau, A**, **D'Ortenzio, F**, **Ras, J**, **Drapeau, S**, **Haëntjens, N**, **Barbieux, M.** 2017. Recommendations for obtaining unbiased chlorophyll estimates from *in situ* chlorophyll fluorometers: A global analysis of WET Labs ECO sensors. *Limnology and Oceanography: Methods* **15**(6): 572–585. DOI: http://dx.doi.org/10.1002/lom3.10185.

Ross, PS, **Chastain, S**, **Vassilenko, E**, **Etemadifar, A**, **Zimmermann, S**, **Quesnel, S-A**, **Eert, J**, **Solomon, E**, **Patankar, S**, **Posacka, AM**, **Williams, B.** 2021. Pervasive distribution of polyester fibres in the Arctic Ocean is driven by Atlantic inputs. *Nature Communications* **12**: 106. DOI: http://dx.doi.org/10.1038/s41467-020-20347-1.

Rudels, B. 2015. Arctic Ocean circulation, processes and water masses: A description of observations and ideas with focus on the period prior to the International Polar Year 2007–2009. *Progress in Oceanography* **132**: 22–67. DOI: http://dx.doi.org/10.1016/j.pocean.2013.11.006.

Rudels, B, **Björk, G**, **Nilsson, J**, **Winsor, P**, **Lake, I**, **Nohr, C.** 2005. The interaction between waters from the Arctic Ocean and the Nordic Seas north of Fram

Strait and along the East Greenland Current: Results from the Arctic Ocean-02 Oden expedition. *Journal of Marine Systems* **55**(1–2): 1–30. DOI: http://dx.doi.org/10.1016/j.jmarsys.2004.06.008.

Rudels, B, **Carmack, E.** 2022. Arctic Ocean water mass structure and circulation. *Oceanography* **35**(3–4): 52–65.

Rudels, B, **Korhonen, M**, **Schauer, U**, **Pisarev, S**, **Rabe, B**, **Wisotzki, A.** 2015. Circulation and transformation of Atlantic water in the Eurasian Basin and the contribution of the Fram Strait inflow branch to the Arctic Ocean heat budget. *Progress in Oceanography* **132**: 128–152. DOI: http://dx.doi.org/10.1016/j.pocean.2014.04.003.

Rudels, B, **Schauer, U**, **Björk, G**, **Korhonen, M**, **Pisarev, S**, **Rabe, B**, **Wisotzki, A.** 2013. Observations of water masses and circulation with focus on the Eurasian Basin of the Arctic Ocean from the 1990s to the late 2000s. *Ocean Science* **9**(1): 147–169. DOI: http://dx.doi.org/10.5194/os-9-147-2013.

Rybakova, E, **Kremenetskaia, A**, **Vedenin, A**, **Boetius, A**, **Gebruk, A.** 2019. Deep-sea megabenthos communities of the Eurasian Central Arctic are influenced by ice-cover and sea-ice algal falls. *PloS one* **14**(7): e0211009. DOI: http://dx.doi.org/10.1371/journal.pone.0211009.

Schanke, NL, **Bolinesi, F**, **Mangoni, O**, **Katlein, C**, **Anhaus, P**, **Hoppmann, M**, **Lee, PA**, **DiTullio, GR.** 2021. Biogeochemical and ecological variability during the late summer–early autumn transition at an ice-floe drift station in the Central Arctic Ocean. *Limnology and Oceanography* **66**(S1): S363–S382. DOI: http://dx.doi.org/10.1002/lno.11676.

Schauer, U, **Rudels, B**, **Jones, E**, **Anderson, L**, **Muench, R**, **Björk, G**, **Swift, JH**, **Ivanov, V**, **Larsson, A-M.** 2002. Confluence and redistribution of Atlantic water in the Nansen, Amundsen and Makarov basins. *Annales Geophysicae* **20**(2): 257–273. DOI: http://dx.doi.org/10.5194/angeo-20-257-2002.

Schewe, I. 2001. Small-sized benthic organisms of the Alpha Ridge, Central Arctic Ocean. *International Review of Hydrobiology* **86**(3): 317–335. DOI: http://dx.doi.org/10.1002/1522-2632(200106)86:3<317::AID-IROH317>3.0.CO;2-V.

Schmidt, K, **Birchill, AJ**, **Atkinson, A**, **Brewin, RJ**, **Clark, JR**, **Hickman, AE**, **Johns, DG**, **Lohan, MC**, **Milne, A**, **Pardo, S**, **Polimene, L**, **Smyth, TJ**, **Tarran, GA**, **Widdicombe, CE**, **Woodward, EMS**, **Ussher, SJ.** 2020. Increasing picocyanobacteria success in shelf waters contributes to long-term food web degradation. *Global Change Biology* **26**(10): 5574–5587. DOI: http://dx.doi.org/10.1111/gcb.15161.

Schnack-Schiel, SB. 2003. The macrobiology of sea ice, in Thomas, DN, Dieckman, GS eds., *Sea ice: An introduction to its physics, chemistry, biology and geology.* Wiley: 211–239. DOI: http://dx.doi.org/10.1002/9780470757161.

Schulz, K, **Koenig, Z**, **Muilwijk, M**, **Bauch, D**, **Hoppe, CJM**, **Droste, E**, **Hoppmann, M**, **Chamberlain, EJ**, **Laukert, G**, **Stanton, T**, **Quintanilla Zurita, A**, **Fer, I**, **Heuzé, C**, **Karam, S**, **Mieruch-Schnuelle, S**, **Baumann, T**, **Vredenborg, M**, **Tippenhauer, S**, **Granskog, MA.** 2024. The Eurasian Arctic Ocean along the MOSAiC drift (2019–2020): An interdisciplinary perspective on properties and processes. *Elementa: Science of the Anthropocene* **12**: 00114. DOI: https://doi.org/10.1525/elementa.2023.00114.

Sen, A, **Jordà Molina, E**, **Ricardo de Freitas, T**, **Hess, S**, **Reiss, H**, **Bluhm, BA**, **Renaud, PE.** 2024. Benthic remineralization under future Arctic conditions: Evaluating the potential for changes in carbon sequestration in warming sediments. *Scientific Reports* **14**: 23336. DOI: http://dx.doi.org/10.1038/s41598-024-73633-z.

Sherr, EB, **Sherr, BF**, **Wheeler, PA**, **Thompson, K.** 2003. Temporal and spatial variation in stocks of autotrophic and heterotrophic microbes in the upper water column of the central Arctic Ocean. *Deep Sea Research Part I: Oceanographic Research Papers* **50**(5): 557–571. DOI: http://dx.doi.org/10.1016/S0967-0637(03)00031-1.

Simon, M, **Azam, F.** 1989. Protein content and protein synthesis rates of planktonic marine bacteria. *Marine Ecology Progress Series* **51**: 201–213.

Skjøldal, HR. 2022. Ecosystem assessment of the Central Arctic Ocean: Description of the ecosystem. ICES Cooperative Research Reports (CRR). DOI: http://dx.doi.org/10.17895/ices.pub.20191787.v2.

Slagstad, D, **Ellingsen, IH**, **Wassmann, P.** 2011. Evaluating primary and secondary production in an Arctic Ocean void of summer sea ice: An experimental simulation approach. *Progress in Oceanography* **90**: 117–131. DOI: http://dx.doi.org/10.1016/j.pocean.2011.02.009.

Slagstad, D, **Wassmann, PF**, **Ellingsen, I.** 2015. Physical constrains and productivity in the future Arctic Ocean. *Frontiers in Marine Science* **2**: 85. DOI: http://dx.doi.org/10.3389/fmars.2015.00085.

Smith, DC, **Azam, F.** 1992. A simple, economical method for measuring bacterial protein synthesis rates in seawater using 3H-leucine. *Marine Microbial Food Webs* **6**: 107–114.

Snoeijs-Leijonmalm, P, **Flores, H**, **Volckaert, F**, **Niehoff, B**, **Schaafsma, F**, **Hjelm, J**, **Hentati-Sundberg, J**, **Niiranen, S**, **Crépin, AS**, **Österblom, H.** 2020. Review of the research knowledge and gaps on fish populations, fisheries and linked ecosystems in the Central Arctic Ocean (CAO). Executive Agency for Small and Medium-sized Enterprises (EASME), EASME/EMFF/2018/003: "Framework Contract for the Provision of Scientific Support to the High Seas Fisheries in the Central Arctic Ocean (CAO)." DOI: http://dx.doi.org/10.2826/387890.

Snoeijs-Leijonmalm, P, **Gjøsæter, H**, **Ingvaldsen, RB**, **Knutsen, T**, **Korneliussen, R**, **Ona, E**, **Skjøldal, HR**, **Stranne, C**, **Mayer, L**, **Jakobsson, M**, **Gårdfeldt, K.** 2021. A deep scattering layer under the North Pole pack ice. *Progress in Oceanography* **194**: 102560. DOI: http://dx.doi.org/10.1016/j.pocean.2021.102560.

Solomon, A, **Heuzé, C**, **Rabe, B**, **Bacon, S**, **Bertino, L**, **Heimbach, P**, **Inoue, J**, **Iovino, D**, **Mottram, R**, **Zhang, X**, **Aksenov, Y**, **McAdam, R**, **Nguyen, A**, **Raj, RP**, **Tang, H.** 2021. Freshwater in the Arctic Ocean 2010–2019. *Ocean Science* **17**(4): 1081–1102. DOI: http://dx.doi.org/10.5194/os-17-1081-2021.

Soltwedel, T, **Mokievsky, V**, **Schewe, I.** 2000. Benthic activity and biomass on the Yermak Plateau and in adjacent deep-sea regions northwest of Svålbard. *Deep Sea Research Part I: Oceanographic Research Papers* **47**(9): 1761–1785. DOI: http://dx.doi.org/10.1016/S0967-0637(00)00006-6.

Spreen, G, **Kaleschke, L**, **Heygster, G.** 2008. Sea ice remote sensing using AMSR-E 89-GHz channels. *Journal of Geophysical Research: Oceans* **113**(C2): C02S03. DOI: http://dx.doi.org/10.1029/2005JC003384.

Stedmon, CA, **Amon, RM**, **Bauch, D**, **Bracher, A**, **Gonçalves-Araujo, R**, **Hoppmann, M**, **Krishfield, R**, **Laney, S**, **Rabe, B**, **Reader, H**, **Granskog, MA.** 2021. Insights into water mass origins in the central Arctic Ocean from in-situ dissolved organic matter fluorescence. *Journal of Geophysical Research: Oceans* **126**(7): e2021JC017407. DOI: http://dx.doi.org/10.1029/2021JC017407.

Steer, A, **Divine, D.** 2023. Sea ice concentrations in the northern Barents Sea and the area north of Svalbard at Nansen Legacy stations during 2017–2021 [dataset]. Norwegian Polar Institute. DOI: https://doi.org/10.21334/npolar.2023.24f2939c.

Stein, R, **Grobe, H**, **Wahsner, M.** 1994. Organic carbon, carbonate, and clay mineral distributions in eastern central Arctic Ocean surface sediments. *Marine Geology* **119**(3–4): 269–285. DOI: http://dx.doi.org/10.1016/0025-3227(94)90185-6.

Steiner, NS, **Bowman, J**, **Campbell, K**, **Chierici, M**, **Eronen-Rasimus, E**, **Falardeau, M**, **Flores, H**, **Fransson, A**, **Herr, H**, **Insley, SJ**, **Kauko, HM**, **Lannuzel, D**, **Loseto, L**, **Lynnes, A**, **Majewski, A**, **Meiners, KM**, **Miller, LA**, **Michel, LN**, **Moreau, S**, **Nacke, M**, **Nomura, D**, **Tedesco, L**, **van Franeker, JA**, **van Leeuwe, MA**, **Wongpan, P.** 2021. Climate change impacts on sea-ice ecosystems and associated ecosystem services. *Elementa: Science of the Anthropocene* **9**(1): 00007. DOI: http://dx.doi.org/10.1525/elementa.2021.00007.

Stevenson, TC, **Davies, J**, **Huntington, HP**, **Sheard, W.** 2019. An examination of trans-Arctic vessel routing in the Central Arctic Ocean. *Marine Policy* **100**: 83–89. DOI: http://dx.doi.org/10.1016/j.marpol.2018.11.031.

Stocker, AN, **Renner, AHH**, **Knol-Kauffman, M.** 2020. Sea ice variability and maritime activity around Svalbard in the period 2012–2019. *Scientific Reports* **10**: 17043. DOI: http://dx.doi.org/10.1038/s41598-020-74064-2.

Stroeve, J, **Notz, D.** 2018. Changing state of Arctic sea ice across all seasons. *Environmental Research Letters* **13**(10): 103001. DOI: http://dx.doi.org/10.1088/1748-9326/aade56.

Sugie, K, **Fujiwara, A**, **Nishino, S**, **Kameyama, S**, **Harada, N.** 2020. Impacts of temperature, CO_2, and salinity on phytoplankton community composition in the western Arctic Ocean. *Frontiers in Marine Science* **6**: 821. DOI: http://dx.doi.org/10.3389/fmars.2019.00821.

Sumata, H, **de Steur, L**, **Divine, DV**, **Granskog, MA**, **Gerland, S.** 2023. Regime shift in Arctic Ocean sea ice thickness. *Nature* **615**: 443–449. DOI: http://dx.doi.org/10.1038/s41586-022-05686-x.

Svensen, C, **Halvorsen, E**, **Vernet, M**, **Franzè, G**, **Dmoch, K**, **Lavrentyev, PJ**, **Kwasniewski, S.** 2019. Zooplankton communities associated with new and regenerated primary production in the Atlantic inflow north of Svalbard. *Frontiers in Marine Science* **6**: 293. DOI: http://dx.doi.org/10.3389/fmars.2019.00293.

Tamelander, T, **Renaud, PE**, **Hop, H**, **Carroll, ML**, **Ambrose Jr, WG**, **Hobson, KA**. 2006. Trophic relationships and pelagic–benthic coupling during summer in the Barents Sea Marginal Ice Zone, revealed by stable carbon and nitrogen isotope measurements. *Marine Ecology Progress Series* **310**: 33–46. DOI: https://doi.org/10.3354/meps310033.

Tank, SE, **McClelland, JW**, **Spencer, RGM**, **Shiklomanov, AI**, **Suslova, A**, **Moatar, F**, **Amon, RMW**, **Cooper, LW**, **Elias, G**, **Gordeev, VV**, **Guay, C**, **Gurtovaya, TY**, **Kosmenko, LS**, **Mutter, EA**, **Peterson, BJ**, **Peucker-Ehrenbrink, B**, **Raymond, PA**, **Schuster, PF**, **Scott, L**, **Staples, R**, **Striegl, RG**, **Tretiakov, M**, **Zhulidov, AV**, **Zimov, N**, **Zimov, S**, **Holmes, RM.** 2023. Recent trends in the chemistry of major northern rivers signal widespread Arctic change. *Nature Geoscience* **16**: 789–796. DOI: http://dx.doi.org/10.1038/s41561-023-01247-7.

Terhaar, J, **Kwiatkowski, L**, **Bopp, L.** 2020. Emergent constraint on Arctic Ocean acidification in the twenty-first century. *Nature* **582**: 379–383. DOI: http://dx.doi.org/10.1038/s41586-020-2360-3.

The Nansen Legacy. 2020. Sampling protocols: Version 5. The Nansen Legacy Report Series 13/2020. DOI: https://doi.org/10.7557/nlrs.5719.

Thibault, D, **Head, EJ**, **Wheeler, PA.** 1999. Mesozooplankton in the Arctic Ocean in summer. *Deep Sea Research Part I: Oceanographic Research Papers* **46**(8): 1391–1415. DOI: http://dx.doi.org/10.1016/S0967-0637(99)00009-6.

Timmermans, ML, **Marshall, J.** 2020. Understanding Arctic Ocean circulation: A review of ocean dynamics in a changing climate. *Journal of Geophysical Research: Oceans* **125**(4): e2018JC014378. DOI: http://dx.doi.org/10.1029/2018JC014378.

Tsubouchi, T, **Våge, K**, **Hansen, B**, **Larsen, KMH**, **Østerhus, S**, **Johnson, C**, **Jónsson, S**, **Valdimarsson, H.** 2021. Increased ocean heat transport into the Nordic Seas and Arctic Ocean over the period 1993–2016. *Nature Climate Change* **11**: 21–26. DOI: http://dx.doi.org/10.1038/s41558-020-00941-3.

Tuerena, RE, **Mahaffey, C**, **Henley, SF**, **de La Vega, C**, **Norman, L**, **Brand, T**, **Sanders, T**, **Debyser, M**,

Dähnke, K, **Braun, J**, **März, C.** 2022. Nutrient pathways and their susceptibility to past and future change in the Eurasian Arctic Ocean. *Ambio* **51**: 355–369. DOI: http://dx.doi.org/10.1007/s13280-021-01673-0.

Ulfsbo, A, **Cassar, N**, **Korhonen, M**, **van Heuven, S**, **Hoppema, M**, **Kattner, G**, **Anderson, LG.** 2014. Late summer net community production in the central Arctic Ocean using multiple approaches. *Global Biogeochemical Cycles* **28**(10): 1129–1148. DOI: http://dx.doi.org/10.1002/2014GB004833.

Utermöhl, H. 1958. Zur Vervollkommnung der quantitativen Phytoplankton-Methodik. *Internationale Vereinigung für theoretische und angewandte Limnologie: Mitteilungen* **9**(1): 1–38. DOI: http://dx.doi.org/10.1080/05384680.1958.11904091.

Vader, A, **Marquardt, M.** 2022. Chlorophyll *a* and phaeopigments Nansen Legacy cruise 2021710. Norwegian Marine Data Centre. DOI: https://doi.org/10.21335/NMDC-1635641464.

Valk, O, **van der Loeff, MR**, **Geibert, W**, **Gdaniec, S**, **Moran, SB**, **Lepore, K**, **Edwards, RL**, **Lu, Y**, **Puigcorbé, V**, **Casacuberta, N**, **Paffrath, R**, **Smethie, W**, **Roy-Barman, M.** 2019. Circulation changes in the Amundsen Basin from 1991 to 2015 revealed from distributions of dissolved ^{230}Th. *Ocean Science Discussions*: 1–27. DOI: http://dx.doi.org/10.5194/os-2019-49.

Vanreusel, A, **Clough, L**, **Jacobsen, K**, **Ambrose, W**, **Jivaluk, J**, **Ryheul, V**, **Herman, R**, **Vincx, M.** 2000. Meiobenthos of the central Arctic Ocean with special emphasis on the nematode community structure. *Deep Sea Research Part I: Oceanographic Research Papers* **47**(10): 1855–1879. DOI: http://dx.doi.org/10.1016/S0967-0637(00)00007-8.

Vedenin, AA, **Mironov, AN**, **Bluhm, BA**, **Käß, M**, **Degen, R**, **Galkin, SV**, **Gebruk, AV.** 2022. Uniform bathymetric zonation of marine benthos on a Pan-Arctic scale. *Progress in Oceanography* **202**: 102764. DOI: http://dx.doi.org/10.1016/j.pocean.2022.102764.

Vihtakari, M, **Hordoir, R**, **Treble, M**, **Bryan, MD**, **Elvarsson, B**, **Nogueira, A**, **Hallfredsson, EH**, **Christiansen, JS**, **Albert, OT.** 2021. Pan-Arctic suitable habitat model for Greenland halibut. *ICES Journal of Marine Science* **78**(4): 1340–1356. DOI: http://dx.doi.org/10.1093/icesjms/fsab007.

Vylegzhanin, AN, **Young, OR**, **Berkman, PA.** 2020. The Central Arctic Ocean Fisheries Agreement as an element in the evolving Arctic Ocean governance complex. *Marine Policy* **118**: 104001. DOI: http://dx.doi.org/10.1016/j.marpol.2020.104001.

Wang, Y, **Kang, J-H**, **Xiang, P**, **Ye, Y-Y**, **Lin, H-S**, **Lin, M.** 2019. Phytoplankton communities and size-fractioned chlorophyll *a* in newly opened summer waters of the central Arctic Ocean. *Marine Ecology Progress Series* **622**: 67–82. DOI: http://dx.doi.org/10.3354/meps13001.

Wassmann, P, **Kosobokova, KN**, **Slagstad, D**, **Drinkwater, KF**, **Hopcroft, RR**, **Moore, SE**, **Ellingsen, I**, **Nelson, RJ**, **Carmack, E**, **Popova, E**, **Berge, J.** 2015. The contiguous domains of Arctic Ocean advection: Trails of life and death. *Progress in Oceanography* **139**: 42–65. DOI: http://dx.doi.org/10.1016/j.pocean.2015.06.011.

Wassmann, P, **Peinert, R**, **Smetacek, V.** 1991. Patterns of production and sedimentation in the boreal and polar Northeast Atlantic. *Polar Research* **10**(1): 209–228. DOI: http://dx.doi.org/10.3402/polar.v10i1.6740.

Wei, CL, **Rowe, GT**, **Escobar-Briones, E**, **Boetius, A**, **Soltwedel, T**, **Caley, MJ**, **Soliman, Y**, **Huettmann, F**, **Qu, F**, **Yu, Z**, **Pitcher, CR**, **Haedrich, RL**, **Wicksten, MK**, **Rex, MA**, **Baguley, JG**, **Sharma, J**, **Danovaro, R**, **MacDonald, IR**, **Nunnally, CC**, **Deming, JW**, **Montagna, P**, **Lévesque, M**, **Weslawski, JM**, **Wlodarska-Kowalczuk, M**, **Ingole, BS**, **Bett, BJ**, **Billett, DSM**, **Yool, A**, **Bluhm, BA**, **Iken, K**, **Narayanaswamy, BE.** 2010. Global patterns and predictions of seafloor biomass using random forests. *PloS one* **5**: e15323. DOI: http://dx.doi.org/10.1371/journal.pone.0015323.

Wickham, H. 2016. *ggplot2: Elegant graphics for data analysis*. Cham, Switzerland: Springer. DOI: https://doi.org/10.1007/978-3-319-24277-4.

Wiedmann, I, **Ershova, E**, **Bluhm, BA**, **Nöthig, E-M**, **Gradinger, RR**, **Kosobokova, K**, **Boetius, A.** 2020. What feeds the benthos in the Arctic Basins? Assembling a carbon budget for the deep Arctic Ocean. *Frontiers in Marine Science* **7**: 224. DOI: http://dx.doi.org/10.3389/fmars.2020.00224.

Wold, A, **Hop, H**, **Svensen, C**, **Assmann, K**, **Søreide, JE**, **Ormacyk, M**, **Kwasniewski, S.** 2023. Atlantification influences zooplankton communities seasonally in the northern Barents Sea and Arctic Ocean. *Progress in Oceanography* **219**: 103133. DOI: http://dx.doi.org/10.1016/j.pocean.2023.103133.

Yunda-Guarin, G, **Brown, TA**, **Michel, LN**, **Saint-Beat, B**, **Amiraux, R**, **Nozais, C**, **Archambault, P.** 2020. Reliance of deep-sea benthic macrofauna on ice-derived organic matter highlighted by multiple trophic markers during spring in Baffin Bay, Canadian Arctic. *Elementa: Science of the Anthropocene* **8**(1): 047. DOI: http://dx.doi.org/10.1525/elementa.2020.047.

Zabłocka, M, **Kowalczuk, P**, **Meler, J**, **Peeken, I**, **Dragańska-Deja, K**, **Winogradow, A.** 2020. Compositional differences of fluorescent dissolved organic matter in Arctic Ocean spring sea ice and surface waters north of Svalbard. *Marine Chemistry* **227**: 103893. DOI: http://dx.doi.org/10.1016/j.marchem.2020.103893.

Zhang, F, **He, J**, **Lin, L**, **Jin, H.** 2015. Dominance of picophytoplankton in the newly open surface water of the central Arctic Ocean. *Polar Biology* **38**: 1081–1089. DOI: http://dx.doi.org/10.1007/s00300-015-1662-7.

Zhang, F, **Lin, L**, **Gao, Y**, **Cao, S**, **He, J.** 2016. Ecophysiology of picophytoplankton in different water masses of the northern Bering Sea. *Polar Biology* **39**: 1381–1397. DOI: http://dx.doi.org/10.1007/s00300-015-1860-3.

Zhukova, NG, **Nesterova, VN**, **Prokopchuk, IP**, **Rudneva, GB.** 2009. Winter distribution of euphausiids (*Euphausiacea*) in the Barents Sea (2000–2005). *Deep Sea Research Part II: Topical Studies in Oceanography* **56**(21–22): 1959–1967. DOI: http://dx.doi.org/10.1016/j.dsr2.2008.11.007.

Zhulay, I, **Iken, K**, **Renaud, PE**, **Kosobokova, K**, **Bluhm, BA.** 2023. Reduced efficiency of pelagic–benthic coupling in the Arctic deep sea during lower ice cover. *Scientific Reports* **13**: 6739. DOI: http://dx.doi.org/10.1038/s41598-023-33854-0.

Ziegler, A, **Bluhm, B**, **Jørgensen, L**, **Åström, E**, **Ricardo de Freitas, T**, **Hess, S**, **Alve, E**, **Jordà-Molina, È**, **Reiss, H**, **Renaud, P**, **Sen, A**, **Schuppe, B**, **Lockwood-Ireland, C**, **Keck, A**, **Kohlbach, D**, **Giebichenstein, J**, **Marquardt, M.** 2024a. Stable isotopic and elemental compositions of carbon and nitrogen in organic matter from sea ice in the Barents Sea, Nansen Basin and Amundsen Basin (Arctic Ocean). DOI: https://doi.org/10.21335/NMDC-245429765.

Ziegler, A, **Bluhm, B**, **Jørgensen, L**, **Åström, E**, **Ricardo de Freitas, T**, **Hess, S**, **Alve, E**, **Jordà-Molina, È**, **Reiss, H**, **Renaud, P**, **Sen, A**, **Schuppe, B**, **Lockwood-Ireland, C**, **Keck, A**, **Kohlbach, D**, **Giebichenstein, J**, **Marquardt, M**. 2024b. Stable isotopic and elemental compositions of carbon and nitrogen in organic matter from sea water, in the Barents Sea, Nansen Basin and Amundsen Basin (Arctic Ocean). DOI: https://doi.org/10.21335/NMDC-1380716613.

Ziegler, A, **Kohlbach, D**, **Bluhm, B.** 2024c. Carbon and nitrogen stable isotope values for pelagic and benthic invertebrate fauna from the Nansen and Amundsen Basins from the Nansen Legacy JC2-2 cruise (2021). DOI: https://doi.org/10.21335/NMDC-1888717245.

Ziegler, AF, **Bluhm, BA**, **Renaud, PE**, **Jørgensen, LL.** 2023. Weak seasonality in benthic food web structure within an Arctic inflow shelf region. *Progress in Oceanography* **217**: 103109. DOI: http://dx.doi.org/10.1016/j.pocean.2023.103109.

Zubkov, MV, **Burkill, PH**, **Topping, JN.** 2007. Flow cytometric enumeration of DNA-stained oceanic planktonic protists. *Journal of Plankton Research* **29**(1): 79–86. DOI: http://dx.doi.org/10.1093/plankt/fbl059.

How to cite this article: Kohlbach, D, Fransson, A, Amargant-Arumi, M, Assmann, KM, Assmy, P, Bratbak, G, Chierici, M, Cristea, A, Divine, DV, Down, E, Eikrem, W, Foss, Ø, Gardner, J, Gradinger, RR, Granskog, MA, Hess, S, Ingvaldsen, RB, Koenig, Z, Kwaśniewski, S, Majaneva, S, Marquardt, M, Müller, O, Ntniou, IV, Ormańczyk, M, Raffel, B, Renaud, P, Renner, AHH, Ricardo de Freitas, T, Sen, A, Smoła, Z, Svensen, C, Vader, A, Våge, S, Wiktor, J, Wold, A, Zabłocka, M, Ziegler, A, Bluhm, BA. 2025. Nansen and Amundsen basins: Gradients of physico-chemical properties and biota composition with implications for future resource management of the central Arctic Ocean. *Elementa: Science of the Anthropocene* 13(1). DOI: https://doi.org/10.1525/elementa.2024.00016

Domain Editor-in-Chief: Jody W. Deming, University of Washington, Seattle, WA, USA

Associate Editor: Jean-Éric Tremblay, Department of Biology, Université Laval, Québec, Canada

Knowledge Domain: Ocean Science

Published: March 06, 2025 **Accepted:** December 09, 2024 **Submitted:** March 01, 2024

ELEMENTA Science of the Anthropocene

Elem Sci Anth is a peer-reviewed open access journal published by University of California Press.

OPEN ACCESS